1
The Electronic Structure of Organic Semiconductors

1.1
Introduction

Organic semiconductors are a class of materials that combine the electronic advantages of semiconducting materials with the chemical and mechanical benefits of organic compounds such as plastics. Thus, the ability to absorb light, conduct electricity, and emit light is united with a material structure that can easily be modified by chemical synthesis, for example, to tailor electronic properties such as the desired emission wavelength, to render it soluble, or to allow for mechanically robust, lightweight, and flexible thin films. These properties imply that semiconductor applications such as displays, lighting panels, or solar cells may be produced with a variety of solution-processing techniques or vacuum deposition methods (Figure 1.1). The technological exploitation is, naturally, in a constant flow of development. At the time of writing this book, industrial interest focuses on replacing vacuum deposition by printing techniques such as the reel-to-reel coating familiar from the fabrication of plastic foil or ink-jet printing. Applications on flexible foils, such as solar cell foils or lighting sheets seem attractive. The already established commercialization of organic semiconductor comprises display applications, lighting applications, and photocopier machines. The large-scale exploitation of organic semiconductor materials in the xerographic process of any common photocopier machine is present in any typical office (Figure 1.1d). Organic light-emitting diode (OLED)-based displays are, for example, employed in the Galaxy smartphone series by Samsung, and are thus also widely distributed (Figure 1.1c). More geared toward a designer market, at the time of writing, are OLED-based lighting panels, for example, from Osram (Figure 1.1e). In addition to established products, there is a constant flow of ideas for novel, innovative products that needs to be evaluated (Figure 1.1a,b). Overall, it is evident that there is a large industry involved in the present day and in the future exploitation of organic semiconductors. Consequently, there is also a need for highly qualified personnel familiar with the conceptual premises that govern electronic processes in organic semiconductors.

Over the last decade, the number of research groups that are active in the field of organic semiconductors has increased strongly. Summer schools, graduate training programs, and advanced lecture courses, typically in the context of an MSc degree or PhD, aim to educate students in many aspects of this field. With this book, we wish to contribute to this process by providing a basic and broad introduction to organic semiconductors that should enable the reader to explore the different aspects of this fascinating field later on in more depth.

1.1.1
What Are "Organic Semiconductors"?

The term *organic semiconductors* implies (i) that the materials are mostly made up by carbon and hydrogen atoms, with a few heteroatoms such as sulfur, oxygen, and nitrogen included and (ii) they show properties typically associated with a semiconductor material. The latter means absorption

Electronic Processes in Organic Semiconductors, First Edition. Anna Köhler and Heinz Bässler.

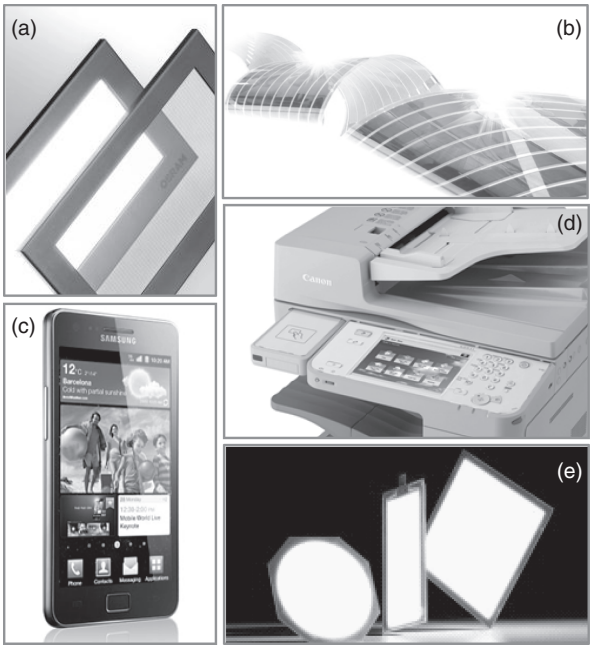

Figure 1.1 Examples of present and perhaps future organic semiconductor applications. (a) Prototype for a luminescent window made by OSRAM with an organic electroluminescent semiconductor. When switched off, the window provides a view to the outside, yet when switched on, it emits light thus functioning as panel lighting. (b) Prototype for a continuous, flexible solar cell foil by Konarka Power Plastic employing an organic semiconductor. (c) Samsung Galaxy smartphone featuring an OLED display. (d) Photocopier using organic semiconductors for the xerographic process by Canon. (e) Lighting tiles by OSRAM.

and emission of light in the visible spectral range and a degree of conductivity that is sufficient for the operation of classical semiconductor devices such as light-emitting diodes (LEDs), solar cells, and field-effect-transistors (FETs). While they show semiconducting properties, one needs to understand that the "semiconducting" nature differs strongly between inorganic and organic materials.

Traditional inorganic semiconductors such as silicon, germanium, and GaAs have low band gaps such as 0.67 (Ge), 1.1 (Si), or 1.4 eV (GaAs). At room temperature, free charges can be created by thermal excitation from a valence band to a conduction band, with a concentration of charge carriers given by $N = N_{\mathrm{eff}} \mathrm{e}^{-E_{\mathrm{g}}/2kT}$, where N_{eff} is the effective density of valence or conduction band states and E_{g} is the band gap. Typical intrinsic conductivities are in the range of about 10^{-8} to $10^{-2}\,\Omega^{-1}\,\mathrm{cm}^{-1}$. Furthermore, the dielectric constant is as large as $\varepsilon_{\mathrm{r}} = 11$ so that coulomb effects between electrons and holes are unimportant due to dielectric screening, and light absorption at room temperature creates free electrons and holes.

In contrast, the conductivity of organic "semiconductors" is extrinsic and results from the injection of charges at electrodes, from intentional or unintentional doping and from the dissociation of photogenerated electron–hole pairs that are bound by their mutual coulomb attraction. This is a result of two characteristic features of organic materials. First, absorption and emission take place mostly in the range of 2–3 eV (about 600–400 nm), which precludes creating any significant charge-carrier concentration by thermal excitation at room temperature. Further, the dielectric constant is low, taking a value of about $\varepsilon_{\mathrm{r}} = 3.5$. This implies that coulomb interactions are significant, so that any

electron–hole pair created by optical (or, hypothetically, thermal) excitation is bound by a coulomb energy of about 0.5–1.0 eV.

This brief exposition on the differences between organic and inorganic semiconductors may be sufficient to demonstrate that detailed knowledge on the electronic structure is needed in order to understand their photophysical properties, and even more if one wishes to design and improve semiconductor devices. It is useful to distinguish between the following three varieties of organic semiconductors:

(I) *Amorphous molecular films.* By this term, we mean organic molecules deposited as an amorphous film through evaporation or spin-coating. Thin amorphous films of molecules are employed for device applications such as LEDs, and molecularly doped polymer (MDP) films are used on a large technological scale in xerography.

(II) *Molecular crystals.* By definition, a crystal consists of a lattice and a basis. In the same way how atoms like silicon can form a crystal by covalent bonding, or sodium and chloride atoms by ionic bonding, molecules such as naphthalene or anthracene can form the basis of a crystal that is held together by van-der-Waals interactions. The charge mobilities that can be obtained in molecular crystals are high compared to those in noncrystalline organic materials. This renders them relevant for transistor applications.

(III) *Polymer films.* Polymers may be considered a chain of covalently coupled molecular repeat units. Usually, they are processed from solution, which allows for a range of deposition techniques including simple spin-coating, ink-jet deposition, or industrial reel-to-reel coating. They are also more suitable to blending than molecules since polymer blends are thermodynamically more stable and less susceptible to crystallization.

The semiconducting properties in all of these types of organic semiconductors have a similar origin, though their excited states and associated photophysical properties vary slightly depending on the order and coupling in the solid. As shall be detailed further below, the semiconducting nature is associated with the energy levels of the prevailing π-electrons. In this book, it is understood that we refer to molecules and polymers with extended π-orbitals unless stated otherwise.

1.1.2 Historical Context

It is useful to have a little background on the origins of this research field in order to place the available literature, be it books or journal articles, into context. This field comprises researchers that come from different disciplines, schools of thought and traditions, and the interpretation of experimental results is usually based on the background a researcher has.

One of the roots goes back to the field of *molecular crystals*. The first studies on conductivity, photoconductivity, the photoelectric effect, and fluorescence of organic solids have already been reported at the beginning of the twentieth century [1–4]. Even electroluminescence had already been reported as early as 1953 by Bernanose [5] on a cellulose film doped with acridine orange. The main period of research on molecular crystals such as naphthalene and anthracene, however, took place in the years from 1950 to 1980. This field gained momentum from the report of electroluminescence in an anthracene crystal by Pope in 1963, and by Helfrich and Schneider in 1965 [6–8]. Unfortunately, molecular crystals, held together by van-der-Waals forces, are brittle and thus require a certain minimum thickness in the range of a few micrometers. This implies the electric field needed for charge injection and conduction can only be obtained by applying a few 100 V across the crystal slice. Clearly, this is not suitable for any consumer application. Lower operating voltages were made possible with the adventure of 100 nm thin films made from amorphous vacuum deposited molecules [9] and from spin-coated polymers [10]. As a consequence, research interest moved on to amorphous organic materials and the concepts developed originally for molecular crystals were transferred to amorphous films. Central ideas that have their origin in the field of molecular crystals are the notion that

charge carriers can move in a narrow band at low temperatures in a defect-free crystal, yet that coherence is destroyed at higher temperatures so that charges move by hopping between molecules at room temperature. A further key concept is that optical excitation in a molecular crystal creates a coulomb-bound electron–hole pair, termed a *Frenkel exciton*, that may move through the crystal. These ideas are well explained in the book by Pope and Swenberg [11] and in the book by Schwoerer and Wolf [12].

Another source of concepts underpinning organic semiconductors lies in the field of molecularly doped crystals (MDPs). When companies such as Xerox and Kodak investigated materials that are suited as photoreceptors for electrophotography in the mid-1970s, it was noted that the until then used inorganic chalcogenides such as As_2Se_3 could be replaced profitably by a few μm thin film of MDPs. The application of xerography requires a material that has a very low dark conductivity, yet a reasonable photoconductivity. This is well fulfilled by MDPs, which consist of an inert polymeric binder material, for example, polycarbonate, that is doped with about 30% by weight of an optically active molecule such as triphenylamines. MDPs have the advantage of being nontoxic and easy to process, and for this reason they are still used in every common photocopying machine today. For this application, it was essential to understand how charge is transported between different molecules. Key concepts for charge transport by hopping evolved in this context [13]. A good introduction into this field can be found in the book by Borsenberger and Weiss [14].

The field of organic semiconductors was also influenced significantly by the discovery in the late 1970s that high conductivities could be obtained in π-conjugated polymers, that is, hydrocarbon chains with alternating single and double bonds, when they are doped. The discovery and development of these *conductive polymers* was rewarded in 2000 with the Nobel Prize in Chemistry to Heeger, MacDiarmid, and Shirakawa [15, 16]. The electronic structure of these polymers was initially interpreted in a traditional inorganic-semiconductor band picture [17, 18]. This model was neglecting electron–electron interactions while giving very strong weight to polaronic effects, that is, the fact that the bond lengths in a polymer chain change when a charge is placed on the polymer. During the early 1990s, however, it became clear that, in contrast to the traditional inorganic semiconductors, coulomb and exchange interactions between charges are so significant in π-conjugated polymers that they cannot be disregarded. Instead, coulomb and exchange interactions were found to be central for a suitable and correct description of the electronic structure. The lively scientific debate that eventually led to this insight is portrayed, for example, in the book edited by Sariciftci [19]. This topic is discussed further in Chapter 2.

The technological development of organic semiconductors took off with the discovery of electroluminescence in about 100 nm thin *amorphous organic films*. In 1987, Tang and Van Slyke [9] reported an amorphous thin film LED made with the molecule Alq_3 with an external quantum efficiency of 1% (emitted photons to injected electrons), a high value at the time. The low film thickness implied the necessary electrical field was already obtained below 10 V, significantly lower than in the case of molecular crystals. The abstract of their paper declares "High external quantum efficiencies (1% photon/electron), luminous efficiency (1.5 lm W^{-1}), and brightness (>1000 cd m^{-2}) are achievable at a driving voltage below 10 V." This was followed in 1990 with the report of electroluminescence below 14 V in a 100 nm thick film of the non-doped π-conjugated polymer poly(*para*-phenylene vinylene (PPV) [10]. From a technological perspective, the two types of materials differ in the way how they are processed into films. While the light-emitting molecules are usually deposited by vacuum-evaporation, the polymer films are fabricated by spin-coating from solution. The observed electroluminescence, and later on any related optoelectronic properties such as field-effect mobility in transistors or photoconductivity in solar cell structures, was interpreted using elements from the three established fields described above. For example, it soon became evident that charge transport is best described by the concept of hopping established for molecular crystals and for MDPs. Further, for amorphous molecular films, the excited state was, and still is, frequently referred to an exciton as in the case of a molecular crystal. Strictly taken, this is not correct and the term *exciton* should only be used in the context of a highly ordered system; yet by now the tradition has evolved of using "excitation" and "exciton" as synonyms. The development of a universally accepted understanding of the

electronic structure prevailing in nondoped π-conjugated polymers took some time and discussion. One line of thought (the "band picture") was inspired from the work on doped, conducting polymers, while another view (the "molecular picture") was to consider the π-conjugated polymer as a chain of chromophores, with a chromophore comprising a few repeat units. The latter is by now the canonical view, with some fundamental aspects still being addressed and developed in contemporary research [20].

1.2 Different Organic Semiconductor Materials

For a first orientation, we list here some examples for the three different classes of organic semiconductor materials.

1.2.1 Molecular Crystals

A straightforward place to start are molecular crystals. Like any crystal, they are characterized by a perfectly ordered point lattice and a basis, that is, the structural unit that is placed at the lattice point. In an inorganic crystal like silicon or germanium, the basis is formed by atoms, while molecular crystals have a basis formed by molecules. Typical crystal-forming molecules are flat, large, aromatic molecules such as the polyacenes, in particular naphthalene, anthracene, tetracene, and pentacene, as well as pyrene, perylene, and similar compounds.(see Figure 1.2) These molecules have filled outer orbitals and they are electrically neutral. Whereas a silicon crystal is kept together by covalent bonds formed only between partially filled orbitals of the atoms, and a sodium chloride crystal takes its cohesion from ionic bonding between the charged Na^+ and Cl^- ions, these forms of strong bonding are not available to a molecular crystal. Instead, the attractive force between the neutral and nonpolar molecules is provided by comparatively weak van-der-Waals interactions.

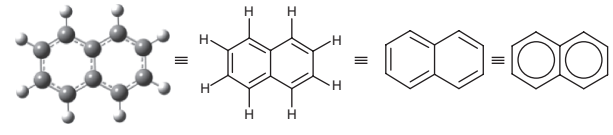

(a)

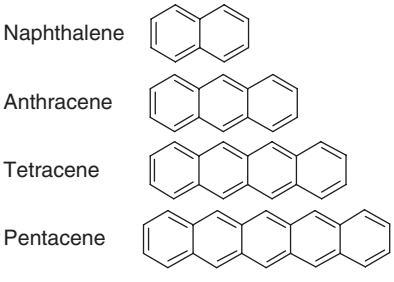

(b)

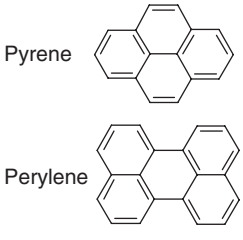

(c)

Figure 1.2 Chemical structures of π-conjugated molecules that tend to form molecular crystals. (a) The structure of naphthalene, explicitly including the H-atoms. In any subsequent figure, the H-atoms shall be omitted as is custom in the field. (b) The structure of the acenes from naphthalene to pentacene. (c) The structures of the molecules pyrene and perylene.

The concept of the van-der-Waals interaction between two molecules is based on the fact that the molecules have no static dipole moment, but that they have a charge distribution that is not entirely rigid. A temporal fluctuation in the charge distribution in a molecule implies an associated temporary fluctuating dipole moment. This will induce a corresponding fluctuating dipole in the second molecule. The electrostatic interaction between the correlated fluctuating dipoles in the two molecules results in an attractive force, the van-der-Waals-attraction. This force depends strongly on the distance r between the molecules, and on the ability to induce dipole moments in a charge distribution, that is, the polarizability α of a molecule. Quantitatively, the potential energy associated with a van-der-Waals interaction is given by $V_{\mathrm{VdW}} \propto \frac{\alpha^2}{r^6}$, that is, the force is proportional to r^{-7} [12].

This has two consequences. First, the dependence on polarizability implies that molecular crystals are preferentially formed by molecules that possess a filled outer orbital that is large and delocalized, so that many electrons can easily be moved over some distance on the molecule. As we shall detail further below, this is the case for flat molecules with π-orbitals, like the polyacenes. In fact, the increase in polarizability explains why the melting points of the polyacene molecular crystals rises with their size (benzene 5.5 °C, naphthalene 80 °C, anthracene 216 °C, tetracene 357 °C) [12]. Second, the strong distance dependence of the comparatively weak van-der-Waals forces leads to tightly packed structures (Figure 1.3). A particularly frequent structure is the herringbone arrangement (see Figure 1.3). This structure is further assisted by electrostatic interactions between the comparatively

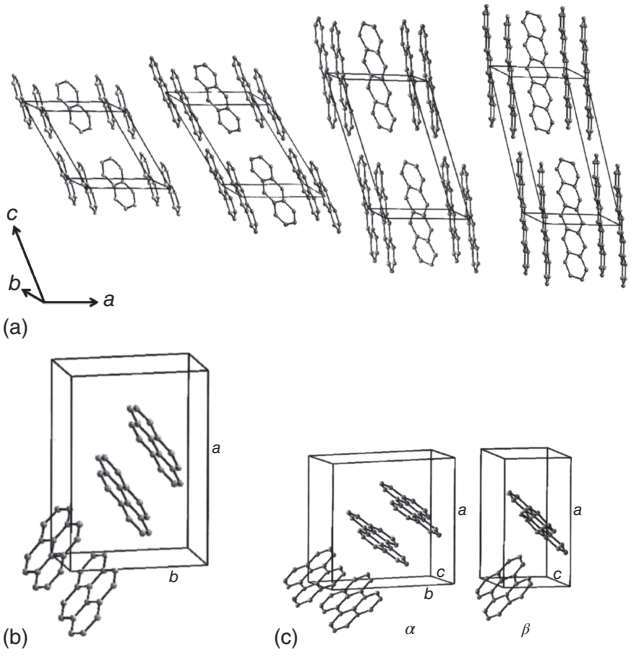

Figure 1.3 Typical crystal structures of organic molecular crystals. (Adapted from Schwoerer and Wolf [12].) (a) The unit cell for the naphthalene, anthracene, tetracene, and pentacene. The crystal has a simple cubic lattice with a basis consisting of two molecules that are arranged in a herringbone stacking, that is, the H-atoms of the second molecule point toward the π system of the first molecule. (b) The unit cell for pyrene. Only the simple cubic lattice and the basis are shown. The basis consists of four molecules, that is, two sandwich-type pairs arranged in a herringbone manner. (c) The unit cell for perylene in two different phases, the α phase and the β phase. Only the simple cubic lattice and the basis are shown. In the α phase, the basis comprises four molecules analogous to pyrene, while in the β phase, the basis is made up by two molecules in herringbone stacking.

electron-deficient hydrogen atoms in the polyacene and the electron-rich π-electrons of the aromatic ring system.

Usually, the crystal structure is made up from individual molecules, as is the case for naphthalene or for the β-phase perylene. It can, however, also occur that it is made up from a weakly interacting pair of two identical molecules, as is the case for pyrene and for α-phase perylene. Since the pair is only weakly bound, it absorbs as a monomer, yet it emits as a dimer. This is referred to as *excimer emission*. There are a number of good monographs on the subject of molecular crystals, to which the interested reader may refer to for more detail [12, 21–23].

Today's technological interest in molecular crystals arises mostly from the field of organic field-effect transistors (OFETs). A basic version of an OFET consists of an organic semiconductor layer with a source and a drain electrode at either end. This is placed on top of an insulating layer that separates the semiconductor from a gate electrode. When a potential is applied to the gate electrode, a current can flow between the suitably biased source and drain electrode (Figure 1.4). This current moves in a very thin layer of the semiconductor, adjacent to the insulator layer. For this application, the total thickness of the organic semiconductor is not relevant while the mobility of the charge is important to yield reasonable switching times of the OFET. Thus, the high degree of order that prevails in molecular crystals and that allows for comparatively high charge mobilities render them of interest for OFET applications, even though their preparation and purification can be demanding. In contrast to OLED or solar cell applications, the layer thickness of a few micrometers needed to prevent the crystal from mechanically breaking does not affect the operation of the OFET in a significant way. During the last 5 years, OFETs employing crystalline materials were reported with hole mobilities in the range of $1-50\ cm^2\ V^{-1}\ s^{-1}$ [24–29]. In passing we note that a relevant parameter for OFET application is not only the purity and structure of the crystalline material, but also the orientation of the molecules relatively to the insulator surface (and thus also relative to the source and drain electrode) [30], as charge transport in molecular crystals is highly anisotropic [11, 12].

1.2.2 Amorphous Molecular Films

With this class of materials we associate molecules that form amorphous films, that is, glasses, which are suitable for organic semiconductor applications. For those new to the field of organic semiconductors, and in particular to those with a background outside chemistry, the wealth and variety of chemical structures they encounter may at first seem overwhelming. After a short inspection, the beginner may notice that most molecules they encounter are made up of similar chemical units, usually phenyl rings, some five- or six-membered rings with heteroatoms like sulfur, nitrogen, or oxygen in it ("heteroaromatic rings"), and occasionally a few carbon atoms, either with alternating single and double bonds when in the center of the molecule, or with a sequence of single bonds when forming a side chain. Scientists who make organic semiconductor devices or who synthesize molecules for such applications tend to distinguish between the molecules according to their processability or

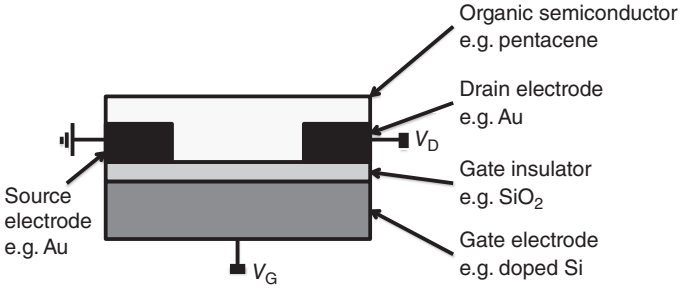

Figure 1.4 Basic structure of an organic field effect transistor (OFET).

according to their function in the device. This tends to be a useful way to order the large amount of compounds that are available, and we shall employ this approach to exemplarily introduce some of the commonly used compounds.

When considering processability, one differentiates between molecules that are deposited by evaporation in vacuum and those that are deposited on a substrate by spin-coating after dissolving them in a common organic solvent such as toluene, chloroform, or chlorobenzene. For vacuum deposition, the molecule needs to be thermally stable, which is often obtained by including the intrinsically stable aromatic rings in the chemical structure and by avoiding side chains, which are more likely to break up. In contrast, for spin-coating, solubility needs to be high, and this requires the use of solubilizing groups such as side chains. Thus, the same core molecule can, in principle, be prepared in a version for either processing method, depending on whether and to which extent solubilizing groups are incorporated in the chemical structure. Examples of such molecules are given in Figure 1.5.

The function a molecule takes in a device structure depends largely on its absorption or emission energy and on the energy of the molecular orbitals relative to the electrode workfunctions or relative to other molecular materials used. In general, it is nearly impossible to chemically optimize the energy levels in a molecule such that it is at the same time well suited to transport positive charge, negative charge, emit light, and absorb light efficiently in the desired wavelength range. Instead, it is common practice to prepare molecules that are particularly suited to one of these tasks. Thus, molecules that have a high quantum yield of luminescence may be employed as efficient emitters in OLEDs, those with a high absorption cross-section at the wavelength of interest are used as absorbers (or "light-harvesting-molecules") in solar cell structures. Molecules that readily give up electrons may be well suited to transport holes and are thus referred to as *hole-transporting molecules*, while the converse is the case for electron-transporting or electron-accepting molecules. A few examples of commonly used compounds can be found in Figure 1.5.

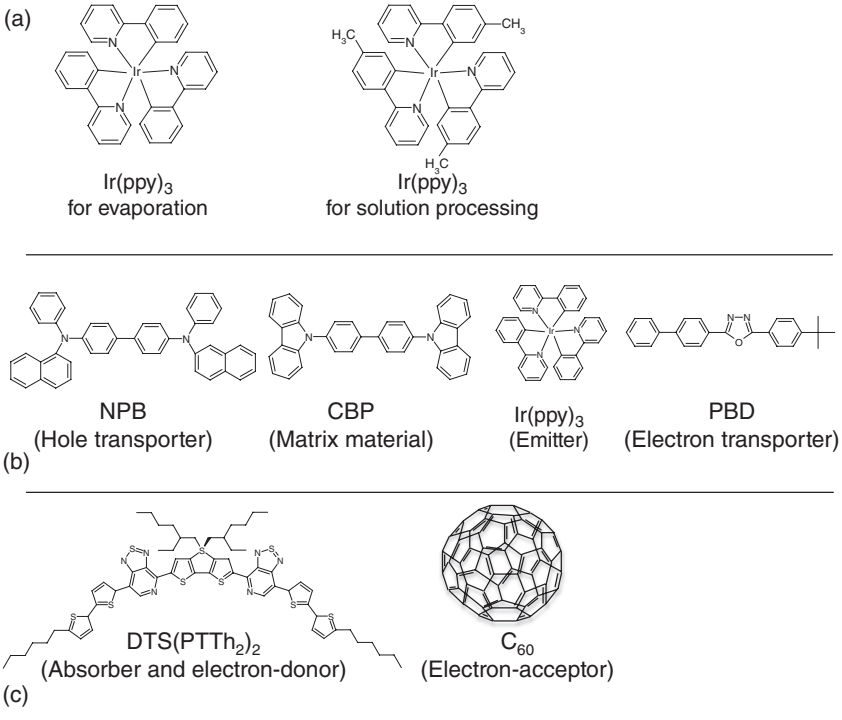

Figure 1.5 Examples and classification of π-conjugated molecules (a) by processing methods, (b) by electronic function in an OLED, and (c) by electronic function in an organic solar cell.

1.2.3 Polymer Films

The name polymer is composed of the Greek words πολυ and μεροσ, meaning "many" and "part." It implies that a polymer is a macromolecule that is composed of many repeating single units, the monomer units. In the context of organic semiconductors, "many" usually means at least 100 repeat units. Commercially available semiconducting polymers such as PPV derivatives and polyfluorenes are offered with molecular weight in the range of 50 000–100 000 Da, implying they contain about 200–400 repeat units (see Box 1.1). Any chain made with up to 20 repeat units is referred to as *oligomer* (ολιγοσ = a few). Molecules containing between 20 and 100 repeat units may be called either a *long oligomer* or a *short polymer*, depending on which aspect the author wishes to emphasize. The arrangement of the repeat units can vary to form homopolymers, copolymers, main-chain polymers, or side-chain polymers (see Box 1.2). Here, we consider main chain homopolymers, which are frequently encountered and straightforward in their structure.

Box 1.1 Average Molecular Weights of Polymers

When polymers are synthesized, they will not all have exactly the same number of repeat units. Instead, there will be a distribution of polymer sizes, with some short chains, many medium-sized chains, and few long chains. A polymer sample can then be characterized by the average weight of the polymer and the width of the associated weight distribution. There are several ways to obtain an average weight, the most important being the *number-average molecular weight* $\overline{M_n}$ and the *weight-average molecular weight* $\overline{M_w}$. In general, any average $\overline{x}$ for a quantity with a distribution of values x_i is given by the sum over all values times the probability p_i of it occurring, that is, $\overline{x} = \sum_i p_i x_i$.

If the probability of a molecular mass M_i occurring in a distribution is considered proportional to the number-fraction of molecules with that mass, you have $p_i = N_i / \sum_j N_j$, where N_i is the number of molecules with mass M_i. This gives you a number-average as

$$M_n = \sum_i p_i M_i = \sum_i \left(\frac{N_i}{\sum_j N_j} \right) M_i = \frac{\sum_i N_i M_i}{\sum_j N_j} \tag{B1.1.1}$$

This is just the arithmetic mean value. If one considers the probability of a molecular mass M_i occurring to be proportional to the weight-fraction of molecules with that mass, one needs to take $p_i = N_i M_i / \sum_j N_j M_j$. This yields the weight-average as

$$M_w = \sum_i p_i M_i = \sum_i \left(\frac{N_i M_i}{\sum_j N_j M_j} \right) M = \frac{\sum_i N_i M_i^2}{\sum_j N_j M_j} \tag{B1.1.2}$$

In most cases, the weight-average molecular weight is more suitable to characterize the weight of a distribution. This can be seen by the following example. Consider a sample that contains 9 mole of polymers with a molecular weight of 10 000 Da and 5 mole of polymers with a molecular weight of 50 000 Da. (The abbreviation Da stands for dalton, a synonym for atomic mass unit u.

It corresponds to 1/12 of the mass of an isolated ^{12}C-atom, that is, 1 Da = 1u = $1.66 \cdot 10^{-27}$ kg.) We find

$$\overline{M_n} = \frac{(9 \cdot 10\,000\,\mathrm{Da}) + (5 \cdot 50\,000\,\mathrm{Da})}{9+5} = 24\,286\,\mathrm{Da} \cong 24\,\mathrm{kDa} \quad \text{and}$$

$$\overline{M_w} = \frac{9 \cdot (10\,000\,\mathrm{Da})^2 + 5 \cdot (50\,000\,\mathrm{Da})^2}{(9 \cdot 10\,000\,\mathrm{Da}) + (5 \cdot 50\,000\,\mathrm{Da})} = 39\ \ 412\,\mathrm{Da} \cong 39\,\mathrm{kDa}$$

Since the sample contains 250 000 Da of polymers with a weight of 50 000 Da and only 90 000 Da of polymers with a molecular weight of 10 000 Da, the weight-average molecular weight of about 39 kDa seems more representative for the bulk of the material than the number-average of about 24 kDa. As an example, the distribution of molecular mass measured by gel permeation chromatography for the polymer MEH-PPV is shown in Figure B1.1.1 shows, along with the values for $\overline{M_n}$ and $\overline{M_w}$.

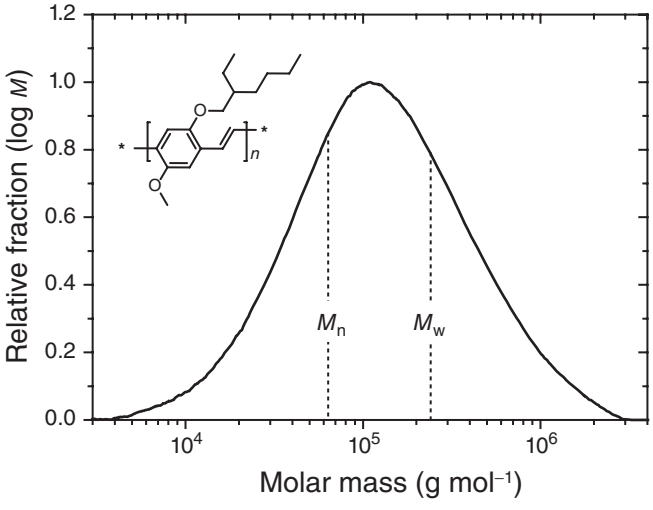

Figure B1.1.1 The distribution of molecular mass for a sample of the polymer MEH-PPV shown as inset. The weight-average molecular weight $\overline{M_w}$ of 234 000 and the number-average molecular weight $\overline{M_n}$ of 64 500 are indicated.

The spread of the distribution can be indicated by the *polydispersity index PDI*, defined as the ratio between the weight-average and the number-average

$$\mathrm{PDI} = \frac{\overline{M_w}}{\overline{M_n}} \tag{B1.1.3}$$

For the example above, $\mathrm{PDI} = 39/24 = 1.62$. Often one is interested in the number *n* of repeat units an average polymer chain contains. This is also called the *degree of polymerization DP*. It can be obtained by dividing the (weight-) average molecular weight of the polymer chain by the calculated weight of a single repeat unit.

Box 1.2 Polymer Structures and Their Names

By definition, a polymer is made up by a sequence of repeating units. There are, however, many ways how such as sequence can be arranged. If all repeat units are identical, they form a *homopolymer*, while *copolymers* are formed when different repeat units are joint. Scientists differentiate *alternating copolymers, statistical copolymers* and *block copolymers,* depending on whether the different repeat units follow in an alternating way, in a random way, or as blocks. For example, for two units A and B, the sequence … ABABABABABABABAB … defines an alternating copolymer, … ABBAABABBBAABAABBA … is a statistical copolymer, and … AAAAAAAABBBBBBBBBB … is a diblock copolymer.

In the majority of currently used semiconducting polymers, the electronically relevant part of the repeat unit forms part of the polymer backbone. They are referred to as *main chain polymers.* There are, however, also a number of *side chain polymers*, where the backbone is formed by electronically inert molecular sections, while the electronically active moiety is located in the side chain of the polymer. A few examples to polymer architectures are illustrated below (Figure B1.2.1).

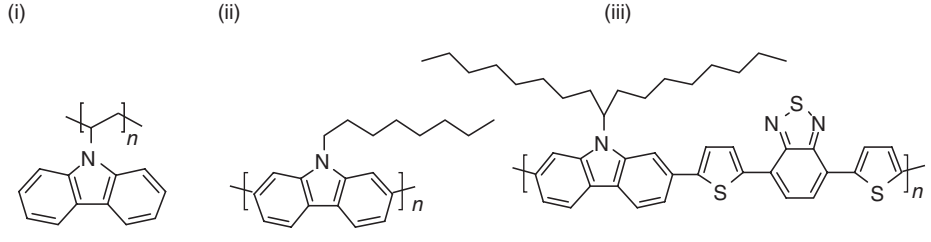

Side chain homopolymer (PVK) | Main chain homopolymer (P(2,7-carbazole)) | Alternating copolymer (PCDTBT)

Figure B1.2.1 The optically and electronically active unit carbazole is used to form (i) a sidechain polymer known as PVK (poly(vinylcarbazole)), (ii) a main chain polymer, and (iii) an alternating copolymer with a carbazole donor that is connected via thiophenes to a benzothiadiazole acceptor unit. This polymer is known as *PCDTBT*.

Semiconducting polymers frequently contain rings such as a phenyl ring. Such rings may be connected at different positions to form a chain. Chemists use the prefixes *para*, *meta*, and *ortho* to indicate at which relative positions two connections are made in a ring, and they abbreviate them by an italic minor letter *p*, *m*, or *o* in the chemical name. For example, if you number the six carbon atoms in a phenyl ring from 1 to 6, then the phenyl rings in a poly(*para*-phenylene) (or poly(*p*-phenylene)) are joint at carbon atom number 1 and 4, that is, opposite to each other. In a poly(*meta*-phenylene) (or poly(*m*-phenylene)) they are joint at carbon atoms 1 and 3, that is, there is one carbon atom in between the connecting ones, and a poly(*ortho*-phenylene) (or poly(*o*-phenylene)) is made by joining the rings at two adjacent carbons, that is, number 1 and 2. The para, meta, and ortho positions are indicated in Figure B1.2.2.

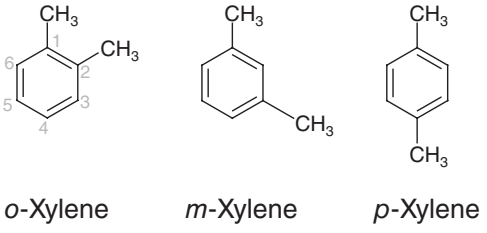

Figure B1.2.2 Substitution with two methyl groups (CH_3) renders a phenyl ring into xylene, also referred to as *dimethylbenzene*. The two methyl groups may be in ortho, meta, or para position with respect to each other, thus giving *o*-xylene (=1,2-dimethylbenzene), *m*-xylene (=1,3-dimethylbenzene), and *p*-xylene (1,4-dimethylbenzene), respectively. For *o*-xylene, the numbering of the carbon atoms is shown in gray.

For some polymer chains, the relative position of the side chain in a sequence can be relevant. For example, in a thiophene ring with the atomic positions numbered as shown below, the alkyl side chain may be attached at the position number 3 or 4. If the side chain is always at the same position (say 3), and the repeat units are always connected from position 2 on one ring unit to 5 on the next (called 2,5′ or *head-to-tail*), you end up with a structure where all side chains point in the same direction. This is a *regioregular* structure. Other combinations, for example, involving 2,2′ ("*head-to-head*") or 5,5′ ("*tail-to-tail*") connections lead to structures with irregular sidechain directions, referred to as *regiorandom* structure. It turns out that regioregular structures form more ordered film morphologies with improved charge carrier mobilities. A prototypical example is the polythiophene P3HT, which contains a hexyl group at the 3 position (Figure B1.2.3).

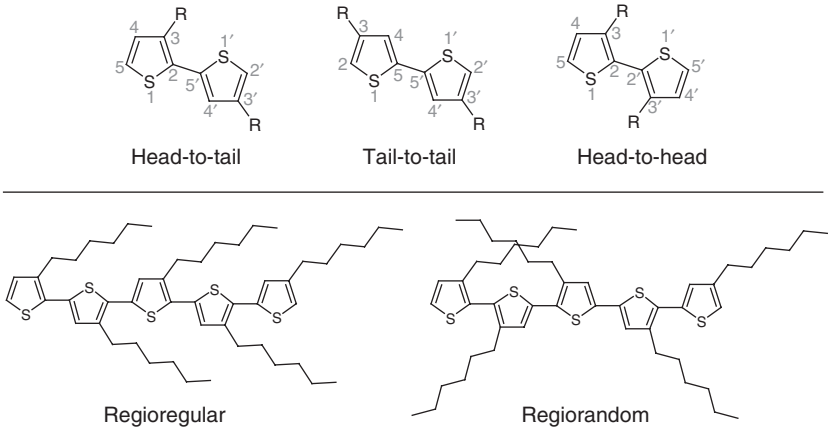

Figure B1.2.3 Thiophene rings may be connected (a) either head-to-tail, tail-to-tail, or head-to-head. The numbering of the atoms is shown in gray. (b) If all connections are head-to-tail, the resulting structure is regioregular, otherwise it is regiorandom.

The backbone of a semiconducting polymer is formed by a chain of carbon atoms with alternating single and double bonds. Aromatic and heteroaromatic rings may also form part of this structure.

The large majority of today's semiconducting polymers contain side chains that render them soluble in common organic solvents. The value of these side chains to the performance of polymer in a device is not always fully appreciated. Not only do they render the polymer soluble, but, equally important, they keep polymer chains at a certain distance from each other once they are deposited in a film, and sometimes they even control the relative orientation of polymer chains to each other. By this, the side chains control the degree of electronic interaction that can take place between polymer chains. Inter-chain interactions, however, determine the efficiency of luminescence that is the key feature in OLEDs [31, 32], and of charge-carrier generation in solar cell structures [33, 34] as well as the mobility of charge carriers in OFETS [35].

Thus, choosing suitable side chains for the monomer unit before proceeding with the polymerization reaction is an important step in the chemical synthesis. The side chains usually consist of a sequence of carbon atoms, joint by single bonds. To keep the structural representation clear, the hydrogen atoms that complement the structure are usually not drawn. If the carbon atoms are linked directly to the backbone, the generic term *alkyl chain* is used (and specified as methyl, ethyl, propyl, butyl, and so on if it contains 1, 2, 3, 4, or more carbon atoms), while the term *alkoxy chain* denotes a chain linked via an oxygen (and again counting methoxy, ethoxy, and so on for 1, 2, and more carbon atoms involved). These side chains may be linear or branched (Figure 1.6). The branched ones are more effective in suppressing inter-chain interactions [33, 36]. The first polymer on which electroluminescence was observed [10], PPV, does not contain any side chain. Thus, it is insoluble and has to be prepared by a precursor route involving a 4–12 h elimination step at temperatures of 220–300 °C, depending on the particular precursor type [37]. Apart from being a time-consuming and thus tiresome additional processing step, the thermal conversion tends to introduce chemical defects in the resulting film, thus adversely affecting the polymers optoelectronic properties. For this reason, the pioneer precursor-polymer PPV was soon replaced by the soluble derivative MEH-PPV. The ease of solution processing, and the associated options for processing including printing techniques is still a major advantage of soluble semiconducting polymers. Soluble polymers can also easily be combined with each other or with molecules such as C_{60}-derivatives to form a blend, a common practice for

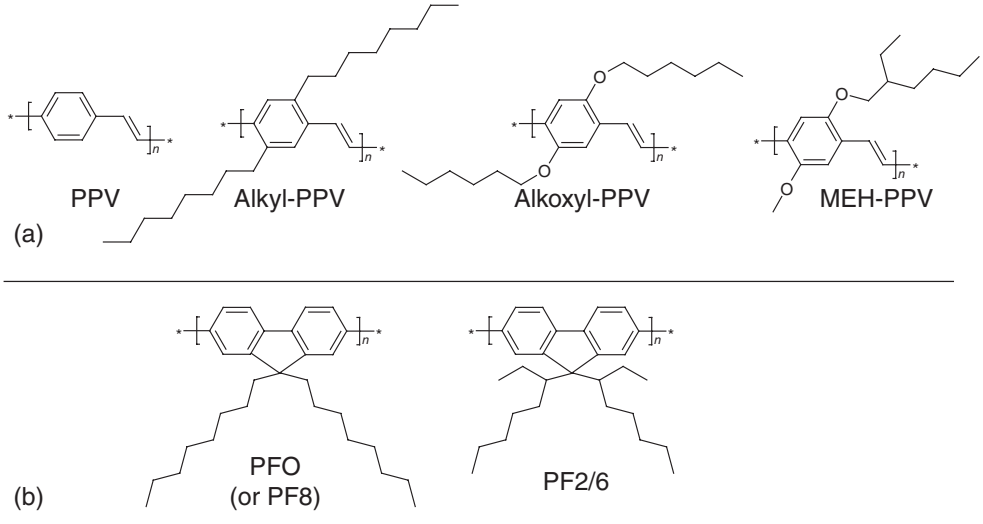

Figure 1.6 Examples for (a) poly(*p*-phenylene vinylene) (PPV) without sidechains, with linear alkyl sidechains, with linear alkoxy sidechains, and with branched, asymmetric alkoxy sidechains. (b) Polyfluorene (PF) with linear octyl sidechains and with branched, ethyl-heptyl side chains.

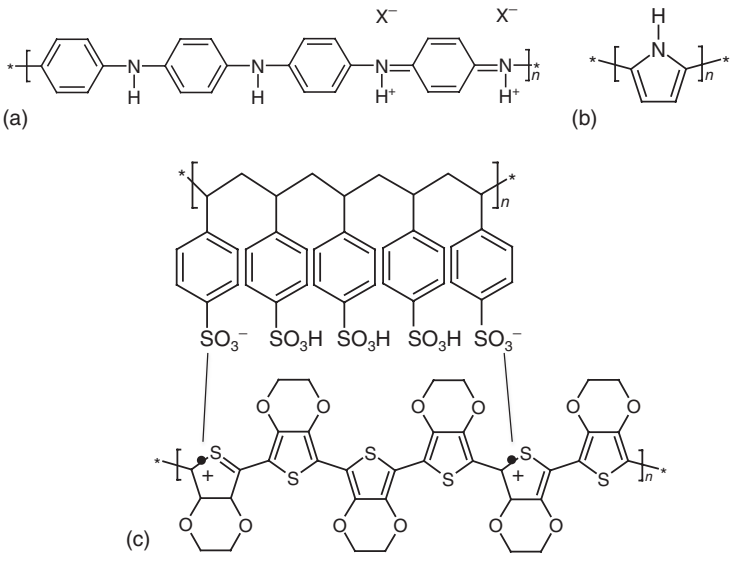

Figure 1.7 Selected conducting polymers. (a) polyaniline (PA). PA exists in different oxidation states and doped forms. The figure here shows the emeraldine salt of PA. For different forms, see MacDiarmid [50] and Smela *et al*. [51]. (b) Polypyrrole. (c) The mixture of PEDOT (bottom) with PSS (top), PEDOT:PSS.

solar cell applications. Multiple layers, however, are difficult to realize with soluble polymers, as it is difficult to deposit a second layer without redissolving the first one. Multiple layers may be realized by synthesizing polymers that are soluble in very different solvents, for example, a highly polar one like alcohol and a nonpolar one like toluene, or by rendering a polymer insoluble after deposition, for example, by chemical cross-linking [38–41]. We have already mentioned that any of the compounds discussed so far are intrinsically insulating in the sense that the intrinsic concentration of charge carriers at room temperature is negligible. Charges are provided extrinsically, for example, by charge injection from electrodes or doping; they are transported across the material and may, for example, result in luminescence. The terms *organic semiconductors* and *semiconducting polymers* are to be understood in this context.

A closely related class of materials that we shall not discuss further in this book are conducting polymers. A "semiconducting" (intrinsically insulating) polymer can become a truly conducting polymer when it is heavily doped as was demonstrated by Heeger, MacDiarmid, Shirakawa and their coworkers for the case of poly(acetylene) [15, 16]. For technological applications, for example, as antistatic, anticorrosive, or conducting paint, a persistent, high, and homogeneous level of doping is required. Conductivities up to a few hundred Siemens per centimeter can be reached for the conducting polymers poly(aniline), poly(pyrrole) and PEDOT:PSS (poly(3,4-ethylene dioxythiophene)–polystyrene sulfonic acid), a mixture of two polymers [42–48] (Figure 1.7). A basic introduction to conducting polymers, focused on PEDOT:PSS, can be found in [49].

1.2.4
Further Related Compounds

A group of compounds associated with organic semiconductors are fullerenes and carbon nanotubes.(Figure 1.8) Both types of macromolecules consist of a sheet of carbon atoms, joint to form six- and five-membered rings. When the sheet forms the surface of a sphere, it is called a *fullerene*. The most prominent fullerene, discovered by Kroto [52], contains 60 carbon atoms and is thus

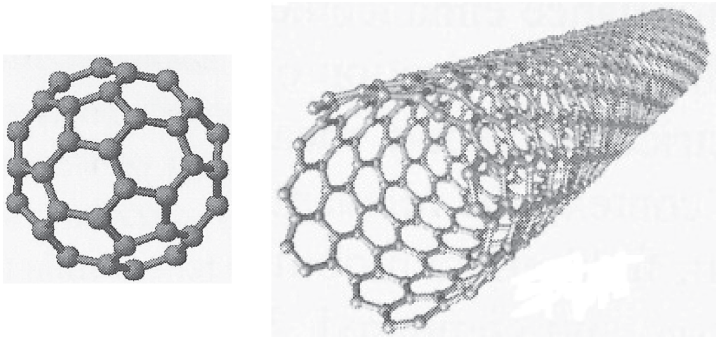

(a) (b)

Figure 1.8 (a) The fullerene C_{60} and (b) a single-wall carbon nanotube.

referred to as C_{60}, though other fullerenes (C_{70}, C_{76}, etc.) are also common. Nanotubes are formed when the sheet is rolled up to form a tube. Depending on the way how the sheet is rolled up, the resulting nanotube may have semiconducting or metallic properties. Nanotubes can be formed by rolling up only one sheet (single wall carbon nanotube) or several sheets (multiwall carbon nanotube). Fullerenes and nanotubes are sometimes employed as electron-accepting materials in organic solar cell applications. For a review on fullerenes and nanotubes, we refer the reader to [53–55].

Some molecular organic semiconductor materials can form liquid crystals (LCs), that is, they adopt a phase that is intermediate between solid and liquid in the sense that the molecules have some orientation as in a crystal yet they can move as in a liquid. The liquid-like behavior is obtained through long flexible side chains while the macroscopic orientation is caused by van-der-Waals interactions between stiff, flat, extended molecular cores. Depending on their orientation, there are different types of LCs. In the context of organic semiconductors, the most frequently encountered types are discotic LCs and nematic LCs. In the former, flat, disk-like molecules pile up to form a columnar stack, while in the latter the molecular axes are all aligned in roughly the same direction (Figure 1.9). The long-range orientational order provided by LCs is exploited in OFETs and organic solar cells where anisotropic and well coupled charge transport is desired. The physics of LCs is explained in dedicated textbooks on polymer or soft matter physics, for example, [56, 57].

1.2.5 A Comment on Synthetic Approaches

Any of the compounds used for a semiconductor application will be made in a synthetic laboratory by a certain synthesis route, and it will be given to the user after some form of purification. The method and care chosen for synthesis and purification will affect the defect levels in the sample, and thus the optoelectronic performance. While we cannot give a review on synthetic approaches, a few general comments may be made.

The synthesis of small molecules (where we use the term to refer to low molecular weight materials as opposed to polymers) is comparatively well controllable. In contrast to polymers, molecules can be purified to a high degree. Purification can also occur during sublimation and during crystallization, so that vacuum-deposited films and molecular crystals are frequently purer than amorphous films of the same molecule obtained by spin-coating.

The synthesis of polymers is elaborate and can lead to nominally the same products yet with some variation in the optoelectronic properties. It is therefore a good idea to be aware of the synthetic approach taken, even for those who try hard to avoid chemistry. First of all, polymerization usually requires the use of metal catalysts such as Pd or Ni. Traces of these metals may remain in the compound even after purification, and they can act as quenching sites to luminescence or as trapping sites

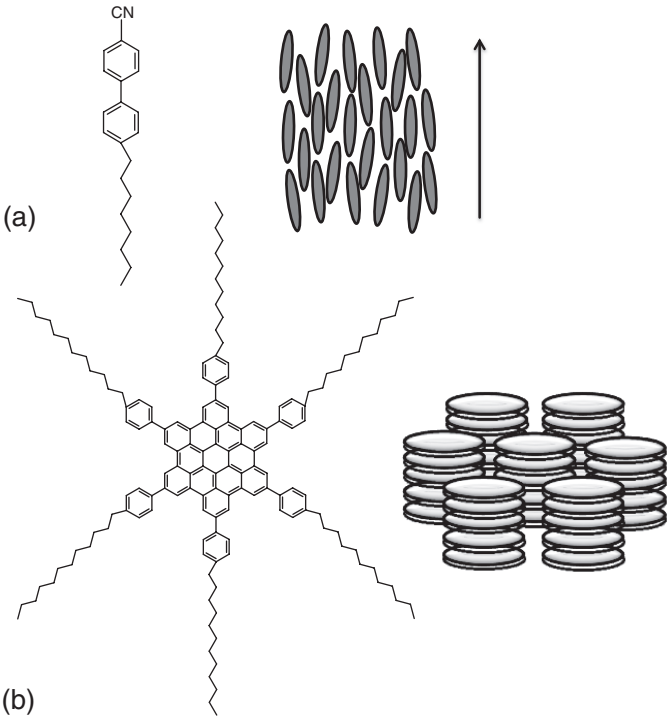

Figure 1.9 Chemical structure and orientation for (a) a nematic liquid crystal and (b) a discotic liquid crystal.

for charges. Second, most polymer synthesis relies on the coupling of monomer units in solution. This process results in a variety of chain length distributions and in a different number of unwanted short chains or branched chains. Purification of polymers requires some effort and skill. As a result, the purity of a compound can vary from batch to batch unless great effort is taken to provide a high level of constant batch-to-batch quality, as is the case for large commercial chemical companies.

Further, the monomeric units used for synthesis contain functional end groups that are reactive to allow for the polymerization reaction. Frequently these are bromines or other halogens. When the polymerization is completed, the polymer formed will have a bromine unit at either end. Such bromine end groups also trap charges and quench luminescence. This can be avoided by replacing the bromine end group by "end caps," for example, phenyl rings.

It is in the core interest of synthetic chemistry to control and improve the outcome of a reaction, and thus different routes provide end products of different quality. For example, when preparing the thiophene polymer P3HT, the regioregularity of the chain can be controlled by the synthetic route chosen, with the approach by McCullough and Lowe [58] giving a higher degree of regioregularity than earlier approaches [59]. Frequently encountered reactions for the preparation of semiconducting polymers include the Yamamoto-coupling [60] and the Suzuki-coupling [61]. In the Yamamoto-coupling, monomer units of the type Br – Ar – Br are connected by eliminating the bromine using Ni as a catalyst. Ar denotes any aromatic group that one wishes to employ as electronically active repeat unit. This reaction can only produce homopolymers or random copolymers. The Suzuki-coupling requires two differently functionalized monomers, $(HO)_2$B-Ar-B$(OH)_2$ and Br-Ar′-Br which are coupled using a Pd catalyst. If Ar and Ar′ are of a different structure, an alternating copolymer results. The Suzuki-coupling is particularly popular as it is comparatively mild, tolerates many functional groups,

and requires only small amounts of catalyst. For a good introduction to synthetic approaches, we recommend the chapters [62, 63].

1.3 Electronic States of a Molecule

1.3.1 Atomic Orbitals in Carbon

Organic semiconductor materials are carbon-based materials, so it is useful to know a little about the electronic structure of carbon. Atomic carbon in its ground state has six electrons, of which two are in a 1s orbital, two in a 2s orbital, and the remaining two in two of the three $2p_x$, $2p_y$, and $2p_z$-orbitals (Box 1.3). The way how electrons are distributed over orbitals is called a *configuration*, and the arrangement can be written as $(1s)^2(2s)^2(2p_x)^1(2p_y)^1(2p_z)^0$, or shorter $1s^2 2s^2 2p_x{}^1 2p_y{}^1$. In this configuration, carbon is only able to make two covalent bonds. If one of the 2s electrons were to move into the empty $2p_z$ orbital, the carbon atom could make four covalent bonds. It turns out that the binding energy gained from making four bonds exceeds the energy needed to promote an electron from the 2s orbital to the orbital $2p_z$. So this happens whenever carbon is not in its elementary atomic form.

Box 1.3 σ- and π-Orbitals

Depending on the angular momentum quantum number of the electrons, the atomic orbitals of carbon are referred to as *s and p-orbitals*, and they are associated with a spherical charge distribution centered around the atom (s-orbital) or with a "figure-of-eight" distribution (p-orbital). Analogously, the molecular orbitals are called *σ-orbitals* when the spatial probability density of the electrons is centered around the axis joining two atoms like a cylinder, and π-orbitals, when the electrons are most likely to be found above and below the line connecting two atoms (Figure B1.3.1).

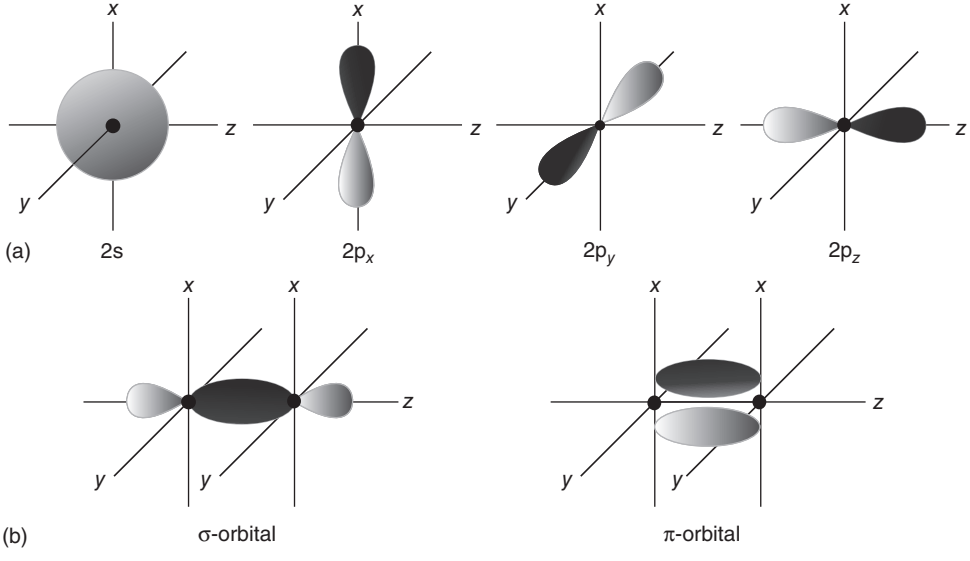

Figure B1.3.1 (a) The atomic s and p orbitals. (b) The molecular σ and π orbitals, formed from constructive overlap of two p_z and two p_x orbitals, respectively.

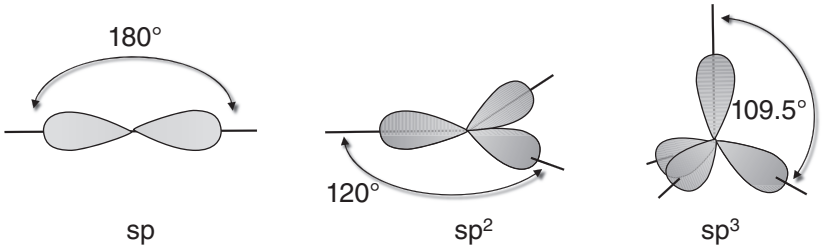

Figure 1.10 The sp, sp^2, and sp^3 hybrid orbitals.

When other atoms like hydrogen or another carbon approach as binding partners, the concomitant external forces compensate the energy difference between the 2s and the 2p orbitals, thus rendering them degenerate. As a result, new *hybrid orbitals* are formed from a linear combination of the 2s with the 2p orbitals (Figure 1.10). Chemists also refer to a combination of orbitals as a "mixing" of orbitals. There can be mixing between all 4 orbitals, between only three of them and between only 2 of them. When all 4 mix, that is, the one 2s and the three 2p orbitals, the resulting four orbitals are called $2sp^3$ orbitals (note a potential source of confusion – the superscript 3 now refers to the number of p-orbitals involved and not to the number of electrons in the orbital). All 4 orbitals being equivalent, they point into the 4 corners of a tetraeder, with an angle of 109.5° between them. This is the case, for example, when two carbon atoms form the molecule ethane (Figure 1.11). Three sp^2 hybrid orbitals are formed when the 2s orbital mixes with two 2p orbitals, say $2p_x$ and $2p_y$. The three orbitals are distributed in the *xy*-plane, with an angle of 120° between them. The remaining $2p_z$ orbital is orthogonal to that plane. This is the form taken by carbon in the molecule ethene, also known as *ethylene*. Finally, the mixing of the 2s orbital with only one 2p orbital results in two sp-hybrid orbitals at an angle of 180° from each other. Two sp-hybridized carbon atoms can join to form the molecule

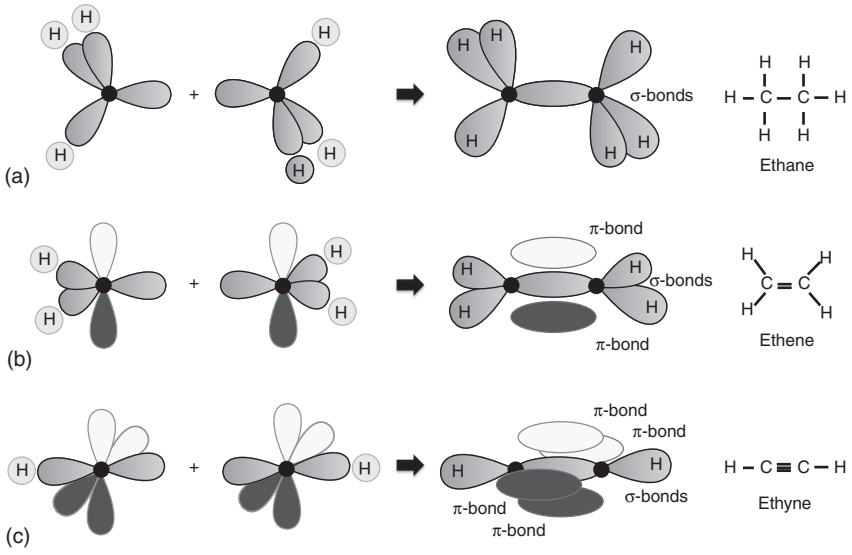

Figure 1.11 The combination (a) of six hydrogen atoms and two sp^3 hybridized carbon atoms to yield the molecule ethane, (b) of four hydrogen atoms and two sp^2 hybridized carbon atoms to give ethene (ethylene), and (c) of two hydrogen atoms and two sp hybridized carbon atoms to form ethyne (acetylene). The σ-bonds are shown in light gray, the two different phases of a π-bond are indicated by black and white color.

ethyne. An older name of ethyne is acetylene. A detailed description of hybridization can be found in any common textbook of physical chemistry or molecular physics [64, 65].

1.3.2 From Atomic Orbitals to Molecular Orbitals

The number of hybrid orbitals and remaining p-orbitals in a carbon atom determine the number of bonds it can form. A very simple yet still useful idea of the chemical bond is to think of it as a pair of electrons that are shared between two atoms. The electrons no longer belong to one atom, but they belong equally to the pair of atoms. As the electrons are now equally probable to be found orbiting around atom number 1 as around atom number 2, they can no longer be assigned to atomic orbitals, but they need to be associated with molecular orbitals.

Consider the ethane molecule, C_2H_6, shown in Figure 1.11. Each of the two carbon atoms has four valence electrons, one in each of the four $2sp^3$ hybrid orbitals. Such an electron may be paired with the electron from the 1s-orbital of a hydrogen, or with the electron in the other carbon's $2sp^3$ orbital. The resulting molecular orbital is called a *σ-orbital*, and the associated bond is correspondingly referred to as a *σ-bond*. Ethane is made up entirely from σ-bonds. Let's compare this to the ethene molecule, C_2H_4. Each carbon atom has three $2sp^2$ hybrid orbitals in a plane and one $2p_z$ orbital orthogonal to this plane. The sp^2 orbitals give rise to three σ-bonds, two of which are formed with hydrogens and one with the other carbon. The electron in the $2p_z$ orbital of one carbon atom will be paired with the electron in the other carbon's $2p_z$ orbital. Now the electrons will have spatial probability density above and below the molecular axis, and the molecular orbital is termed a *π-orbital*. This shared pair of electrons corresponds to a π-bond. Thus, the two carbon atoms in ethene are held together by *two* bonds, a π-bond due to overlapping atomic p_z orbitals and a σ-bond from overlapping atomic sp^3 orbitals. The carbon atoms in ethyne, finally, are joined by *three* bonds, that is one σ-bond and two π-bonds.

If we are interested in optical and electrical processes in organic molecules, we need to know not only that there are molecular orbitals, but also which energy they have. A molecular orbital may be approximated by a linear combination of atomic orbitals (LCAO). Consider, for example, the combination of two 1s orbitals, ϕ_a and ϕ_b, of two hydrogen atoms as the atoms approach. The resulting molecular σ-orbital may be written as $\psi_+ = c_1\phi_a + c_2\phi_b$, with c_1 and c_2 being positive numbers. This can be considered a constructive interference of the two electron wavefunctions. The enhanced charge density between the atomic nuclei associated with this orbital leads to a bonding character. The combination, $\psi_- = c_1\phi_a - c_2\phi_b$ is also possible and may be interpreted as a destructive interference with concomitantly reduced charge density between the nuclei. Since the repulsion between the nuclei is not screened by electron density, this orbital is also referred to as *anti-bonding*, and denoted with a star, as in 1s*. The energy levels associated with the two ways of superposition are different from the energies of ϕ_a or ϕ_b, with the orbital ψ_+ being at lower energy and ψ_- at higher. The energies can be calculated by considering the Schrödinger equation with the Hamilton operator being the sum of the kinetic and potential energy. It turns out that the energy is given by $E_+ = (\alpha + \beta)/(1 + S)$ for the constructive term and $E_- = (\alpha - \beta)/(1 - S)$ for the destructive one. S is the overlap integral, α is the Coulomb integral, and β is the resonance integral (also referred to as *exchange integral*). For the hydrogen-ion, they are given by $S = \int \phi_a\phi_b \mathrm{d}\tau$, $\alpha = \int \phi_a H \phi_a \mathrm{d}\tau$, and $\beta = \int \phi_a H \phi_b \mathrm{d}\tau$, where $\int \mathrm{d}\tau$ denotes the integral over space. The overlap integral is a measure of the extent to which the two orbitals located on different centers overlap, the Coulomb integral gives a measure for the Coulomb interaction of the electron on one nucleus with the other nucleus, and the resonance integral can be seen as expressing the interaction between a nucleus and the overlap of the two atomic orbitals located on different centers.(see also Box 1.4). As the resonance interaction between the two orbitals is essentially controlled by the resonance integral, this is also what largely determines the energy splitting between the two linear combinations of the two atomic orbitals. Assuming a small overlap

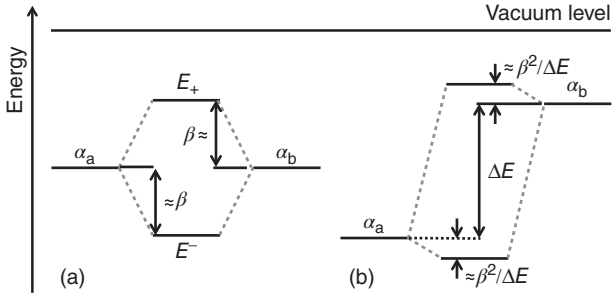

Figure 1.12 The splitting of two molecular orbitals with energies α_a and α_b due to resonance interaction for the case where the two orbitals (a) have the same energies and (b) when they have different energies. (After Atkins [64].)

integral S one finds $\Delta E = E_- - E_+ \approx 2\beta$. So far we considered the case that the two interacting orbitals ϕ_a and ϕ_b have the same energy. If they have different energies, the splitting caused by their interaction reduces. For small S, one finds $E_+ \approx \alpha_a - \beta^2/(\alpha_b - \alpha_a)$ and $E_- \approx \alpha_b + \beta^2/(\alpha_b - \alpha_a)$, implying that $\Delta E = E_- - E_+ \approx (\alpha_b - \alpha_a) + 2\beta(\beta/(\alpha_b - \alpha_a))$. Thus, with increasing difference between the orbitals, their resonance interaction vanishes. This is illustrated in Figure 1.12.

Box 1.4 The Energy Levels of the Hydrogen Ion

For a hydrogen ion, H_2^+, with two atoms a and b, the Hamiltonian consists of the sum of the kinetic energies and potential energies of the nuclei and the electron at a distance r_a and r_b from the two nuclei, which are separated by a distance R. It can be written as

$$H = -\frac{\hbar^2}{2m_e}\nabla^2 + \frac{e^2}{4\pi\varepsilon_0}\left(\frac{1}{R} - \frac{1}{r_a} - \frac{1}{r_b}\right) \tag{B1.4.1}$$

Using the atomic orbitals ϕ_a and ϕ_b, the Coulomb integral $\alpha = \int \phi_a H \phi_a \mathrm{d}\tau$ can be evaluated to give

$$\alpha = E_{1s} + \frac{e^2}{4\pi\varepsilon_0 R} - j', \quad \text{with} \quad j' = \frac{e^2}{4\pi\varepsilon_0}\int \phi_a^2 \left(\frac{1}{r_b}\right)\mathrm{d}\tau \tag{B1.4.2}$$

This j' term in the Coulomb integral corresponds to the total electrostatic energy of interaction between a charge distribution with a probability density ϕ_a^2 and the other nucleus b. Similarly, the resonance integral $\beta = \int \phi_a H \phi_b \mathrm{d}\tau$ can be evaluated to give

$$\beta = \left(E_{1s} + \frac{e^2}{4\pi\varepsilon_0}\right)S - k', \quad \text{with} \quad k' = \frac{e^2}{4\pi\varepsilon_0}\int \phi_a \left(\frac{1}{r_a}\right)\phi_b \mathrm{d}\tau \tag{B1.4.3}$$

The k' term in the resonance integral may be thought of as a representing the interaction of the overlap charge density $-e\phi_a\phi_b$ with the nucleus a. As a result, the two energies of the linear combination of the two atomic orbitals are given by

$$E_+ = E_{1s} + \frac{e^2}{4\pi\varepsilon_0 R} - \frac{j' + k'}{1 + S} \tag{B1.4.4a}$$

$$E_- = E_{1s} + \frac{e^2}{4\pi\varepsilon_0 R} - \frac{j' - k'}{1 + S} \tag{B1.4.4b}$$

that is, E_+ is always lower in energy than E_-, since j' and k' are both positive.

How does this help us now to get an idea on the energies of molecular orbitals? When we construct a molecular orbital as LCAOs, we need to take into account all atomic orbitals. However, to get a first qualitative idea about the energy of the resulting molecular orbitals, it is sufficient to consider only the mutual interaction of orbitals at equal or similar energy, as the contributions from orbitals of different energy is small. To get an idea about the energies of the molecular orbitals in ethene, for example, we consider the interaction of two 1s orbitals, two threefold degenerate $2sp^2$ hybrid orbitals and two $2p_z$ orbitals from the carbon atoms. The 1s orbitals are close to the core with negligible resonance interaction. They form a σ and a σ*-orbital with only little splitting between them. One of the three $2sp^2$ hybrid orbitals on each carbon points along their internuclear axis. Thus, there is a large amount of charge overlap located between the nuclei, leading to a large resonance integral with σ and a σ*-orbitals that are pushed far apart. In a similar way, strongly bonding σ and antibonding σ*-orbitals result from the interaction of the other two carbon $2sp^2$ hybrid orbitals with hydrogen 1s-orbitals. The interaction of the $2p_z$ orbitals, however, takes place at some distance from the nuclei, and thus results in a weaker splitting between the bonding π and anti-bonding π* orbital. Figure 1.13 illustrates this for the interaction between the carbon atoms. The carbon-hydrogen interaction is omitted for clarity of display.

Let us now consider which of the ethene orbitals are filled or empty. The carbon 1s-orbitals each contribute two electrons, that is, a total of four, which are accommodated in the σ and a σ*-orbitals, leading to (at first order) no net interaction. The three $2sp^2$ hybrid orbitals on each carbon contain three single electrons each. When they combine with the electron from the other carbon's $2sp^2$ hybrid orbital, or with the single electron of the hydrogen's 1s-orbital, the pair will fill the low-lying bonding σ-orbital yet leave the anti-bonding σ*-orbital at high energy empty, resulting in a strong net attractive interaction between the nuclei involved. Thus, the σ-bonds hold the molecule together. The two carbon $2p_z$ orbitals each contain one electron to be accommodated. They will fill the π-orbital, leaving the π* orbital empty. In contrast to the σ-orbital, the π-orbital contributes only little to the attractive force between the nuclei. This is a result of the fact that the overlap electron density is further away from the internuclear axis, and it is reflected in the lower splitting between π and π* orbitals compared to σ and σ*. The potential energy gained when placing two electrons in the molecular π-orbital instead of the parent atomic p_z-orbitals is correspondingly lower. In summary, for ethene, we find the highest occupied molecular orbital (HOMO) is a π-orbital. The next higher orbital is the π*-orbital, and it is empty. It is the lowest unoccupied molecular orbital (LUMO). Experimental techniques to measure the energy of the HOMO and LUMO shall be discussed in Chapter 2. Different approaches to calculating molecular orbitals are summarized in Box 1.5.

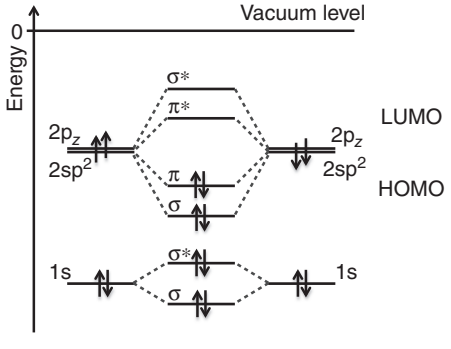

Figure 1.13 Simple energy level diagram illustrating the formation of σ and π bonds from atomic orbitals for ethene. Only orbitals involved in the carbon-carbon interaction are shown. The two $2sp^2$ hybrid orbitals forming σ-bonds with hydrogen atoms are omitted. (After Atkins [64].)

Box 1.5 Calculating Molecular Orbitals

Different Approaches

There are a number of different approaches to calculate molecular orbitals. Among the most frequently accounted ones are the Valence-bond (*VB*) method, the *LCAO*, Hückel-theory, intermediate neglect of differential overlap (*INDO*), and density functional theory (*DFT*) . The *VB method* dates back to the beginning of the twentieth century and introduced concepts such as the chemical bond as a shared pair of electrons. The more contemporary accounts of bonding are expressed in *molecular orbital theory*. The approach is to approximate molecular orbitals as LCAOs, thus also called *LCAO-method*. For large molecules, this can become demanding. In 1931, Erich Hückel noted that calculations become much simpler, yet give still reasonably accurate results, when one treats the π-orbitals separately from the σ-orbitals. This *Hückel-approximation* works for many hydrocarbons with valence electrons in π-orbitals. For molecules such as benzene or butadiene, it can be done in the framework of a student's course [66, 67]. Many further theoretical developments use the *Hartree–Fock approach*, where an initial wavefunction is guessed, used to solve the Hartree–Fock equation for the total energy, and the resulting improved wavefunction is used again for the same procedure in an iterative way, until the change to the previous calculation round is smaller than a predefined criterion. This procedure is called a *self-consistent field method*. When many of the integrals are estimated from spectroscopic data or physical properties such as ionization energies, the calculation is said to be *semi-empirical*. In contrast, in *ab initio methods*, all integrals are calculated without empirical input parameter. Today, ready-to-use software packages are commercially available with these methods implemented. In order to allow for a reasonable computation time, approximations are made. For example, integrals between orbitals that have very small overlap and that thus contribute little to the result are usually neglected. Depending on the degree of approximation, they are called *complete neglect of differential overlap* (*CNDO*) or *INDO*. A different, and increasingly popular technique for the calculation of molecular structure is *DFT*. Instead of considering the electron wavefunction ψ, DFT focuses on the electron density ρ. The energy of the molecule is written as a function of the electron density, which is itself a function of position. Mathematicians refer to the function of a function as a *functional*. The electron density is constructed from a superposition of "Kohn–Sham-orbitals." These orbitals are calculated from iteratively and self-consistently solved Kohn–Sham equations and are not to be confused with the common spatial electron orbitals. DFT theory has shown to be a powerful technique that is still being developed further.

Butadiene as a Worked Example

One of the simplest conjugated molecules for which the molecular energy levels can be calculated is butadiene, CH_2=CH–CH=CH_2, which has 4 sp^2-hybridized carbon atoms. The atoms' sp^2-orbitals associate to molecular σ orbitals that form the backbone of butadiene. Each of the 4 atoms further carries one p_z-orbital ϕ_i that can combine to result in 4 molecular π-orbitals. They can be calculated as LCAOs.

$$\psi_\pi = \sum_{i=1}^{4} c_i \phi_i \qquad \text{(B1.5.1)}$$

The contribution c_i of each p_z-orbital ϕ_i can be obtained from applying the *variational principle*. It says that an approximate solution ψ will solve the Schrödinger equation to give an energy eigenvalue $E = \int \psi^* H \psi \, d\tau / \int \psi^* \psi \, d\tau$ that is somewhat higher than the true eigenvalue that would be obtained with the exact solution. Thus, if the approximate solution is set up as a linear

combination

$$\psi = \sum_{i=1}^{m} c_i \phi_i, \quad i = 1, 2, \ldots, m \tag{B1.5.2}$$

Then the best coefficients c_i can be obtained by minimizing the expectation value of the energy with respect to the coefficients c_i, that is, by solving

$$\frac{\partial}{\partial c_i}\left(\int \psi^* H \psi \mathrm{d}\tau\right) = 0, \quad i = 1, 2, \ldots, m \tag{B1.5.3}$$

When Eq. (B1.5.2) is inserted into Eq. (B1.5.3), this leads to a set of linear equations

$$\begin{aligned}
&c_1(H_{11} - ES_{11}) + c_2(H_{12} - ES_{12}) + \cdots + c_m(H_{1m} - ES_{1m}) = 0\\
&c_1(H_{21} - ES_{21}) + c_2(H_{22} - ES_{22}) + \cdots + c_m(H_{2m} - ES_{2m}) = 0\\
&\vdots\\
&c_1(H_{m1} - ES_{m1}) + c_2(H_{m2} - ES_{m2}) + \cdots + c_m(H_{mm} - ES_{mm}) = 0
\end{aligned} \tag{B1.5.4}$$

with

$$H_{ij} = \int \phi_i^* H \phi_j \mathrm{d}\tau \text{ and } S_{ij} = \int \phi_i^* \phi_j \mathrm{d}\tau$$

Such a set of linear equations has a nontrivial solution when

$$|H_{ij} - ES_{ij}| = 0 \tag{B1.5.5}$$

Thus, solving Eq. (B1.5.5) gives m energies E_i, $i = 1, 2, \ldots, m$. Inserting them into Eq. (B1.5.4) allows calculating the c_i. Of course, this involves calculating all the H_{ij} and S_{ij}, yet since the ϕ_i are known, this is possible (at least numerically).

When the variational principle is applied to calculate the molecular π-orbitals of butadiene, it is convenient to use some approximations that Hückel once suggested (*Hückel-approximation*) and that work reasonably well for conjugated π-systems. This is

(I) For all overlap integrals, use $S_{ij} = 0$ and $S_{ii} = 1$.
(II) Let all diagonal elements of the Hamiltonian be identical, that is, $H_{ii} = \alpha$.
(III) Let all off-diagonal elements of the Hamiltonian be 0, except for nearest neighbors which are set to $H_{ij} = \beta$.

If we apply the Hückel approximation to Eq. (B1.5.5) for the case of butadiene, we obtain

$$\begin{vmatrix}
\alpha - E & \beta & & \\
\beta & \alpha - E & \beta & \\
 & \beta & \alpha - E & \beta \\
 & & \beta & \alpha - E
\end{vmatrix} = 0 \tag{B1.5.6}$$

Solving this gives $E_{1,4} = \alpha \pm 1.62$, $E_{2,3} = \alpha \pm 0.62$ for the four energies (note that $\beta < 0$). The four molecular π-orbitals are obtained as

$$\begin{aligned}
\psi_{\pi 4} &= 0.37\phi_1 - 0.60\phi_2 + 0.60\phi_3 - 0.37\phi_4\\
\psi_{\pi 3} &= 0.60\phi_1 - 0.37\phi_2 - 0.37\phi_3 + 0.60\phi_4\\
\psi_{\pi 2} &= 0.60\phi_1 + 0.37\phi_2 - 0.37\phi_3 - 0.60\phi_4\\
\psi_{\pi 1} &= 0.37\phi_1 + 0.60\phi_2 + 0.60\phi_3 + 0.37\phi_4
\end{aligned} \tag{B1.5.7}$$

These orbitals and their energies are indicated in Figure B1.5.1.

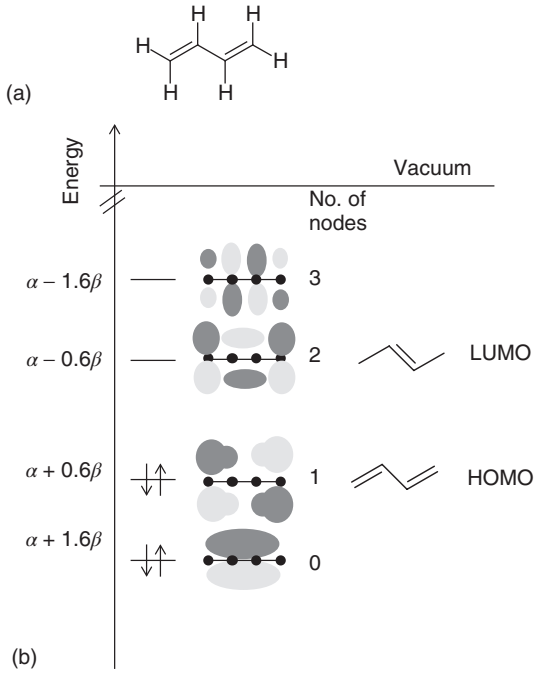

Figure B1.5.1 (a) The chemical structure of butadiene, explicitly showing the hydrogen atoms. (b) Schematic showing (from left to right) the energies of the four molecular π-orbitals of butadiene ($\alpha, \beta < 0$), their occupation with π-electrons, the orbital wavefunctions with light and dark gray indicating their sign, the number of nodes in the wavefunction, and the resulting sense of bond alternation for the HOMO and LUMO.

Since the block of filled orbitals ends with the HOMO and the sequence of unfilled ones starts with the LUMO, they are also called the *frontier orbitals*. They take a critical role in the optical and electrical processes of the molecule. When an electron is to be placed on a molecule, it will go into that empty orbital that is at the lowest energy, the LUMO. Similarly, the injection of a hole corresponds to taking an electron out of the highest occupied orbital, the HOMO and placing it in the electrode. Whether electron or hole injection can occur depends therefore on the relative HOMO and LUMO energy of the molecule in a solid film compared to the work function of the metal electrode (Figure 1.14). Because of the large resonance interaction involved, σ and σ* orbitals are at fairly low and high energies, rendering charge injection from electrodes into molecular solids very difficult. When the frontier orbitals are formed by π-orbitals, in contrast, their moderate amount of splitting implies a moderate energy difference to typical electrode work function. Similarly, in a simple picture, absorption of light takes place by promoting an electron from the HOMO to the LUMO. When the frontier orbitals are σ-orbitals, the $\sigma \rightarrow \sigma^*$ transition is in the ultraviolet spectral range, while the lower splitting associated with π-orbitals implies $\pi \rightarrow \pi^*$ transitions can take place in the visible spectral range, in particular for large π-orbitals that extend over several carbon atoms. Of course, this also applies to the light emission due to the transition of an electron from the LUMO to HOMO.

What is the key message to take away from this consideration of molecular orbitals? *The ability of a molecule to partake in electronic processes such as absorption and emission of visible light and such as charge injection from metal electrodes depends on the energy levels of the frontier orbitals.* It is the weaker splitting of π and π*-orbitals compared to σ and σ* orbitals that results in favorable energy

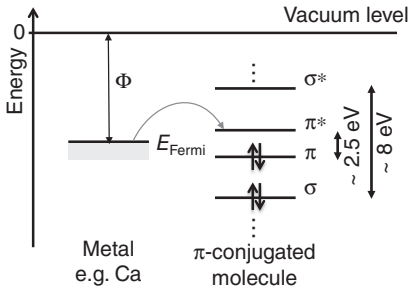

Figure 1.14 Illustration of approximate, typical energetic positions of the frontier orbitals in organic carbon-based molecules relative to metal work functions for the case of π-orbitals and for the case of σ-orbitals. HOMO–LUMO dominated transitions based on π and π* orbitals tend to be around 2.5 ± 0.5 eV, well suitable for absorption or emission in the visible spectral range. With the π*-LUMO located at about −2 eV and the π-HOMO at about −5 eV, injection of charges from suitable electrode materials, for example, calcium (workfunction of about 2.8 eV) for electron injection and indium-tin-oxide (ITO) (workfunction of about 4.8 eV) for hole injection, is possible. In contrast, if σ and σ* orbitals are the HOMO and LUMO, the optical transitions are in the vacuum-UV range, and charge injection from electrodes is impossible, with a σ*-LUMO close to the vacuum level, and a σ-HOMO typically near −8 eV.

levels and that thus renders a molecule suitable for organic semiconductor applications. In passing we note that when replacing carbon by either silicon or germanium, as realized in polysilylenes (polysilanes) or polygermylenes, the energy gap between the σ and σ* orbitals diminishes and the polymer films become p-type semiconductors [68, 69].

1.3.3 From Orbitals to States

How do we move conceptually from the molecular orbitals to the ground state and excited states of the molecule? When the molecular orbital $\psi = \sum_i c_i \phi_i$ is constructed as LCAOs ϕ_i, the coefficients c_i need to be determined by solving the Schrödinger equation $\hat{H}\psi = E\psi$ using the variational principle. Considering the nuclei as static, the Hamiltonian should contain the kinetic energy of each electron and the potential energies due to (i) the repulsion between the nuclei, (ii) the interaction between the electrons and the nuclei, and (iii) the interaction between the different electrons (electron–electron correlation). As this cannot be solved analytically for more than one electron (because the electrons are moving), one considers the hypothetical case of a molecule with only *one* electron. The potential energy of the other electrons is approximated by some mean field. The molecular orbitals thus obtained are *one-electron* orbitals. One can calculate the energy of the one-electron orbitals, as outlined in the previous section, and fill them with the number of electrons that happen to be part of the molecule. The associated many-electron wavefunction, corresponding to the ground state of the molecule, is then formed by the product of the molecular one-electron orbitals. $\Psi = \prod_i \psi_i$. Note that in doing so, one has ignored any interaction between electrons, and this is a very rough approximation.

One way to obtain an excited state energy that includes electron-correlation effects is to compose the excited state as a linear combination of different configurations. This is called *configuration interaction* (*CI*). The term *configuration* denotes the way how electrons are distributed over the molecular orbitals. For example, one particular configuration is that all electrons are pairwise in the lowest possible orbitals. In this case, the molecule has the lowest possible energy, so this is the configuration of the ground state. Other configurations may be that there is only one electron in the HOMO, and another electron in the LUMO, or in the orbital above the LUMO (called LUMO+1), or in the

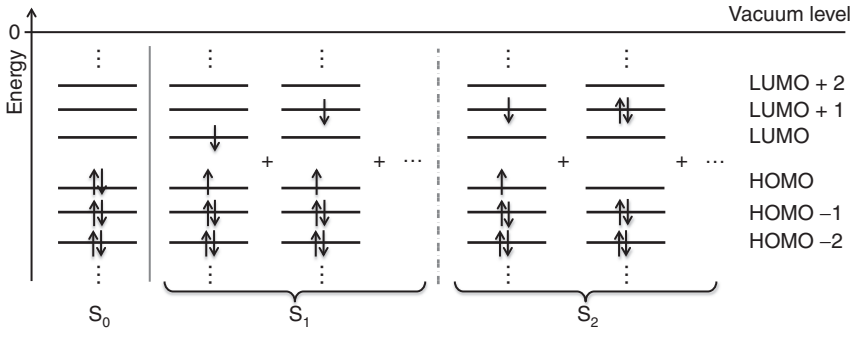

Figure 1.15 Illustration of configuration interaction. The configuration associated with the ground state S_0 is shown, as well as configurations that may contribute, to different degrees, to the first excited state S_1 and to the second excited state S_2. While several contributing configurations are shown here, it is common practice to only depict the dominating configuration for each state.

LUMO+2. Alternatively, the HOMO may contain two electrons, but the orbital below contains only one electron, and the LUMO contains another. It is easy to see that many different configurations are possible. If there were no electron–electron interactions, the configuration with one electron each in HOMO and LUMO would appropriately describe the excited state in terms of energy and wavefunction. However, as there are interactions between electrons, the nature of the excited state in a molecule is not well described by a single arrangement of electrons in one-electron orbitals. A better approximation is obtained by a superposition of different configurations. This is illustrated in Figure 1.15. For many organic molecules one finds that the first excited state can be well described by a superposition containing a predominant contribution, say 80–95%, of the configuration with one electron in the HOMO, one in the LUMO. The remaining contributions are then frequently made up from configurations containing single excitations such as "one electron in HOMO, none in LUMO, one in LUMO+1" (illustrated for S_1 in Figure 1.15), or "one electron in HOMO-1, two in HOMO, one in LUMO," and so on, or containing double excitations such as "no electron in HOMO, no electron in LUMO, two electrons in LUMO+1" (illustrated for S_2 in Figure 1.15). The composition needed for a good approximation of the next highest excited state is then usually made up by several configurations with different weights.

When discussing molecules, it is important to distinguish between orbitals, configurations, and states. This is different from the case of atoms containing only one electron that is discussed in introductory lectures on atomic physics or quantum mechanics. For a single-electron atom, the state of the atom is indeed defined by the orbital the one electron occupies, and thus the two terms may be used synonymously. The important distinction between orbitals, configurations, and states can also be seen by considering the configuration with one electron in the HOMO and one electron in the LUMO. The two single electrons may have a parallel spin or an antiparallel spin. The configuration of the molecule, that is, the number of electrons in the one-electron molecular orbitals, is the same in both cases. However, the spin-parallel and spin-antiparallel case correspond to different excited states of the molecule, with different energies and different overall wavefunctions. As detailed further below, the spin-anti-parallel case corresponds to a spin-singlet excited state, the spin-parallel case yields a spin-triplet excited state, which is at lower energy.

When drawing an energy diagram, care needs to be taken to be clear whether the diagram shows (one-electron) orbitals, or (many-electron) states. Electrons in orbitals are bound to the nuclei, so orbital energies are below the vacuum energy at 0 eV. The energy of a HOMO may be at −5 eV, the energy of a LUMO could be at −2.5 eV. Even if there are only HOMO and LUMO drawn, there will be molecular orbitals at energies below and above. In such an orbital picture, it is usually not possible to indicate effects due to electron–electron interactions, such as the effects of electron spin or of Coulomb attraction. Different from this is a state picture. The lowest possible state of a molecule,

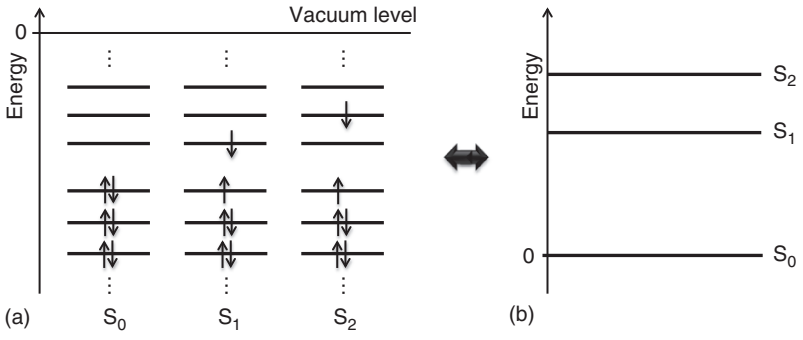

Figure 1.16 The singlet states S_0, S_1, and S_2 represented (a) in an orbital diagram, showing the one-electron orbital energies for the dominant configuration and (b) in a state diagram, showing the relative energies of the molecular electronic state.

the ground state, serves as a reference and is therefore arbitrarily set to zero. The energies of excited states have positive values above zero. There may be many excited states above the ground state, but there are none below it. The different energies of spin-singlet and spin-triplet states can readily be indicated. Figure 1.16 compares an orbital picture and a state picture for singlet states.

We finally add a few comments on the difference between orbitals and states that may appear trivial, but that may help to avoid occasionally encountered misconceptions.

(I) It is not possible to draw a meaningful diagram that contains both orbitals and states. In particular, when comparing the energies of orbitals with the work functions of metals in order to explain the operation of an OLED, it is a good idea to refrain from the occasional temptation to indicate the relative position of singlet and triplet states. Similarly, it is difficult to indicate the Coulomb energy that exists between the electron in the LUMO and the missing electron in the HOMO, that is, the hole, in a reasonable quantitative way.

(II) When an electron is promoted from a HOMO to LUMO, the molecule changes from being in a configuration yielding the ground state to a configuration that dominates the excited state. Thus, the HOMO → LUMO transition of the electron results in the transition of the molecule from the ground to the excited state. However, the HOMO itself is not a ground state, and a LUMO is not an excited state. They are (one-electron) orbitals.

(III) The energy difference between HOMO and LUMO is, in fact, only a very rough approximation for the energy difference between the ground state and the excited state. It ignores any electron–electron interactions such as the coulomb attraction between the additional electron in the LUMO and the missing electron (=hole) in the HOMO, or the relative spin of the two electrons.

(IV) Keep in mind that the molecular orbital picture is based on one-electron orbitals and that it neglects electron correlation effects. The energies calculated for HOMO and LUMO on this (one-electron) basis deviate from the energy experimentally needed to remove an electron from a real, previously neutral (many-electron) molecule or to add an electron to a neutral molecule. By the way, the energy to remove an electron from a neutral molecule, thus creating a molecular cation, is called *ionization potential* (*IP*), while the term *electron affinity* (*EA*) is used for the energy gained when placing an electron onto a neutral molecule, thus creating a molecular anion. The IP and the EA may be experimentally determined by cyclovoltammetry or photoemission spectroscopy.

(V) From points (II) to (IV) it follows that the (calculated) one-electron energies for HOMO and LUMO differ from the IP and EA derived experimentally (cf. Ref. [70]). Note that in the field it has become a common though misleading practice to employ the terms *HOMO* and *LUMO* as convenient approximation for IP and EA. Further, the energy difference between the molecule

in the ground state and excited state that can be read of absorption or emission spectra, does not correspond to the energy difference between HOMO and LUMO (cf. Section 2.4.4.3). Thus, the common procedure of measuring the IP by cyclovoltammetry, associating it with the HOMO, and then adding the excited state energy observed in the optical spectra yields an energy that one may nominally associate with a LUMO energy, but that is only a poor approximation for the energy level of an additional electron in a real molecule. This is because neither the coulomb-binding energy nor energy differences due to the relative spins of electrons are taken into account. Further, it is not considered that the energy levels of the electrons in a molecule change as soon as another electron is brought in or taken out or moved around. Accurately describing the electronic state of a molecule including electron correlation effects is one of the current challenges in quantum chemistry.

1.3.4 Singlet and Triplet States

So far our description concerning the electronic states of a molecule focused on the wavefunction of its electrons. This *electronic wavefunction* is a function of the electron's spatial coordinates and the positions of the nuclei. The square of the electronic wavefunction tells us the probability of finding an electron at a particular point in space for a fixed position of the nuclei. We have already indicated that this is not sufficient for a complete description of the molecule's state. For example, we need to also consider the spin the electrons have. This can be done by introducing a *spin wavefunction* that is a function of the electron's spin. The spin of a state is given by the total spin of all electrons in all orbitals, yet the electrons in filled orbitals are paired with anti-parallel spins and so contribute zero to the total spin. It is therefore sufficient to consider the unpaired electrons of an excited state configuration, usually one electron in a π^*-orbital and one in a π-orbital. To clarify the terminology, we refer to a singlet (triplet) state when the spin of electron in the π^* orbital and that of the remaining electron in the π-orbital are antiparallel (parallel) and so add up to a total spin of zero (one) in units of $\hbar$, and we number excited states in energetic order, that is, S_1, S_2, or T_1, T_2, and so on, for the energetically lowest or second lowest singlet or triplet excited state. There are also other, more sophisticated terminologies in use (see Box 1.6). Spin angular momentum is a vectorial quantity that couples according to the rules of quantum mechanics. The unpaired electrons in the π^* and the π orbital that comprise the configuration dominating the excited state form a two-particle system. From quantum mechanics, we know that two particles with spin angular momentum have simultaneous eigenstates to $\widehat{\boldsymbol{S}}^2$ and $\widehat{S}_z$, with eigenvalues S and M_s, where $\widehat{\boldsymbol{S}}$ is the spin angular momentum operator, and $\widehat{S}_z$ denotes its z-component. There are four such eigenstates of the two-particle-system. The wavefunction of an electron can be written as the product of the electronic wavefunction that depends only on the electron's spatial coordinates and of a spin wavefunction Ψ_{spin} that is a function of the electron's spin. When α and β denote the spin wavefunctions of the one-electron states with eigenvalues $s = 1/2$, $m_s = 1/2$ and $s = -1/2$, $m_s = -1/2$, the spin wavefunctions of the four eigenstates to the two particle system can be written as

$$\begin{aligned}
&\Psi_{\text{spin,T+}} = \alpha_1\alpha_2, && \text{yielding } S = 1 \text{ and } M_s = 1\\
&\Psi_{\text{spin,T0}} = \frac{1}{\sqrt{2}}(\alpha_1\beta_2 + \beta_1\alpha_2), && \text{yielding } S = 1 \text{ and } M_s = 0\\
&\Psi_{\text{spin,T-}} = \beta_1\beta_2 && \text{yielding } S = 1 \text{ and } M_s = -1\\
&\Psi_{\text{spin,S}} = \frac{1}{\sqrt{2}}(\alpha_1\beta_2 - \beta_1\alpha_2) && \text{yielding } S = 0 \text{ and } M_s = 0
\end{aligned} \tag{1.1a}$$

The index 1 and 2 on α and β refer to electron 1 and 2. The first three spin wavefunctions with $S = 1$ only differ in the z-component of the spin, which takes the eigenvalues $M_s = 1, 0, -1$. This

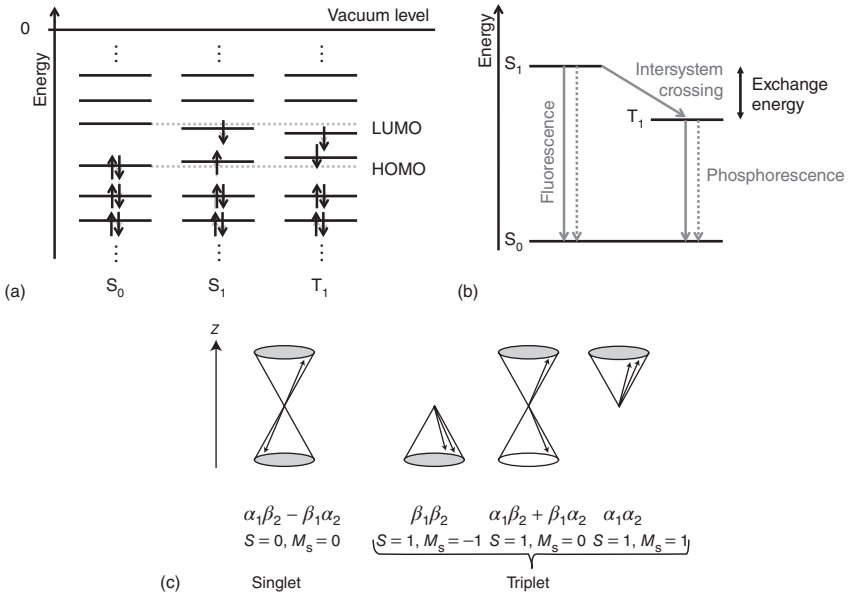

Figure 1.17 Singlet and triplet states. (a) Singlet and triplet states in an orbital configuration scheme. The arrows indicate the electron spin, the horizontal gray line is a guide to the eye. In this representation, Coulomb and exchange energies are explicitly included in the positions of the frontier orbitals. For the triplet state, only one spin configuration is shown. (b) Singlet and triplet states in a state diagram. Solid and dotted lines represent radiative and nonradiative decay channels, respectively. (c) Singlet and triplet states as a vector diagram illustrating the relative orientations of the two electron spins for the singlet and the triplet state. The two spins, indicated by arrows, process around a local magnetic field in *z*-direction. The antiparallel and 180° out of phase configuration corresponds to the situation in a singlet state, while the other three in phase configurations yield a triplet state. The corresponding spin wavefunctions and the eigenvalues of S and M_s are also given.

arrangement is therefore called a *triplet*. The fourth wavefunction with $S = 0$ has only a single possible value of the *z*-component, that is $M_s = 0$ and is therefore referred to as *singlet*. A vectorial representation is given in Figure 1.17, along with a representation in terms of molecular orbitals and in a state picture. Note that for the triplet wavefunctions, the spins are always in phase, while they are 180° out of phase for the singlet state. The energies of the first singlet and triplet state differ by the exchange energy, which is twice the value of the exchange integral. To a first order approximation, the exchange interaction scales exponentially with the overlap of the respective electron wavefunctions. If the wavefunctions of the electron in the HOMO and that in the LUMO overlap significantly, this results in a large exchange energy in the order of 0.7 – 1.0 eV. Smaller exchange energies, in the range of 0.2 – 0.5 eV, occur in molecules where HOMO and LUMO are located on different parts of the molecule.

Box 1.6 Nomenclatures

In molecular spectroscopy, the excited states are sometimes labeled by a symbol denoting how the excited state wavefunction transforms with respect to the symmetry group of the molecular Hamiltonian. The notations are derived from group theory. It turns out that in a system with an even number of π-electrons the ground state is always totally symmetric (under any symmetry operation) and is designated as ^1A_g. Capital letters like A or B specify the symmetry of the state

according to the transformations laid out in group theory [66, 67]. The subscript g defines the parity of the state. A "g" indicates that the state is *gerade* under spatial inversion as opposed to "u" (*ungerade*). In optical absorption, it is a necessary yet not sufficient condition for a transition being allowed that the parity changes, for example, from g to u and vice versa. This is a consequence of the fact that a photon has an angular momentum of $\hbar$ that is added or removed upon photon absorption or emission. By this token, a g → g transition can only occur via an intermediate – real or virtual – u state, for example, by two-photon absorption. Similarly, luminescence can take place only from an "ungerade" to a "gerade" state. For example, the ground state S_0, and the first and second singlet excited states S_1 and S_2 are 1^1A_g, 1^1B_u, and 2^1A_g, respectively, for luminescent polymers such as MEH-PPV. In contrast for nonluminescent polymers such as polyacetylene, S_0, S_1, and S_2 are 1^1A_g, 2^1A_g, and 1^1B_u, respectively. The luminescence is precluded by S_0 and S_1 having the same parity. The superscript 1 designates that the state is a singlet state with spin 0. For a triplet state with spin 1, the superscript would be 3. Thus, the first excited triplet state is, for example, 1^3B_u.

The commonly encountered eigenstates in Eq. (1.1a) are only well defined when a magnetic field exists that defines the z-direction. Without a magnetic field, $\widehat{S}_z$ cannot be defined, implying that M_s is not a good quantum number. In the absence of a magnetic field, four linearly independent and orthonormal spin eigenstates of a two-particle-system are given by [12]

$$\begin{aligned}
\Psi_{\text{spin,T}x} &= \frac{1}{\sqrt{2}}(\beta_1\beta_2 + \alpha_1\alpha_2)\\
\Psi_{\text{spin,T}z} &= \frac{1}{\sqrt{2}}(\alpha_1\beta_2 + \beta_1\alpha_2)\\
\Psi_{\text{spin,T}y} &= \frac{i}{\sqrt{2}}(\beta_1\beta_2 + \alpha_1\alpha_2)\\
\Psi_{\text{spin,S}} &= \frac{1}{\sqrt{2}}(\alpha_1\beta_2 - \beta_1\alpha_2)
\end{aligned} \tag{1.1b}$$

They are eigenstates to $\widehat{\boldsymbol{S}}^2$ with eigenvalue $S = 0$ or 1, and to the $\widehat{S}_u$ component (u = x, y, or z) of the spin angular momentum operator with the eigenvalue 0, that is, $\widehat{S}_u\Psi_{\text{spin,T}u} = 0$. The total spin is thus oriented in the $u = 0$ plane.

Even in the absence of a magnetic field, the three triplet sublevels are not degenerate. Rather, they are separated by a small energy, the *zero-field splitting*, that tends to be in the order of 0.1 cm^{-1} (=10 μeV) for hydrocarbon-type molecules (Box 1.7).

Box 1.7 The Zero-Field Splitting

The zero-field splitting between the triplet substates is caused by the interaction of the two spins with each other, for example, dipole–dipole coupling of the magnetic moments of the two electrons [71]. In organometallic complexes such as $Ir(ppy)_3$, the zero-field splitting increases by a factor of 10–100 compared to purely organic compounds, depending on how much the wavefunctions of the heavy metal contribute to the HOMO and LUMO [72]. The increased zero-field splitting in organometallic complexes arises from the spin–orbit coupling, induced by the heavy transition metal (cf. Section 1.4.3.3 below), that allows that the electrons' orbital angular momenta to also contribute to the splitting.

The magnitude of the zero-field splitting becomes relevant when radiative transitions from the triplet state to the singlet ground state are considered. Since the different triplet sublevels differ

in their spin–orbit coupling, they also differ in their radiative decay rate. At room temperature, all three sublevels are usually equally populated so that phosphorescence occurs from the level that has the highest oscillator strength. This is no longer granted at low temperature, for example, below 10 K for a level splitting of 1 meV.

When the molecule is exposed to an external magnetic field, the triplet levels split further apart due to the Zeeman effect (Figure B1.7.1).

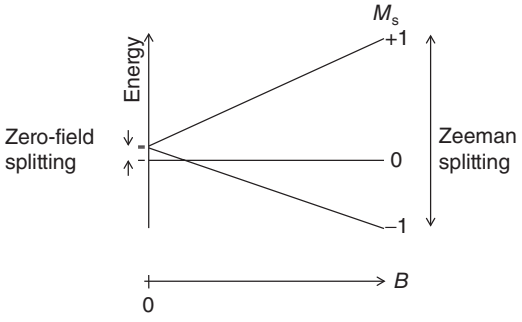

Figure B1.7.1 The zero-field splitting and the Zeeman splitting of the triplet state.

In order to preserve the Pauli exclusion principle, the symmetric spin wavefunctions of the triplet state are always combined with an antisymmetric electronic wavefunction, while the converse is the case for the singlet state. A more detailed introduction to the quantum mechanical description of singlet and triplet excited states in molecules can be found in common textbooks on molecular quantum mechanics such as the ones by Atkins [64] or by Haken and Wolf [71]. For experimental results on triplet states organic molecules, we refer to the book by Schwoerer and Wolf [12]. A detailed description of the nature of triplet states in organic semiconductors, how they are generated, which processes they may engage in during their lifetime, and how they decay is given in a dedicated review article [73].

1.4
Transitions between Molecular States

1.4.1
The Potential Energy Curve

Up to now, we have considered the atomic nuclei in the molecule to be stationary, and we have considered the ground and excited state energies with the nuclei in a particular fixed positions R_i. When the energy of the molecule is calculated for many different positions of the nuclei, one obtains an energy surface. There is a different potential energy surface for each state of the molecule. Next we need to consider that nuclei in real molecules are not stationary. Rather, they oscillate around their equilibrium position with a certain vibrational frequency ω and associated vibrational energy $(n + (1/2))\hbar\omega$, where n denotes the number of excited quanta. For low vibrational energies, the potential that the nuclei experience is approximated as a harmonic oscillator potential. The vibrational motion of the nuclei may be described by a separate nuclear vibrational wavefunction Ψ_{vib}. The total wavefunction Ψ_{total} of a molecular state can then be approximated by the product of the (many-electron) electronic wavefunction Ψ_{el}, the spin wavefunction Ψ_{spin} and the vibrational wavefunction Ψ_{vib},

$$\Psi_{total} = \Psi_{el}\Psi_{spin}\Psi_{vib} \tag{1.2}$$

The electronic wavefunction $\Psi_{el}(\mathbf{r_i}, \mathbf{R_i})$ depends on the positions $\mathbf{r_i}$ of the electrons and on the positions $\mathbf{R_i}$ of the nuclei. The overall spin wavefunction $\Psi_{spin}(\alpha_i, \beta_i)$ is expressed in terms of the electrons' individual spin wavefunctions α_i and β_i, and the vibrational wavefunction $\Psi_{vib}(\mathbf{R_i})$ is a function of the nuclei's positions $\mathbf{R_i}$. The squares of the wavefunctions, $|\Psi|^2$ give the probability of finding the electrons, their spins, and the nuclei at a particular point in space. The part of the total wavefunction that contains only spatial coordinates, that is, the product of the electronic and vibrational wavefunction, $\Psi_{el}\Psi_{vib}$, is also referred to as *spatial wavefunction*. For a fixed position of the nuclei, it is identical to the electronic wavefunction.

Remember that the many-electron (electronic) wavefunction Ψ_{el}, may be approximated by the product of the one-electron wavefunctions ψ, which, in turn, are approximated by the linear combination of atomic electron wavefunction. Just for reference and clarity, we list them here.

$$\Psi_{el} = \prod_i \psi_i \tag{1.3}$$

$$\psi_i = \sum_j c_j \phi_j$$

Approximating an overall wavefunction by a product of wavefunctions works as long as there is no significant interaction between them. With regard to the electronic and nuclear wavefunctions, this is fulfilled in many cases – for example, during the process of light absorption and emission – since electrons move fast compared to nuclei due to their large difference in mass. Theoreticians refer to this approximation of the wavefunction as the *Born–Oppenheimer approximation*, while the term *Franck–Condon principle* is used for underlying phenomenon. This approximation breaks down when there is significant interaction between the electrons and the vibrations (vibronic coupling). Note that as a result of the Born–Oppenheimer approximation, potential energy surfaces do not cross.

When the different atoms constituting the molecule oscillate, they form a system of coupled oscillators. Analogous to the mechanical equivalent system of pendula coupled by springs, such a system of coupled oscillators is mathematically best treated by defining a set of normal mode coordinates Q_i from the nuclear coordinates R_i. Note that in an organic semiconducting molecule, there are many normal modes. When you take a slice through the potential energy surface along a normal mode coordinate Q_i, the energy of the vibrational quanta for that mode can be indicated by horizontal lines, and labeled *0*, *1*, *2*, and so on (Figure 1.18). This energy is typically given in wavenumbers $\tilde{\nu}$, that is, in

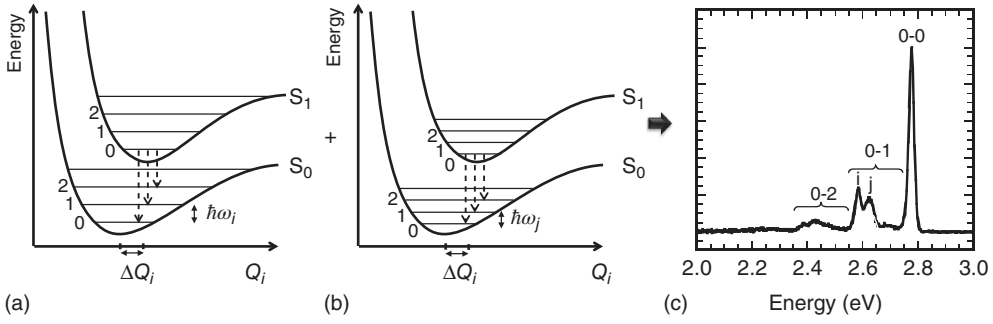

Figure 1.18 Curves of potential energy of a molecule as a function of the displacement (a) in the normal mode coordinate Q_i and (b) in the normal mode coordinate Q_j. The energies of vibrational excitations with quanta $\hbar\omega_i$ and $\hbar\omega_j$ are also indicated, and the vibrational levels are labeled with 0, 1, 2. (c) The emission spectrum of polyfluorene, taken in a thin film at 10 K. The 0-0 electronic transition is indicated, as well as the 0-1 and 0-2 transitions for modes *i* and *j*. For polyfluorene, the higher energy mode *i* is a phenyl ring stretching mode at 1605 cm^{-1} (198 meV), and the lower energy mode *j* at 1282 cm^{-1} (158 meV) can largely be associated with a mode consisting of a C–C stretching motion coupled to a C–H bending.

units of cm^{-1} (see Box 1.8). The energies of the different vibrational modes can be observed directly by Raman spectroscopy or, sometimes, by Fourier transform infrared spectroscopy (FTIR) spectroscopy (see Box 1.9), and they are reflected in the absorption and fluorescence spectra. Typical normal mode vibrations that occur in the organic molecules discussed in this book are C=C stretching modes, C–C stretching modes, C–H in-plane bending modes, and torsions of the phenyl ring.

Figure 1.18 above shows how the potential energies associated with a molecular ground state and excited state depend on a normal mode coordinate Q_i, also referred to as *configuration coordinate*. As the nuclei approach, the resonance interaction between the atomic orbitals takes place, as outlined above, and it reduces the total energy of the molecular state. Repulsive interactions due to the Pauli exclusion principle raise the energy for very small internuclear distances, and in between, a minimum is formed. The functional form of the associated potential is analogous to the Morse potential for a diatomic molecule with interatomic distance R and equilibrium distance R_0, which is $V(R) = D[1 - e^{-\alpha(R-R_0)}]^2$. D is the dissociation energy, that is, the potential energy if both atoms do not interact ($R = \infty$), and α is a measure for the strength of the interaction between the two nuclei. As the nuclei approach from $R > R_0$, the total energy reduces until the minimum value $V(R_0) = 0$ is obtained at the equilibrium distance R_0. For small values of R, that is, $\alpha|R - R_0| \ll 1$, the exponential function can be developed, so that $V(R) \approx D[1 - (1 - \alpha(R - R_0))]^2$, that is, $V(R) \approx D\alpha^2(R - R_0)^2$. Thus, near the equilibrium position, the potential can be approximated as a harmonic oscillator potential. For small internuclear distances, the exponential term in the Morse potential dominates, that is, $V(R) \approx De^{-2\alpha(R-R_0)}$ for $R < R_0$, and the potential raises steeply due to the Pauli exclusion principle. Of course, such a potential energy curve exists and can be calculated not only for the ground state, but also for the excited states of the molecules.

Optical transitions take place between the ground and excited state potential energy curves as detailed in the next section. On top of the electronic energies, the vibrational energy levels need to be added. They are indicated as horizontal lines and numbered 0, 1, 2, and so on. Rotational levels are usually omitted, since for organic molecules, the spectra are typically broader than the splitting of the rotational energy levels, even for gas phase spectroscopy. When an optical transition takes place, such as an absorption or emission, it can occur to different vibrational levels for different normal modes. This is illustrated in Figure 1.18 for two different normal coordinates, Q_i, and Q_j, though in a real molecule, there are many more. The resulting emission spectrum arises from a superposition of these different transitions. If the spectra are sufficiently well resolved, the different normal modes and their overtones can be identified separately, as shown in Figure 1.18 and in Box 1.9. If the spectra are broadened, often only one *effective mode* with a mean energy can be seen. The mathematical formalism for this superposition is discussed in Section 1.4.2 and is known as a *Franck–Condon-Progression*

Box 1.8 Wavelengths, Wavenumbers, and Energy Conversion Units

When measuring absorption or fluorescence, it is natural to be interested in the color of the light absorbed or emitted. This information is contained in absorption and emission spectra that are given as a function of the light's wavelength λ. When thinking about electronic processes, it is often more useful to know the energy

$$E = h\nu = \frac{hc}{\lambda} = hc\tilde{\nu} \tag{B1.8.1}$$

of the light's photons that are absorbed or emitted. Here h is Planck's constant $h = 6.626 \times 10^{-34}$ J s, c is the speed of light in vacuum, $c = 2.997 \times 10^8$ m s^{-1}, and

$$\tilde{\nu} = \frac{1}{\lambda} = \frac{E}{hc} \tag{B1.8.2}$$

is the wavenumber, usually given in units of cm^{-1}. The wavenumber is thus proportional to the photon energy, with 1 eV = 8066 cm^{-1}. If one is interested in color, displaying spectra against

wavelength gives most information. If one needs the photon energy, the spectra are most usefully displayed against wavenumbers (in per centimeter) or photon energy (in electron volts). When comparing against the properties of molecules, such as bond energies, it is helpful to know that 1 eV = 23 kcal mol^{-1}. To convert from wavelength to energy, use $E(\mathrm{eV}) = 1239/\lambda(\mathrm{nm})$. For example, a wavelength of 620 nm corresponds to $1239/620\,\mathrm{eV} = 2.0\,\mathrm{eV}$. By the way, 1 kJ mol^{-1} corresponds to 10.4 meV mol^{-1}. It is useful to have a few approximate reference numbers in mind (or on a notice board), such as the following (Table B1.8.1).

Table B1.8.1 Approximate reference values for wavelengths and energies.

Color/vibrational mode	λ	Energy	$\tilde{\nu}$(cm^{-1})	kcal mol^{-1}
Blue	400 nm	3.1 eV	25 000	71
Green	500 nm	2.5 eV	20 000	57
Red	600 nm	2.1 eV	16 666	47
Phenyl ring torsions [74, 75]	138 μm	9 meV	70	0.2
C–C stretching mode	8.3 μm	150 meV	1 200	3.5
C=C stretching mode	6.2 μm	200 meV	1 600	4.6
C≡C stretching mode	4.8 μm	260 meV	2 100	6.0
C–H stretching mode	3.3 μm	380 meV	3 000	8.7

When converting an absorption spectrum taken in wavelength to an energy scale, one simply needs to convert the abscissae from wavelength to energy by dividing 1239 by the wavelength in nanometer. This works because the absorption or extinction coefficients yield a relative quantity, which is the ratio of the absorbed to the incident intensity, I/I_0. In contrast, when a luminescence spectrum is taken, a detector measures the number of photons emitted from the sample per time interval and, most importantly, per wavelength interval $\mathrm{d}\lambda$. To convert a spectrum $u(\lambda)\mathrm{d}\lambda$ into a spectrum $u(E)\mathrm{d}E$, one needs to consider that $E = hc/\lambda$ results in $\mathrm{d}E = -(hc/\lambda^2)\mathrm{d}\lambda$, implying that $u(E)\mathrm{d}E = -hc(u(\lambda)/E^2)\mathrm{d}\lambda$. In words, one needs to take the intensity taken in wavelength steps and divide it by the square of the photon energy (at each wavelength), before plotting it against an energy scale. Be aware that this procedure is not always followed in the literature. Frequently, only the wavelength scale is changed to an energy scale, yet the spectral intensity is left unaltered.

Box 1.9 Raman and FTIR Spectroscopy

One of the processes that can happen when light interacts with a molecule is that the incident photon gets scattered. Some of this scattering incidents will happen without change in the photon energy (*Rayleigh scattering*) yet some of it may involve a change in the photon's energy (*Raman scattering*). The photon will either transfer energy to a vibrational mode of the molecule or take up a vibrational energy quantum from it. By measuring the scattered photon's energy and comparing it to the incident photon energy, one can obtain the energy of the vibrational mode. The energy difference between incident and scattered energy is referred to as *Raman shift*. Today, Raman measurements are typically done using commercial table-top spectrometers, often combined with a microscope. Laser light of a wavelength well below the optical gap (to avoid a fluorescence background) is directed onto the sample, and the scattered light is collected and dispersed by a monochromator. This is quick and efficient, yet the spectrometers are frequently limited to minimum Raman shifts around 500 cm^{-1}. Accessing smaller Raman shifts, for example, to detect torsional modes, requires the use of a dedicated set-up with large monochromators.

In a classical description of the scattering process, the incident electromagnetic light wave causes the electron cloud of the molecule to oscillate (thereby absorbing the incident photon) and then to emit a "new" photon, thus ceasing to oscillate. For a rigid molecule, the electrical dipole μ induced by the incident electromagnetic wave $E = E_0 \cos(\omega_0 t)$ is simply given by

$$\mu = \alpha E = \alpha E_0 \cos(\omega_0 t) \tag{B1.9.1}$$

implying that the electron oscillates with the frequency of the incident photon. α is the polarizability of the molecule. It is a measure for the ease by which the electron cloud can be polarized. For a molecule vibrating with frequency ω_R, however, the polarizability changes periodically with the change in the normal mode coordinate $Q = Q_0 \cos(\omega_R t)$. This can be taken into account by using a Taylor expansion of α around $Q = 0$,

$$\alpha = \alpha_0 + \left(\frac{\partial \alpha}{\partial Q}\right)_{Q=0} \cdot Q + \cdots \tag{B1.9.2}$$

and inserting this into Eq. (B1.9.1) to yield

$$\mu = \left[\alpha_0 + \left(\frac{\partial \alpha}{\partial Q}\right)_{Q=0} \cdot Q_0 \cos(\omega_R t)\right] E_0 \cos(\omega_0 t) \tag{B1.9.3}$$

This expression can be rearranged as

$$\begin{aligned}\mu = {} & \alpha_0 E_0 \cos(\omega_0 t) + \frac{1}{2}\left(\frac{\partial \alpha}{\partial Q}\right)_{Q=0} \cdot Q_0 E_0 \cos((\omega_0 - \omega_R)t) \\ & + \frac{1}{2}\left(\frac{\partial \alpha}{\partial Q}\right)_{Q=0} \cdot Q_0 E_0 \cos((\omega_0 + \omega_R)t)\end{aligned} \tag{B1.9.4}$$

The first term in Eq. (B1.9.4) describes the resonant scattering process, that is, Rayleigh scattering. The second and third term in the induced dipole moment lead to Raman scattering, with photon frequencies below that of the incident photon (Stokes lines) or above (Anti-Stokes lines). One can show [76] that the intensity of the scattered light depends quadratically on the change of polarizability with normal mode displacement.

$$I \propto I_0 (\omega_0 - \omega_R)^4 \left(\frac{\partial \alpha}{\partial Q}\right)^2 \tag{B1.9.5}$$

What is this good for? Equations (B1.9.4) and (B1.9.5) show, that the occurrence of Raman scattering requires a change in molecular polarizability upon vibration. In organic semiconductors, the electrons that contribute most to the molecular polarizability are the ones in the conjugated π and π^* frontier orbitals as they are only weakly bound and well delocalized. Raman spectroscopy therefore yields the frequencies of those vibrational modes that couple particularly well to the π-conjugated system. One experimentally finds that the modes that feature intensely in a Raman spectrum are also the modes that contribute to the vibrational progression in the luminescence spectra.

The energies of vibrational modes can also be measured by infrared absorption spectroscopy which probes the transition between vibrational levels. The common technique is *FTIR absorption spectroscopy*, where an interferometer setup is used to record the data, which are subsequently Fourier transformed to give the spectrum [77]. Whereas Raman spectroscopy requires a change in polarizability upon vibration, FTIR spectroscopy needs a change in dipole moment. The latter is not directly linked to the conjugated π-system of the molecule, so FTIR spectra give little information relating to the electronic structure. While selection rules for Raman and for FTIR spectra are complementary for centrosymmetric molecules in the gas phase, the symmetry requirements are usually not fulfilled in a strict manner for amorphous films of organic molecules or polymers.

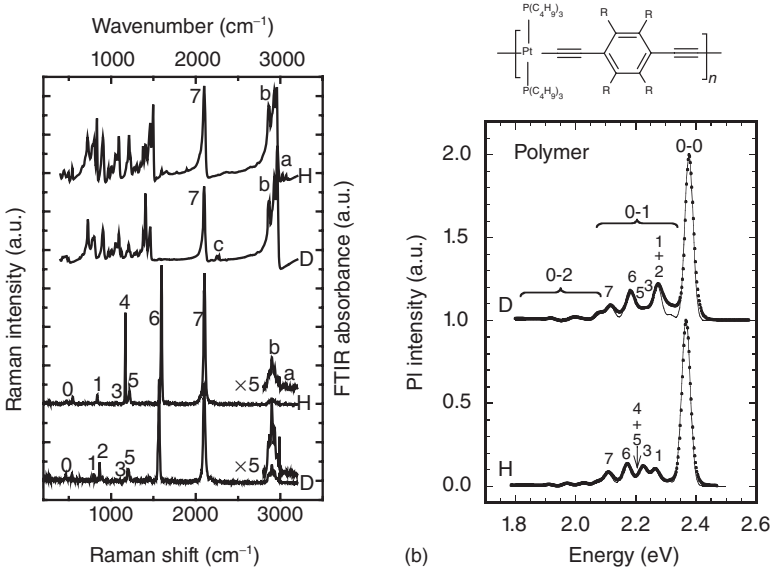

Vibrational modes *i* and assignment		Wavenumber (cm^{-1})	Energy (meV)
0	Pt–C stretch	470	61
1	C–C–C quadrant in plane stretch	840	104
2	C–D in plane bend on Benzene ring	860	107
3	Not assigned	1055	131
4	C–H in plane bend on Benzene ring	1170	145
5	C–C/C=C stretch in Benzene ring	1200	148
6	Benzene breathing mode	1600	198
7	C≡C stretch	2100	260
a	C–H Stretch on Benzene ring	3050	378
b	C–H stretch on the alkyl side chains	2900	360
c	C–D Stretch on Benzene ring	2255	280

(c)

Figure B1.9.1 (a) FTIR and Raman spectra for the Pt-polymer shown in (b), with R = H and with R = D. (Data from Khan [80].) (b) Phosphorescence spectra of the Pt-polymer (dotted line) along with a Franck–Condon fit using the vibrational modes listed in (c). For the 0-1 vibrational overtone, the position of the different modes are indicated. (Data from Khan [80].) (c) Assignment and energies of the different vibrational modes. (From Khan, Köhler *et al*. [80, 81].)

Figure B1.9.1a shows FTIR and Raman spectra taken for two Pt-containing polymers, one with hydrogen atoms attached to the phenyl ring, labeled H, and one with them being replaced by deuterium atoms ("D"). The frequency ω_R of a vibration is related to the reduced mass μ of the vibrating atoms by $\omega_R = \sqrt{k/\mu}$, with k being the force constant of the vibrating bond. Approximating the C–H stretching mode as diatomic molecule, $\mu = m_C m_H/(m_C + m_H)$, with m_C and m_H being the atomic masses of carbon and hydrogen, respectively. Substituting hydrogen by deuterium reduces the energy of the vibration by a factor of 0.74 (the *isotope effect*). From Figure B1.9.1 one can observe:

- Except for the C≡C stretching bond vibration, the intensities of the Raman and FTIR signals are complementary.
- In the FTIR signal, the C–H stretching vibration on the phenyl ring, denoted by "a," disappears upon deuteration and the corresponding C–D mode appears at lower energy, denoted "c." Similarly, in the Raman signal, the C–H in plane bending vibration "4" is replaced by the lower energy C–D in plane bending mode "2."
- The modes visible in the Raman spectra match the energies of the vibrational peaks in the phosphorescence spectrum.

The modes featuring prominently in the Raman spectra are listed and assigned in the table in Figure B1.9.1c. They have been used to model the phosphorescence spectra of Figure B1.9.1b by using Eq. (1.17a). In the figure, the 0-0, 0-1, and 0-2 vibrational transitions are indicated. For the 0-1 transition, the energetic position of the modes used is also indicated through the numbers.

1.4.2 Radiative Transitions: Absorption and Emission

The intensity of light absorption (emission), I, depends on the number n of photons absorbed (emitted) per second per molecule (mathematically, $I \propto \mathrm{d}n/\mathrm{d}t$). This is expressed by the rate of the transition, k. It is the number of transition events that take place per second ($k = \mathrm{d}n/\mathrm{d}t$), that is, for an absorption process k_{abs} is the number of photons absorbed per second. Similarly, for emission, the radiative decay rate k_{r} is the number of photons emitted per second.

The absorption of light increases the total energy of the molecule, while emission decreases it. In terms of quantum mechanics, this means a corresponding term needs to be added to the Hamiltonian of the molecule. For the case of light absorption or emission, a suitable operator is the electric dipole operator $e\hat{\boldsymbol{r}}$. Now new wavefunctions are required that are eigenfunctions to this operator, and the eigenvalues should correspond to the energy of the molecule in the excited state. If a new term $\hat{H}'$ is added to a Hamiltonian $\hat{H}_0$ to give $\hat{H} = \hat{H}_0 + \hat{H}'$, and this changes the original Hamiltonian $\hat{H}_0$ only a little, it is reasonable to assume that the wavefunction and eigenvalues also change only by a small amount. One can then calculate the new wavefunction and eigenvalues by the quantum mechanical approach of perturbation theory. Theoreticians have derived an expression that tells us how the rate of the transition k_{if} between an initial state Ψ_{i} and a final state Ψ_{f} depends on the perturbing Hamiltonian $\hat{H}'$ that causes the transition. Because it is so useful, it is called *Fermi's golden rule*. It says

$$k_{\mathrm{if}} = \frac{2\pi}{\hbar}|\langle\Psi_{\mathrm{f}}|\hat{H}'|\Psi_{\mathrm{i}}\rangle|^2\rho \tag{1.4}$$

ρ is the density of the final states. If we insert the molecular wavefunction $\Psi_{\mathrm{total}} = \Psi_{\mathrm{el}}\Psi_{\mathrm{spin}}\Psi_{\mathrm{vib}}$ into this expression and use the dipole operator, $e\hat{\boldsymbol{r}}$, for the perturbing Hamiltonian, we obtain

$$k_{\mathrm{if}} = \frac{2\pi}{\hbar}|\langle\Psi_{\mathrm{el,f}}\Psi_{\mathrm{vib,f}}\Psi_{\mathrm{spin,f}}|e\hat{\boldsymbol{r}}|\Psi_{\mathrm{el,i}}\Psi_{\mathrm{vib,i}}\Psi_{\mathrm{spin,i}}\rangle|^2\rho \tag{1.5}$$

The dipole operator acts only on the electronic wavefunction $\Psi_{\mathrm{el}}(\mathbf{r_i}, \mathbf{R_i})$. Physically, the incident electromagnetic wave with its time-dependent electrical dipole causes only the electrons to move in resonance. The nuclei are too heavy to respond on the time scale of the oscillations, and the spins are not affected by the changing electric field. The spins would only be affected by the changing magnetic field of the electromagnetic wave, but this is too small in magnitude to have any effect. The spin wavefunction $\Psi_{\mathrm{spin}}(\alpha_i, \beta_i)$ and the vibrational wavefunction $\Psi_{\mathrm{vib}}(\mathbf{R_i})$ are thus insensitive to the dipole operator. They can therefore be treated like constant factors, leading to the expression.

$$k_{\mathrm{if}} = \frac{2\pi}{\hbar}\rho|\langle\Psi_{\mathrm{el,f}}|e\hat{\boldsymbol{r}}|\Psi_{\mathrm{el,i}}\rangle|^2|\langle\Psi_{\mathrm{vib,f}}|\Psi_{\mathrm{vib,i}}\rangle|^2|\langle\Psi_{\mathrm{spin,f}}|\Psi_{\mathrm{spin,i}}\rangle|^2 \tag{1.6}$$

From this we see that the rate of an optical transition, and consequently also the macroscopic intensity of absorption or emission, depends on three factors that we shall now consider in turn. Note that when any of these factors is zero, the transition is said to be forbidden.

1.4.2.1 The Electronic Factor

Let us first turn to the integral $\langle \Psi_{el,f} | e\hat{\mathbf{r}} | \Psi_{el,i} \rangle$. If this expression is different from zero, the transition is said to be dipole-allowed, otherwise it is dipole-forbidden. Note that the dipole operator is of an odd symmetry under spatial inversion. The ground state wavefunction of most molecules transforms in the same manner as the identity representation A_g, that is, is of an even parity. If the excited state wavefunction was also of an even parity, the integral would vanish. It will yield finite values only if the excited state wavefunction has an odd parity, that is, the transition is from a *gerade* state to an *ungerade* state (see Box 1.6). Further, one can see that the value of the integral scales with the overlap of the initial and final state wavefunctions. Rates between orbitals that are centered on the same parts of the molecules (e.g., $\pi-\pi^*$ transitions) will thus be larger than rates between orbitals that

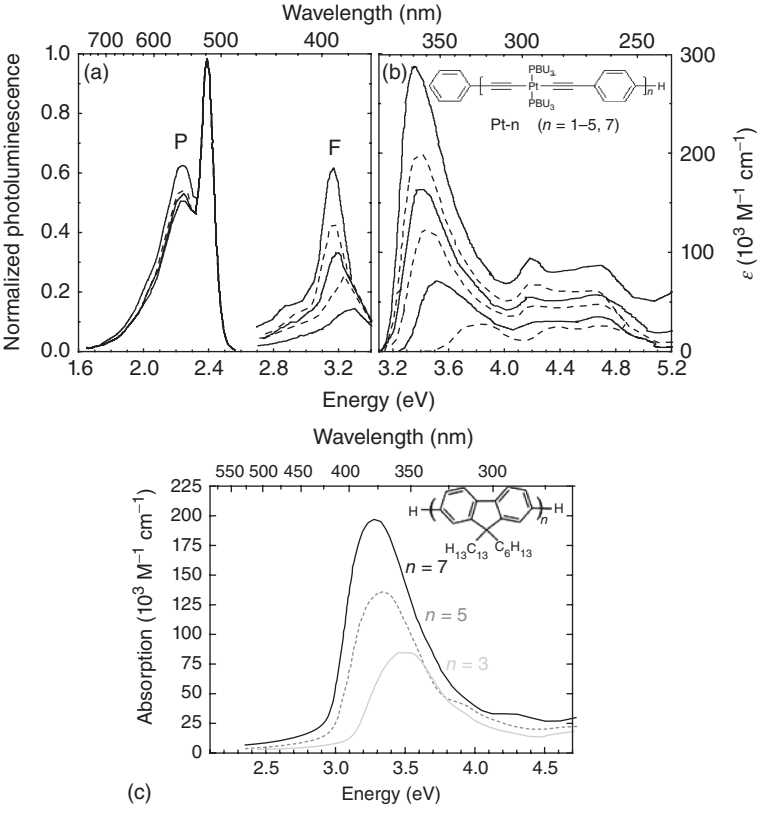

Figure 1.19 The intensity of optical transitions as a function of oligomer length. (a) The photoluminescence spectra of the Pt-containing phenylene ethylene shown in deoxygenated THF solution. F is the fluorescence, P is the phosphorescence. The fluorescence intensity is magnified by 100× as compared to the phosphorescence. The spectra are Pt-2, Pt-3, Pt-4, Pt-5, Pt-7 in order of increasing intensity for F and in order of decreasing intensity in the 0-1 band in P. (Data from Liu *et al*. [78].) (b) The absorption spectra in THF solution. In order of increasing intensity Pt-1, Pt-2, Pt-3, Pt-4, Pt-5, Pt-7. (Data from Liu *et al*. [78].) (c) The absorption spectra of a fluorene trimer, pentamer, and heptamer. (Data from Albuquerque *et al*. [79].)

occupy different spaces (e.g., charge-transfer (CT) transitions, n–π* transitions or metal-to-ligand charge transfer (MLCT transitions – see Box 1.10). Similarly, the integral will scale with the value of the transition dipole moment e**r**, that is, it will be large if the orbitals involved are not only well overlapping but also well extended (and the transition dipole moment is along the molecular axis). For example, the absorption and fluorescence intensity from conjugated oligomers is well known to increase with oligomer length. Figure 1.19 illustrates this for the absorption and emission of the delocalized S_1 state in Pt-containing oligomers and for the absorption of fluorene oligomers.

Box 1.10 Absorption and Oscillator Strength

The rate of an electronic transition, and thus the intensity of the resulting absorption or emission signal, to zero order approximation, depends on the spatial overlap between initial and final state wavefunctions. This is reasonably large for a π-π*-transition that promotes an electron from a π HOMO to a π* LUMO, when both orbitals are delocalized over a similar area of the molecular backbone. The overlap is reduced when the HOMO and the LUMO are located on the different regions of the molecule, as is the case for a charge transfer (CT) transition. CT transitions are common in donor–acceptor-type copolymers or in many organometallic complexes. In the latter case, the transition takes place from a HOMO orbital centered on the metal, usually a metal d-orbital, to a LUMO orbital centered on the ligand, typically a π* orbital is therefore known as *metal-to-ligand charge transfer* (MLCT) transition. A low spatial overlap is also associated with HOMO–LUMO n–π*-transitions. There, the HOMO involves mainly a non-bonding (n) orbital, such as the lone pairs on nitrogen or oxygen, which may lie in the plane of the molecule having some σ character while the π*-LUMO is located above and below the molecular plane. In Figures B1.10.1 and B1.10.2, the relative intensities of different types of transitions are illustrated schematically.

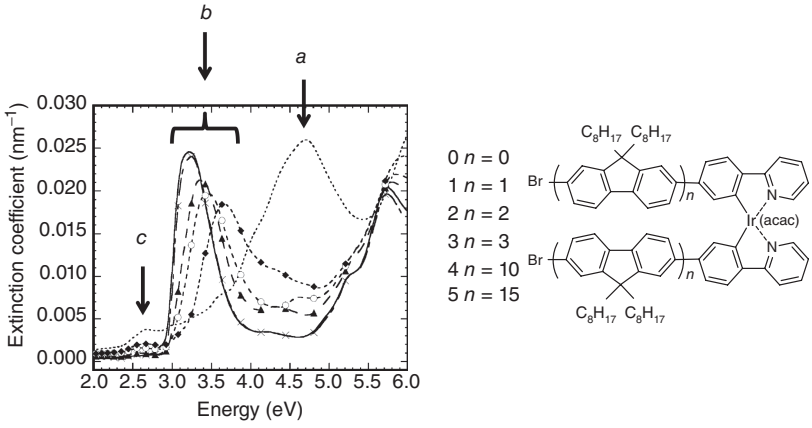

Figure B1.10.1 The absorption spectrum for the molecule shown (0: dotted line, 1: full diamonds, 2: open circles, 3: full triangles, 4: crosses, 15: solid line). The intense absorption indicated by the arrow a is due to a π–π* transition on the phenyl-pyridine ligand of the metal complex. Similarly, the intense absorption b is due to a π–π* transition on the oligo-fluorene extension of the ligand. Note how the intensity of this transition raises with increasing oligomer lengths. The weak absorption feature c arises from a CT type transition between the Iridium atom and the phenyl-pyridine ligand. (Data from Sandee *et al*. [84].)

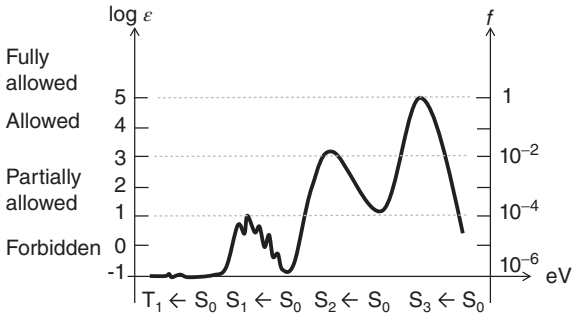

Figure B1.10.2 Illustration for the oscillator strength f and extinction coefficient ε, on a logarithmic scale, for the absorption of an organic molecule with transitions that are forbidden by spin, for example, $T_1 \leftarrow S_0$, by symmetry, for example, here $S_1 \leftarrow S_0$, that have poor overlap, for example, here $S_2 \leftarrow S_0$ or good overlap, for example, here $S_3 \leftarrow S_0$. The correlation between f and ε is only approximate (see Eq. (1.7)). (After Turro [86].)

The strength of the absorption signal can therefore be used to identify the nature of the transitions. An experimental measure for the strength of the transition is given by the *oscillator strength f*. If $\varepsilon(\tilde{\nu})$ denotes the *molar decadic extinction coefficient* at a certain wavenumber $\tilde{\nu}$, and n_0 is the refractive index of the surrounding medium, then the oscillator strength is given by

$$f = \frac{4.39 \times 10^{-9}}{n_0} \int \varepsilon(\tilde{\nu}) \mathrm{d}\tilde{\nu} \tag{1.7}$$

that is, it is related to the total area under the absorption band (see Eq. (1.58a) further below for a derivation). f gives the ratio between the experimentally observed, spectrally integrated absorption coefficient and the absorption coefficient calculated for a single electron in a three-dimensional harmonic potential well. The maximum value it could take is thus 1. For a rough, zero order orientation, singlet transitions with a $\pi-\pi^*$ character tend to have an oscillator strength in the range 10^{-2} to 1, singlet transitions with a charge transfer character (involving $n-\pi^*$ transitions or MLCT transitions) are in the range of 10^{-5} to 10^{-3}, and the oscillator strength of triplet transitions range from 10^{-9} for organic molecules to about 10^{-4} for organometallic complexes, depending on the amount of spin–orbit coupling involved (see further below). These values are intended only as a rough guide for orientation. A more detailed discussion on the oscillator strength is given in Section 1.4.3.

Experimentally, one measures absorption by placing the sample, for example, in the form of a thin film on a quartz substrate or as a solution in a quartz cuvette, in the path of a monochromated collimated light beam with wavelength λ, and one considers which fraction of light is transmitted. The sample should not scatter or reflect light, that is, the film or solution must be clear and homogeneous. For a film with total thickness d, the incident intensity I reduces by $\mathrm{d}I$ with each slab $\mathrm{d}x$ of the film penetrated, according to $\mathrm{d}I(\lambda) = -\alpha(\lambda) I(\lambda) \mathrm{d}x$, where the proportionality constant $\alpha(\lambda)$ is called the *absorption coefficient of the film at the wavelength* λ. The unit of $\alpha(\lambda)$ is cm^{-1}. Integration over x from 0 to the position d readily yields

$$I(\lambda) = I_0 \mathrm{e}^{-\alpha(\lambda) d} \tag{1.8}$$

The absorption coefficient relates to the absorption cross section $\sigma'(\lambda)$ with unit square centimeter as $\alpha(\lambda) = \sigma'(\lambda) n'$, where n' is the number of absorbing chromophores per cubic centimeter. (We use the $'$ to differentiate σ' and n' from the symbols σ and n that we use throughout this book to denote the disorder parameter and the refractive index, respectively.) Often, it is convenient to consider instead

the dimensionless decadic parameter $A(\lambda)$, referred to as *absorbance* or *optical density*. It is defined by

$$I(\lambda) = I_0 10^{-A(\lambda)} \tag{1.9}$$

Absorption coefficient and optical density are related by $\alpha d = A \cdot \ln(10) = A \cdot 2.3$. When using solutions, one needs to consider the concentration c of the solution in moles/liter. The corresponding equation is

$$I(\lambda) = I_0 10^{-\varepsilon(\lambda) c d} \tag{1.10}$$

with $\varepsilon(\lambda)$ being the decadic extinction coefficient in $\text{mole}^{-1} \cdot \text{liter} \cdot \text{cm}^{-1} = 10^3\,\text{cm}^2 \cdot \text{mole}^{-1}$.

Regarding the extinction coefficient, a little care is advisable when considering publications with experimental data. While some authors use the decadic extinction coefficient, others use the extinction coefficient to the basis of the natural logarithm, so that the values differ by a factor of 2.3. In passing we note that comparison of Eqs. (1.8) and (1.10) relates the decadic extinction coefficient to the absorption cross section.

$$\sigma' = \frac{\varepsilon}{n'} c \cdot \ln(10) = \frac{2303}{6.022 \times 10^{23}} \varepsilon = 3.82 \cdot 10^{-21} \varepsilon \tag{1.11}$$

The oscillator strength concept applies to emission in the same way. A high oscillator strengths thus implies not only a strong absorption signal, but also an intense luminescence signal.

1.4.2.2 The Vibrational Factor

So far we have considered the electronic part of the wavefunction. While the electronic part controls the overall intensity of the transition, the product of the vibrational wavefunctions, $\langle \Psi_{\text{vib,f}} | \Psi_{\text{vib,i}} \rangle$, can be said to control the spectral shape of the absorption and emission. Absorption takes place from the molecule in the zeroth vibrational level of the ground state. Typical vibrational energy quanta are in the range of 100–300 meV, implying that at room temperature only the lowest vibrational level is occupied. In the excited state, the potential energy curve is frequently displaced by ΔQ along the configuration coordinate with respect to the ground state potential energy curve. The reason for this is straightforward. When a molecule is in an excited state, one of its electrons will not be in a bonding orbital but in an antibonding orbital. This reduces the overall electron density between the atomic cores and leads to a larger equilibrium distance, which translates into a larger value of the configuration coordinate Q. When a photon is absorbed, the molecule changes from the ground to the excited state. The interaction with the electromagnetic light wave causes the electron distribution to change, while the nuclei are too heavy to respond to the fast oscillating electromagnetic field of the light wave. Thus, in a potential energy diagram (Figure 1.20), the transition can be indicated by a vertical arrow. Following Eq. (1.12), the intensity of the transition is controlled by the overlap of the vibrational wavefunctions, $\langle \Psi_{\text{vib,f}} | \Psi_{\text{vib,i}} \rangle$, also referred to as *Franck–Condon-overlap-integral* . The square of it, $|\langle \Psi_{\text{vib,f}} | \Psi_{\text{vib,i}} \rangle|^2$, is the *Franck–Condon-factor F*. It gives the probability of the transition from the 0th vibrational level of the ground state to the mth vibrational level of the exited state and may be denoted by I_{0-m}. It turns out that this can be described by a Poisson distribution, provided that the vibrational energy $\hbar\omega_m$ is large compared to thermal energies, $kT \ll \hbar\omega_m$, otherwise a Laguerre distribution prevails [11]. If the oscillation of the normal mode is treated as a single harmonic oscillator with reduced mass M, force constant $k = M\omega^2$, and angular frequency ω_m, the Franck–Condon factor can be related to the change in equilibrium coordinate ΔQ by

$$I_{0-m} = |\langle \Psi_{\text{vib,f}} | \Psi_{\text{vib,i}} \rangle|^2 = \frac{S^m}{m!} \mathrm{e}^{-S} \tag{1.12}$$

$$\text{with } S = \frac{1}{2} k \frac{\Delta Q^2}{\hbar\omega_m} = \frac{1}{2} M \omega_m \frac{\Delta Q^2}{\hbar} \tag{1.13}$$

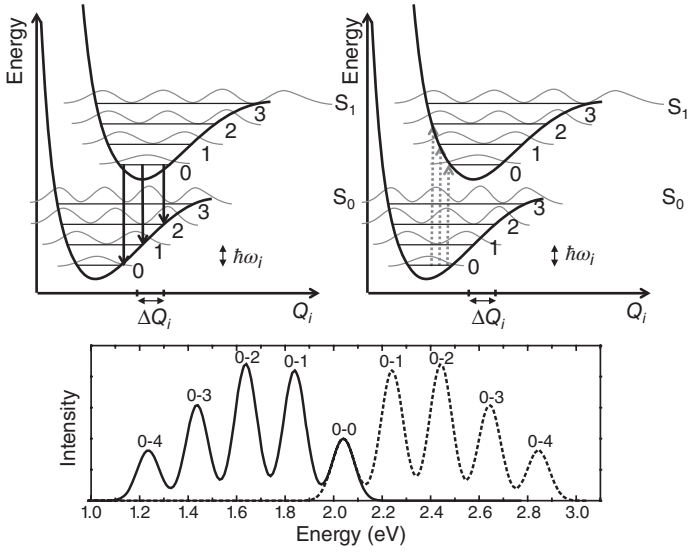

Figure 1.20 Illustration of the Franck–Condon principle. The simplified potential energy curves (for one normal mode) with vibrational wavefunctions show how the overlap of vibrational wavefunctions determines the shape of the absorption (dotted lines, right diagram) and emission spectra (solid lines, left diagram) according to Eq. (1.14a) and (1.14b). (After Kearwell and Wilkinson [82].)

S is called the *Huang–Rhys-parameter*. These equations are very useful and shall be discussed in more detail below. Let us first consider what happens to the molecule immediately after absorption of a photon. If, for example, absorption takes place into the third vibrational level of the S_1 excited state, the transition is denoted as $S_1 \leftarrow S_0$ 0-3 transition (in spectroscopic notation, the higher energy state is always on the left and the arrow gives the direction of the transition). The molecule will loose its vibrational energy by internal conversion, that is, by emission of phonons with energy $\hbar\omega$ and return to the 0 vibrational level of the S_1 excited state within roughly a picosecond. In the same way as the absorption of a photon leads to a transition from the ground state to the excited state potential energy curve, the converse occurs when a photon is emitted. As illustrated in Figure 1.20, the transition takes place vertically from the zeroth vibrational level of the S_1 state to any of the vibrational levels of the ground state, with an intensity governed by Eq. (1.12). This implies that the shape of the absorption and emission band is governed by Eq. (1.12). For a stiff molecule with rigid bonds and correspondingly small displacement between the excited and ground state potential energy curve, the 0-0 transition is dominant, while for a flexible molecule, a higher vibrational level such as 0-2 may form the peak of the distribution of transitions.

In amorphous films or solutions, one does not observe sharp lines for the transitions. Instead, the transitions are inhomogeneously broadened. The reasons for this broadening will be discussed in the next chapter. The consequence of it is that to model the absorption and emission spectra, the vibrational intensities need to be multiplied with a lineshape function Γ such as a Lorentzian or Gaussian distribution function in the case of homogeneous or inhomogeneous broadening, respectively. To model the absorption and emission spectra, one further needs to take into account the influence of the photon density-of-states in the medium surrounding the emitter on its emission rate [83]. As detailed in Section 1.4.3 (Eq. (1.43)) this implies inserting a factor $[n(\hbar\omega) \cdot \hbar\omega]^3$ for the photoluminescence spectra, where $n(\hbar\omega)$ is the refractive index at the transition energy $\hbar\omega$. If a single vibrational mode dominates, the normalized spectra for photoluminescence $I_{\mathrm{PL}}(\hbar\omega)$ and for absorption $I_{\mathrm{Abs}}(\hbar\omega)$

can then be described by

$$I_{\mathrm{PL}}(\hbar\omega) = [n(\hbar\omega)\cdot\hbar\omega]^3 \cdot \sum_m \frac{S^m}{m!}\mathrm{e}^{-S}\cdot\Gamma\cdot\delta(\hbar\omega-(\hbar\omega_0 - m\hbar\omega_m)) \tag{1.14a}$$

$$I_{\mathrm{Abs}}(\hbar\omega) = [n(\hbar\omega)\cdot\hbar\omega]\cdot \sum_m \frac{S^m}{m!}\mathrm{e}^{-S}\cdot\Gamma\cdot\delta(\hbar\omega-(\hbar\omega_0 + m\hbar\omega_m)) \tag{1.14b}$$

$m = 0, 1, 2, \ldots$ denotes the number of vibrational levels considered for the vibration with vibrational energy $\hbar\omega_m$. $\hbar\omega_0$ is the energy of the 0-0 transition. δ is the Delta-function, and for the lineshape function Γ either a Gaussian or a Lorentzian or a linear combination of both may be taken. Usually, a Gaussian profile is sufficient, that is,

$$\Gamma = \exp\left(-\frac{(\hbar\omega)^2}{2\sigma^2}\right) \tag{1.15a}$$

with σ^2 being the variance, that is, a measure for the width of the Gaussian. The full width at half maximum (FWHM) relates to σ by $\mathrm{FWHM} = 2\sqrt{2\ln 2}\sigma = 2.354\,\sigma$. In case a Lorentzian lineshape is needed,

$$\Gamma = \frac{(\gamma/2)^2}{(\hbar\omega)^2 + (\gamma/2)^2} \tag{1.15b}$$

where the parameter γ is the FWHM. Note that the Gaussian and Lorentzian here are defined such that the peak height is normalized to 1.

Equation (1.14a) may look intimidating, yet it simply means that at an energy separation of $m\cdot\hbar\omega_m$ from the 0-0 transition energy, one places a Gaussian peak with a fixed variance σ^2 and height $(S^m/m!)e^{-S}$. This can be done for as many vibrational levels m as desired. In most cases considering $m = 4$ overtones is fully sufficient. Eventually one adds them all up and multiplies the result with the cube of refractive index times the photon energy. The resulting curve is the photoluminescence spectrum. The procedure is analogous for the absorption spectrum, given by equation (1.14b).

It is important to be aware that real molecules are rarely dominated by a single normal mode vibration. Rather, there are several vibrations at different energies, for example, a benzene ring breathing mode and a C–H in plane wagging mode. Consequently, one potential energy may be drawn along a configuration coordinate representing the benzene ring breathing mode and another along a coordinate representing the C–H wagging mode. In the resulting spectrum, the transitions involving these different vibrational modes superimpose, as illustrated in Figure 1.18 above. When several vibrational modes m_i are considered, the equations for the Franck–Condon expressions change to

$$\begin{aligned} I_{0-m_i} &= \frac{{S_i}^{m_i}}{{m_i}!}\mathrm{e}^{-S_i} \\ S_i &= \frac{1}{2}M_i\omega_{m_i}\frac{\Delta {Q_i}^2}{\hbar} \end{aligned} \tag{1.16}$$

$$I_{\mathrm{PL}}(\hbar\omega) = [n(\hbar\omega)\cdot\hbar\omega]^3 \cdot \sum_{m_i}\prod_i \frac{{S_i}^{m_i}}{{m_i}!}\mathrm{e}^{-S_i}\cdot\Gamma\cdot\delta\left(\hbar\omega - \left(\hbar\omega_0 - \sum_i m_i\hbar\omega_{m_i}\right)\right) \tag{1.17a}$$

$$I_{\mathrm{Abs}}(\hbar\omega) = [n(\hbar\omega)\cdot\hbar\omega]\cdot \sum_{m_i}\prod_i \frac{{S_i}^{m_i}}{{m_i}!}\mathrm{e}^{-S_i}\cdot\Gamma\cdot\delta\left(\hbar\omega - \left(\hbar\omega_0 + \sum_i m_i\hbar\omega_{m_i}\right)\right) \tag{1.17b}$$

A final word of caveat. The expression for the Franck–Condon factor in Eq. (1.12) applies to the case of a *displaced* oscillator, which is the most frequently encountered case. It does not apply to a *distorted* oscillator (Box 1.11).

Box 1.11 Franck–Condon Factors for Displaced and Distorted Oscillators

A vibration is said to arise from a *displaced oscillator* when the electronic transition causes a change ΔQ in the equilibrium bond length, while the angular frequency remains constant ($\Delta\omega = 0$) (Figure B1.11.1). The Franck–Condon factor $F(E)$ for a displaced oscillator is given by

$$F(E) = \frac{S^m e^{-S}}{m!} \tag{B1.11.1}$$

where the vibrational quantum m, the vibrational energy $\hbar\omega$, and the energy difference E between the overlapping vibrational wavefunctions are related by $m = E/\hbar\omega$. A typical example for a displaced oscillator is the carbon–carbon stretching vibration with a vibrational energy of about 1200 cm^{-1}.

When the electronic transition causes a change in the angular frequency $\Delta\omega$ and the equilibrium distance remains the same ($\Delta Q = 0$), vibration is said to arise from a *distorted oscillator*. The carbon–hydrogen stretching vibration with 3000 cm^{-1} is an example for a distorted oscillator. The Franck–Condon factor for a distorted oscillator is

$$F(E) = \frac{2\sqrt{\omega_i \omega_f}}{\omega_i + \omega_f}\left(\frac{\Delta\omega}{\omega_i + \omega_f}\right)^m \frac{1, 3, 5, \ldots, (m-1)}{2, 4, \ldots, m} \tag{B1.11.2}$$

for m = even, and it is $F(E) = 0$ for m = odd.

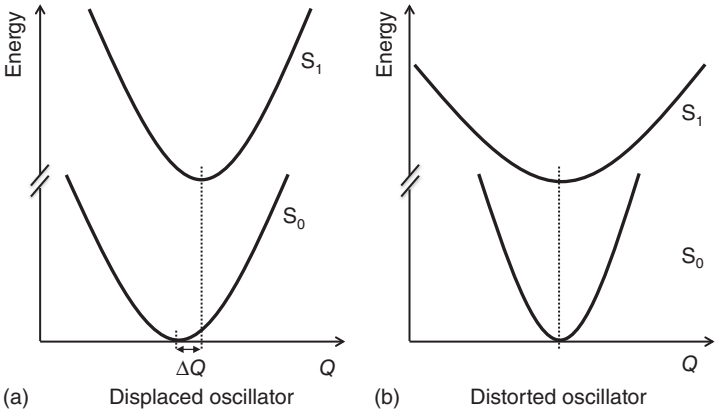

Figure B1.11.1 Illustration of the potential energy for (a) a displaced oscillator and (b) a distorted oscillator.

There are also expressions for the general, displaced, *and* distorted case and for the degenerate cases, which can be found in Ref. [85]. Evidently, the evolution of the Franck–Condon Factors with energy differs for displaced and distorted oscillators. They cross at about 4000 cm^{-1} (about 0.5 eV). Below 4000 cm^{-1}, the FC factor for displaced oscillators is larger, above that for distorted oscillators.

We shall now consider the meaning of the Huang–Rhys-parameter S in more detail. From Eq. (1.16) it is evident that a value for S can be derived from the ratio of the 0-0 to the 0-1 vibrational peak by

$$S = \frac{I_{0\text{-}1}}{I_{0\text{-}0}} \tag{1.18}$$

Further, from Eq. (1.13) one can see that S is a measure for the ratio between the potential energy associated with a vibrational excitation, $k\Delta Q^2/2$ and the energy of the vibrational quanta, $\hbar\omega_m$. The Huang–Rhys-parameter can thus be considered to yield the number of quanta involved in the vibrational excitation. Upon absorption of a photon, the molecule is at first still at the equilibrium position of the ground state, Q_{GS} and has excess potential energy with respect to the equilibrium position of the excited state, Q_{ES}. This excess energy is released by emission of vibrational quanta when the nuclei adapt to the change in electronic charge distribution. It is referred to as *geometric reorganization energy* or *relaxation energy* and is given by

$$E_{rel} = S\hbar\omega \qquad \text{for a single mode, and}$$
$$E_{rel} = \sum_i S_i\hbar\omega \qquad \text{for several modes } i. \tag{1.19}$$

The same reorganization energy is released following the emission of a photon, when the molecule returns from the excited state geometry to the ground state geometry. This is indicated in Figure 1.21.

1.4.2.3 **The Spin Factor**

The final term to consider in determining the rate of a transition according to Eq. (1.6) is the spin wavefunction $\Psi_{spin}(\alpha_i, \beta_i)$, that is, the value of the integral $\langle\Psi_{spin,i}|\Psi_{spin,f}\rangle$. This integral takes only two values, that is 0 if the spins of initial and final state differ, and 1 if they are equal. Thus, transitions between singlet states or between triplet states, such as $S_1 \leftarrow S_0$ or $T_n \leftarrow T_1$ are *spin-allowed* yet transitions from triplet to singlet or vice versa, such as $T_1 \rightarrow S_0$ are *spin-forbidden.* Nevertheless, luminescence arising from the $T_1 \rightarrow S_0$ transition is experimentally observed and it is referred to as *phosphorescence* to distinguish it from the $S_1 \rightarrow S_0$ transition, the *fluorescence*.

How does such a spin-forbidden transition acquire a finite transition rate? This is possible only if, by some perturbation, the triplet state wavefunction obtains some contribution from a singlet state wavefunction and vice versa. The transition then takes place between the singlet admixture in the

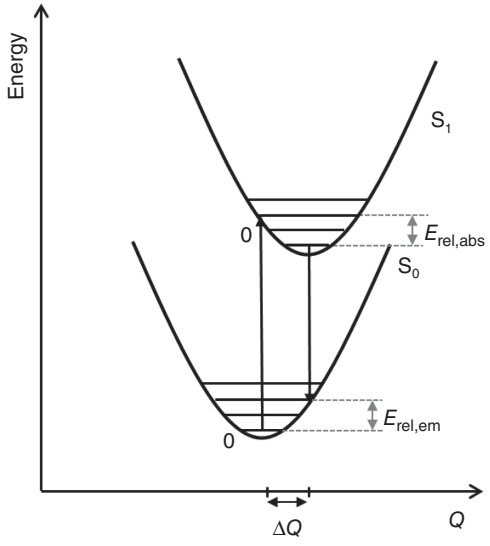

Figure 1.21 Potential energy diagram showing the relaxation energies $E_{rel,\,abs}$ and $E_{rel,\,em}$ associated with the process of absorption and emission, respectively.

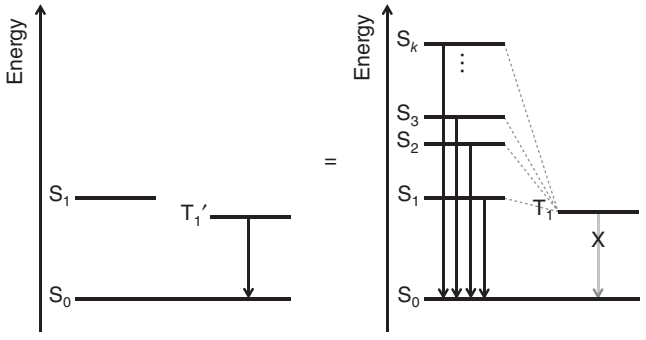

Figure 1.22 State diagram illustrating how a nominal triplet state T_1' acquires oscillator strength for the spin-forbidden $T_1' \rightarrow S_0$ transition through admixtures of the singlet states S_1 to S_k into the pure triplet state T_1.

triplet exited state wavefunction and the singlet ground state, and the triplet state admixture in the triplet ground state wavefunction and the triplet excited state (Figure 1.22).

Such a perturbation is provided by the mechanism of spin–orbit coupling. If the spin angular momentum s and the orbital angular momentum l of an electron couple, then a change in spin angular momentum can be compensated by an opposite change in orbital angular momentum, since only the total angular momentum $j = l + s$ needs to be conserved during the optical transition. For example, a spin flip of an electron can occur when it is accompanied by a change in the associated angular momentum from l_y to l_x. If the energy associated with the spin–orbit coupling is small compared to the total energy of the molecule, the effect of spin–orbit coupling on the wavefunction of a state can be described in the framework of perturbation theory. Let ${}^3\Psi_1^0 := {}^3(\Psi_{\text{el}}\Psi_{\text{spin}})_1^0$ denote the wavefunction of a pure triplet excited state, ${}^1\Psi_0^0$ be the wavefunction of a pure singlet ground state, ${}^1\Psi_k^0$ the pure kth singlet excited state and $\hat{H}_{\text{SO}}$ be the Hamiltonian of the perturbing spin–orbit interaction. The pure triplet excited state ${}^3\Psi_1^0$ will obtain admixtures of higher-lying singlet states ${}^1\Psi_k^0$. The amount of their contributions depends on how well they overlap with the pure triplet state (after the spin–orbit coupling has happened), and how far the two states are separated in energy. Mathematically, this is expressed as

$$|{}^3\Psi_1'\rangle = |{}^3\Psi_1^0\rangle + \sum_k \frac{\langle {}^1\Psi_k^0|\hat{H}_{\text{SO}}|{}^3\Psi_1^0\rangle}{E(T_1) - E(S_k)}|{}^1\Psi_k^0\rangle \tag{1.20}$$

with ${}^3\Psi_1'$ denoting the perturbed triplet state. An analogous expression can be written for the singlet ground state

$$|{}^1\Psi_0'\rangle = |{}^1\Psi_0^0\rangle + \sum_k \frac{\langle {}^3\Psi_k^0|\hat{H}_{\text{SO}}|{}^1\Psi_0^0\rangle}{E(S_0) - E(T_k)}|{}^3\Psi_k^0\rangle \tag{1.21}$$

Due to the large energy separation between the singlet ground state and higher-lying triplet states, the triplet admixture in the singlet ground state wavefunction is small. To obtain the rate for the transition, the wavefunctions of the perturbed triplet excited state and singlet ground state are inserted

into Fermi's golden rule (Eq. (1.12)).

$$k_{\text{if}} = \frac{2\pi}{\hbar}\rho|\langle {}^3\Psi_1'|e\hat{\boldsymbol{r}}|{}^1\Psi_0'\rangle|^2 = \frac{2\pi}{\hbar}\rho(A+B+C+D)^2 \quad \text{with} \tag{1.22}$$

$$A = \langle {}^3\Psi_1^0|e\hat{\boldsymbol{r}}|{}^1\Psi_0^0\rangle$$

$$B = \sum_k \frac{\langle {}^1\Psi_k^0|\hat{H}_{\text{SO}}|{}^3\Psi_1^0\rangle}{E(T_1)-E(S_k)}\langle {}^1\Psi_k^0|e\hat{\boldsymbol{r}}|{}^1\Psi_0^0\rangle$$

$$C = \sum_k \frac{\langle {}^3\Psi_k^0|\hat{H}_{\text{SO}}|{}^1\Psi_0^0\rangle}{E(S_0)-E(T_k)}\langle {}^3\Psi_1^0|e\hat{\boldsymbol{r}}|{}^3\Psi_k^0\rangle$$

$$D = \sum_k \frac{\langle {}^1\Psi_k^0|\hat{H}_{\text{SO}}|{}^3\Psi_1^0\rangle}{E(T_1)-E(S_k)}\sum_j \frac{\langle {}^3\Psi_j^0|\hat{H}_{\text{SO}}|{}^1\Psi_0^0\rangle}{E(S_0)-E(T_j)}\langle {}^1\Psi_k^0|e\hat{\boldsymbol{r}}|{}^3\Psi_j^0\rangle$$

Remembering that our wavefunction contains both, the spatial and the spin wavefunction, it is evident that terms A and D vanish as they contain a product of orthogonal spins. The remaining contributing terms are B and C, with C being only a minor contribution due to the large energy difference between S_0 and T_k's, compared to that between T_1 and S_k's.

This illustrates how the intensity of phosphorescence results mainly from the admixture of singlet wavefunctions in the nominal triplet state. Detailed quantum mechanical studies have been performed for the polyacenes [87]. It turns out that the spin–orbit coupling admixes states of the same parity, yet of different symmetry. As a result of spin–orbit coupling, the triplet state can have a different polarization to the singlet state. This has been observed for molecules such as naphthalene, phenanthrene, chrysene, picenene, and corone [87], but also for polymers such as a Pt-containing phenylene ethynylene [88] and polyfluorene [89].

The amount of the singlet admixture to the nominal triplet state depends not just on the energy separation between T_1 and S_k's, but also on the magnitude of the spin-orbit coupling. For atoms, one can show that the perturbing Hamiltonian $\hat{H}_{\text{SO}}$ is proportional to the fourth power of the atomic charge, $\hat{H}_{\text{SO}} \propto Z^4/(n^3(l+1)(l+0.5)l)$, with n and l being the quantum numbers, and for molecules, a similar expression exists with a dependence between the fourth and fifths power of the atomic charge. As a result, strong phosphorescence is observed when atoms with a high mass are incorporated in the chromophore, as is the case for the organometallic complexes such as the Ir-complexes used for phosphorescent OLEDs, or for halogen-substituted polyacenes (*internal heavy atom effect*) (Figure 1.23) as illustrated in Table 1.4 further below. Sometimes, sufficient interaction between orbitals can even be obtained if the heavy atom is placed immediately next to an organic chromophore, for example, by using a brome or iodine-containing solvent in solution [90, 91], or by having some metal like Pd present in the film as a residue from the metal-catalyzed synthesis [92]. This is referred to as *external heavy atom effect*.

Even in the absence of heavy metals, phosphorescence can still occur, albeit at much weaker intensity. In a semiclassical picture, one can attribute this to the fact that only the sum $j = s + l$ of spin s and orbital angular momentum l needs to be preserved. If the orbital angular momentum changes as a result of vibrations, the spin can flip. In a quantum mechanical picture, the torsions provide the perturbation to mix orbitals with different angular momentum such as σ and π [95, 93, 96]. Vibrationally induced spin–orbit coupling is an example where the Born–Oppenheimer approximation no longer provides a suitable description. Overall, vibrationally induced spin–orbit coupling is weak compared to heavy-metal induced spin–orbit coupling. As a result, radiative rates for phosphorescence are in the range of 10^6 s^{-1} for organometallic complexes, yet reach only 1 s^{-1} for purely organic compounds.

In summary, from the Fermi golden rule expression (Eq. (1.4)) follows that a high rate of absorption and emission requires two states that are of the same parity and spin, with frontier orbitals that contain a well delocalized, well overlapping π-electron system. Transitions with reduced orbital overlap between the initial and final state, such as CT type transitions, have a concomitantly reduced intensity. There are no transitions between states of different parity. The intensity of the transition between

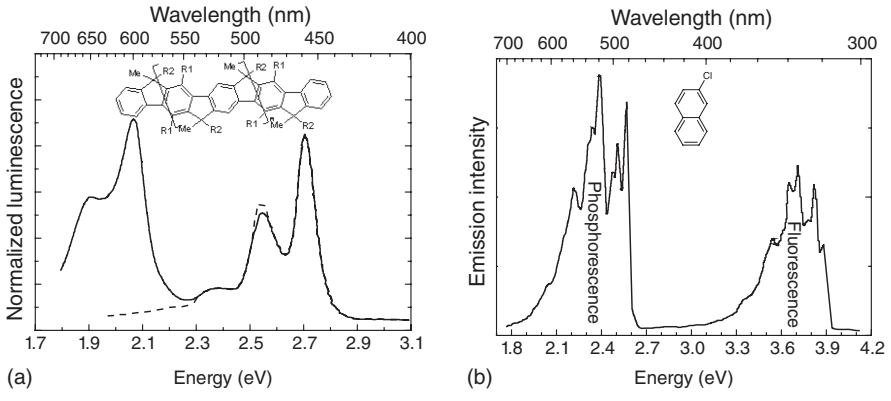

Figure 1.23 (a) Luminescence of MeLPPP at room temperature for optical excitation (dotted line) showing only fluorescence (Fl) and for electrical excitation (solid line), displaying both fluorescence and phosphorescence (Ph). The phosphorescence observed for electrical excitation is enhanced by the presence of palladium in the film. (After Lupton *et al*. [92].) (b) Fluorescence and phosphorescence of Cl substituted Naphthalene, taken in Me-THF at 77 K. (Data from Turro [93].) (c) Phosphorescence from blue, green, and red emitting Ir-complexes FIrpic, Irppy, and Btplr, respectively. (Data from Forrest *et al*. [94].)

singlet and triplet states depends on the strength of the spin–orbit coupling. The spectral shape of the transition is modulated by the Franck–Condon Factor.

1.4.3 A Classical Picture of Light Absorption

In addition to the quantum mechanical description of light absorption presented in the previous chapter, it is useful to be aware of the corresponding classical picture that leads to the macroscopic quantities of such as the refractive index and absorption coefficient. Further, it is instructive to see how the quantum mechanical description and the experimental macroscopic measurements on a sample connect.

1.4.3.1 The Lorentz Oscillator Model and the Complex Refractive Index

Classically, the process of light absorption or emission may be understood as a driven, damped oscillation. The changing electromagnetic field of the light wave accelerates the electron distribution in the molecule and causes it to follow the field almost instantly. As with any driven oscillation, the transfer of energy from the driving electromagnetic field to the oscillating electron cloud is at maximum when the frequency of light wave matches the resonance frequency ω_0 of the electron distribution. This transfer of energy corresponds to the absorption of a photon.

The mathematical formalism is straightforward if one is familiar with the driven damped oscillator and is known as the *Lorentz oscillator model*. We shall sketch it briefly. For simplicity we consider a single electron of mass m and charge e that is bound to an atom by an elastic force with spring constant k. It has a resonance frequency of oscillation $\omega_0^2 = k/m$. The electromagnetic field of the light exerts a force F_{EM} on the electron,

$$\mathbf{F}_{\mathrm{EM}} = e\mathbf{E} + e\mathbf{v} \times \mathbf{B} \tag{1.23}$$

where $\mathbf{E}$ and $\mathbf{B}$ are the electric and magnetic field, respectively, and $\mathbf{v}$ is the velocity of the electron. In this expression, the second, magnetic term is small compared to the first, electric term and can thus be neglected. Considering one-dimensional motion and using $E(t) = E_0 \mathrm{e}^{-i\omega t}$ for the oscillating

electric field yields

$$F_{\mathrm{EM}} \cong eE_0 \mathrm{e}^{-i\omega t} \tag{1.24}$$

for the force that accelerates the electron with an acceleration $\ddot{x}$. The electron resists the resulting motion through its inertia with $F_{\mathrm{inert}} = -m\ddot{x}$, and it is held back by the elastic restoring force that binds it to the atom, $F_{\mathrm{spring}} = -kx$. x is the displacement of the electron from its original position. The whole motion is usually damped by a force that is proportional to the velocity $\dot{x}$ of the object and to its mass. This proportionality is expressed by a phenomenological damping constant γ, so $F_{\mathrm{damp}} = \gamma m\dot{x}$. It is equivalent to friction in a mechanical system. In the present case, damping arises from coupling of the object to its environment. Equating the forces acting on the electron

$$F_{\mathrm{inert}} + F_{\mathrm{damp}} + F_{\mathrm{spring}} = -F_{\mathrm{EM}} \tag{1.25}$$

yields the equation of motion

$$m\ddot{x} - \gamma m\dot{x} + kx = eE_0 \mathrm{e}^{-i\omega t} \tag{1.26}$$

This equation describes how the electron follows the field in an oscillatory motion. The general solution to this equation is

$$x(t) = x_{\mathrm{trans}}(t)\mathrm{e}^{-\frac{t\gamma}{2}} + x_0 \mathrm{e}^{-i\omega t} \tag{1.27}$$

with $x_{\mathrm{trans}}(t) = x_{t0} \exp\left[-i\sqrt{\left(\omega_0^2 - \gamma^2/4\right)}t\right]$. The first term, $x_{\mathrm{trans}}(t)\mathrm{e}^{-t\gamma/2}$, represents a damped oscillation of frequency $(\omega_0^2 - \gamma^2/4)$ that disappears for $t > \gamma^{-1}$. After this transient feature, the electron follows the oscillation of the electromagnetic field. The amplitude of the electron's displacement can be found by inserting Eq. (1.27) into Eq. (1.26) for $t > \gamma^{-1}$. It is

$$x_0 = \frac{eE_0}{m} \frac{1}{(\omega_0^2 - \omega^2) - i\omega\gamma} \tag{1.28}$$

What is this classical model good for? It turns out that this simple picture of an electron forced into oscillations by a periodically changing electric field vector can be helpful to develop an intuitive understanding of the quantum mechanical process of light absorption. For a quantitative description, correction terms are needed that are beyond the scope of this book. They can be found in [97].

Consider for example, the quantum mechanical selection rule that says, light absorption (or emission) must be accompanied by a change in angular momentum by one unit. This can be readily rationalized in this oscillator model (Figure 1.24). The incident oscillating electromagnetic field vector causes the electron cloud to follow and thus to redistribute. Instead of the symmetric charge distribution that was there before the action of the electromagnetic field, there is now an oscillating, polar

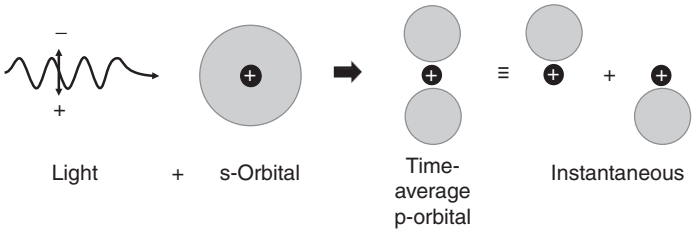

Figure 1.24 Light absorption in the framework of the Lorentz Oscillator Model. The oscillating electric field vector of the incident electromagnetic light wave causes the electron cloud of the atom to follow in resonance. The time-averaged charge distribution thus changes from an initially spherical shape to one with large probabilities at the turn-around points of the oscillation, and a low one in the middle. In this example, light absorption introduces a node by changing the time-averaged charge distribution from an s-orbital to a p-orbital. (After Turro [93].)

charge distribution. Looking at the time-average, there is an additional node. In a single-electron atom such as hydrogen, the electron distribution may change from one corresponding initially to a 1s orbital to one corresponding to a 2p orbital. In a molecule, the distribution may change from a π to a π* orbital. This additional node, induced by the oscillating field, corresponds to a unit change in angular momentum upon absorption of a photon.

In a classical picture, an oscillating charge distribution implies that there is an electromagnetic dipole, just like in the simple antenna of an ordinary household radio receiver. The magnitude of the dipole moment scales with the amount of charge that oscillates and the distance over which it oscillates. This dipole is induced by the incident electromagnetic wave. It is referred to as *transition dipole* μ since it is associated with the optical transition, and, for a single oscillating electron, it is given by

$$\mu = ex_0 \tag{1.29}$$

The dipole moment per unit field strength that can be induced in an atom or molecule defines the *polarizability* α of the atom or molecule,

$$\alpha = \frac{\mu}{E_0} \tag{1.30}$$

It gives a measure for the ease by which an electric field can distort the electron distribution of the molecule. Keep in mind that, in general, the force due to an electric field is opposed by the elastic restoring force, $eE_0 = -kx_0$. Using Eqs. (1.29) and (1.30) one can see that the restoring force constant is inverse proportional to the polarizability, $k = e^2/\alpha$.

In the framework of this classical picture, the frequency dependence of the refractive index of a molecule and of its absorption coefficient can be derived. We shall outline the essential steps. In a macroscopic sample, there is not just one oscillating dipole, but N of them per unit volume. This gives a dipole moment per unit volume, that is, a macroscopic polarization density P,

$$P = N\mu = N\alpha E_0 = N\frac{ex_0}{E_0}E_0 = \frac{Ne^2}{m}\frac{1}{(\omega_0^2 - \omega^2) - i\omega\gamma}\,E_0 \tag{1.31}$$

The overall electric field inside a macroscopic sample then is given by a superposition of the electromagnetic field inside the sample and of the induced dipole field. As it involves displaced charges, it is referred to as *dielectric displacement field* D

$$D = \varepsilon_0 E_0 + P \tag{1.32}$$

Using Eq. (1.31), this can be expressed as

$$D = \varepsilon_0\left(1 + \frac{Ne^2}{\varepsilon_0 m}\frac{1}{\left(\omega_0^2 - \omega^2\right) - i\omega\gamma}\right)E_0 \tag{1.33}$$

The term in the bracket is the *dielectric constant* $\varepsilon_r(\omega)$ of the macroscopic sample. It describes how the field present in the macroscopic sample is altered due to the fact that the electron distributions of the molecules interact with the electromagnetic light wave. From this derivation, it should be evident that the dielectric constant is the macroscopic equivalent of the polarizability α.

$$\varepsilon_r(\omega) = 1 + \frac{Ne^2}{\varepsilon_0 m}\frac{1}{(\omega_0^2 - \omega^2) - i\omega\gamma} \tag{1.34}$$

Maxwell has shown that the dielectric constant of a nonmagnetic material relates to its refractive index as $\tilde{n}^2 = \varepsilon_r(\omega)$. Here, the dielectric constant is a complex number, and thus the refractive index is also a complex number, indicated here by a tilde over the symbol. What does a complex refractive index mean? If one writes

$$\tilde{n} = n - i\kappa \tag{1.35}$$

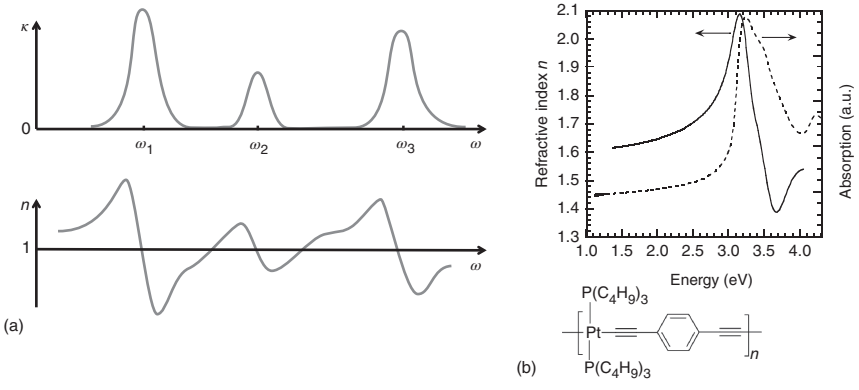

Figure 1.25 The dependence on the energy $\hbar\omega$ of the incident light for the two components n and κ of the complex index of refraction $\tilde{n} = n - i\kappa$. (a) Schematic illustration for three optical transitions at ω_1, ω_2, and ω_3. (After Demtröder [99]) (b) Measured refractive index and absorption for the Pt-polymer shown. (Data from Khan [80].)

and uses this to describe the propagation of an electromagnetic wave in matter

$$E = E_0 e^{i(\omega t - \tilde{n} k_0 z)} = E_0 e^{-\kappa k_0 z} E_0 e^{i(\omega t - n k_0 z)} \tag{1.36}$$

one can immediately see that κ relates directly to the absorption coefficient (see Eq. (1.8)) as $\alpha = 2\kappa k_0$, since the intensity relates to the amplitude of a wave as $I = E^2$. Thus, κ is responsible for an attenuation of the propagating wave. n is simply the usual, real refractive index that describes the dispersion of a light wave. For dilute media, not too far away from the resonance frequency ω_0, one can approximate the combination of Eqs. (1.34) and (1.35) to [97, 98]

$$n(\omega) \approx 1 + \frac{Ne^2}{4\varepsilon_0 m} \frac{(\omega_0 - \omega)/\omega}{(\omega_0 - \omega)^2 + (\gamma/2)^2} \quad \text{and} \quad \kappa(\omega) \approx \frac{Ne^2}{4\varepsilon_0 m} \frac{\gamma/2\omega}{(\omega_0 - \omega)^2 + (\gamma/2)^2} \tag{1.37}$$

with the frequency dependence as indicated in Figure 1.25. Two features are to be noted.

First, there is a steep change of the refractive index close to the resonance frequency, where absorption is at the maximum. A wavelength dependence of the refractive index thus needs to be taken into account near the absorption edge, for example, when modeling the fluorescence spectrum according to Eq. (1.14a), while it can be neglected at some distance from the absorption edge, for example, when modeling phosphorescence.

Second, κ is proportional to the classical expression for the power that is transferred from an external driving force to an oscillating object in the framework of the driven damped oscillator. That power is simply $P = F\dot{x}$, that is, for an incident electromagnetic light wave that interacts with a single electron bound to an atom, $P = eE\dot{x}$. Taking the time average, near the resonance frequency this approximates to

$$P(\omega) \approx \frac{e^2 E_0^2}{4m} \frac{\gamma/2}{(\omega_0 - \omega)^2 + (\gamma/2)^2} = \frac{e^2 E_0^2 \pi}{4m} \mathcal{L}(\omega) \tag{1.38}$$

with

$$\mathcal{L}(\omega) = \frac{1}{\pi} \frac{\gamma/2}{(\omega_0 - \omega)^2 + (\gamma/2)^2}$$

being the Lorentzian curve. It has a FWHM of γ and a maximum of $\mathcal{L}(\omega) = 2/\pi\gamma$. Here, we used the normalization $\int_0^\infty \mathcal{L}(\omega) d\omega = 1$.

This Lorentzian lineshape can indeed be observed in molecular transitions, provided that one looks at a single molecule or at a group of molecules that all have exactly the same resonance frequency. The

latter can be realized through techniques such as site-selective spectroscopy on molecules embedded in inert glasses and Shpol'skii matrices, or through hole-burning spectroscopy. Some of these techniques are discussed in Chapter 2.

1.4.3.2 Relating Experimental and Quantum Mechanical Quantities: The Einstein Coefficients, the Strickler–Berg Expression, and the Oscillator Strength

Experimentally measured quantities such as the absorption coefficient or the emission lifetime can be related to quantum mechanical entities with the help of the Einstein coefficients and the Strickler–Berg relationship. In 1917, Einstein [100] derived the fundamental relationship between the transition probabilities for induced absorption and emission and that for spontaneous emission. His result showed that the spontaneous emission probability is directly proportional to the corresponding absorption probability and to the third power of the frequency of the transition. In the derivation of his equations, it is necessary to assume that the absorption band is sharp and that the fluorescence occurs at the same wavelength as the absorption. This implies that his equations are strictly applicable only to atomic transitions. Strickler and Berg extended his work in 1962 so that it becomes applicable to polyatomic molecules [83, 87]. While the Einstein coefficients are treated in many textbooks on optics, the extension of Strickler and Berg that includes vibrational levels is not commonly summarized at a textbook level, which is why they are included here in a more detailed way. For the practically minded student, it may suffice to merely take note of the gray shaded equations (Eqs. (1.43), (1.49b), (1.53), (1.58b), (1.61b), (1.63), and (1.65)).

Consider a large number of chromophores that are embedded in a medium of refractive index n and that are in thermal equilibrium within a cavity of temperature T. These chromophores will absorb photons and they will emit photons. Let N_l be the number of chromophores in the lower state and N_u those in the upper state, and $h\nu$ be the energy separating the two states. For a given frequency ν, the energy density of radiation (in $10^{-7}\,\mathrm{J\,cm^{-3}}$ per unit frequency range dν) in the medium is given by Planck's black-body law

$$u(\nu) = \frac{8\pi h\nu^3}{c^3}\left(\mathrm{e}^{\frac{h\nu}{kT}} - 1\right)^{-1} \tag{1.39}$$

Let us now introduce a probability coefficient for transitions between a lower electronic state l with vibrational level n and a upper electronic state u with vibrational level m. For spontaneous emission, this shall be $A_{un\to lm}$ (the *Einstein A coefficient*), for stimulated emission (SE), this shall be $B_{un\to lm}$ and for absorption, we use $B_{lm\to un}$ (the *Einstein B coefficient*). The frequency of the transition is $\nu = \nu_{un\to lm} = \nu_{lm\to un}$. Spontaneous emission is a random process that determines the normal radiative lifetime of an excited state. In contrast, SE or absorption occurs when an incident photon induces the transition between the two states. Thus, the rate ΔN for chromophores going from one state to the other by spontaneous emission depends only on the number of chromophores present in the initial state In contrast, for SE and absorption, the rate ΔN also depends on the energy density of the radiation, $u(\nu)$. The rate for molecules going from the lower state to the upper state by absorption is then [83]

$$\Delta N_{lm\to un} = N_{lm} B_{lm\to un} u(\nu) \tag{1.40}$$

while the rate for molecules going the opposite direction by emission is

$$\Delta N_{un\to lm} = N_{un}[B_{un\to lm} u(\nu) + A_{un\to lm}] \tag{1.41}$$

Einstein showed that $B_{un\to lm} = B_{lm\to un}$. Furthermore, the populations of lower and upper state are related by the Boltzmann distribution

$$N_{un} = N_{lm} \exp\left(-\frac{h\nu}{kT}\right) \tag{1.42}$$

In thermal equilibrium, the expressions of Eqs. (1.40) and (1.41) must be equal. Considering this and inserting Eqs. (1.39) and (1.42) yields the *Einstein relation*

$$A_{un\to lm} = 8\pi\left(\frac{h\nu n}{c}\right)^3 B_{lm\to un} \tag{1.43}$$

The feature to notice is that in between the probability of spontaneous emission, given by the Einstein A coefficient, and the probability of absorption, given by the Einstein B coefficient, there is the cube of the transition energy that arises from the photon density of states.

How do these coefficients relate to experimentally measured quantities? $u(\nu)/h\nu$ is the photon density in a frequency range $\mathrm{d}\nu$. When a beam of photon density $u(\nu)/h\nu$ passes through a material, photons are absorbed so that the photon density changes by

$$\frac{\mathrm{d}u(\nu)}{h\nu} = -\sigma' N_{lm}\frac{u(\nu)}{h\nu} \tag{1.44}$$

where N_{lm} is the number of absorbing chromophores per square centimeter and σ' is the absorption cross section of a chromophore. The absorption results in a number of excited chromophores $\Delta N_{lm\to un}$ per second, that is

$$\Delta N_{lm\to un} = -\nu\frac{\mathrm{d}u(\nu)}{h\nu} = \frac{c}{n}\sigma' N_{lm}\frac{u(\nu)}{h\nu} \tag{1.45}$$

with $\nu = c/n$ being the velocity of the light wave (take care not to confuse the similar appearing symbols for velocity, ν, and frequency, ν). Be aware that the same symbol, n, is used to indicate the refractive index, as in $\nu = c/n$, and to indicate the vibrational level, as in $\Delta N_{lm\to un}$. The meaning, however, should be evident from the context. One obtains the excitation rate per unit volume over the entire vibronic band by integration over the entire frequency range from the zeroth vibrational level of the lower state ($l0$) to the mth vibrational level of the upper state (um).

$$\Delta N_{l\to u} = N_l\frac{c}{hn}\int_{l0}^{un}\frac{\sigma'(\nu)u(\nu)}{\nu}\mathrm{d}\nu \tag{1.46}$$

If one assumes, that the energy density is approximately constant in this range, one can write this as

$$\Delta N_{l\to u} = N_l\left[\frac{c}{hn}\int_{l0}^{un}\frac{\sigma'(\nu)}{\nu}\mathrm{d}\nu\right]u(\nu) \tag{1.47}$$

which, by comparison with Eq. (1.40) immediately yields

$$B_{l0\to u} = \sum_n B_{l0\to un} = \frac{c}{hn}\int\frac{\sigma'(\nu)}{\nu}\mathrm{d}\nu \tag{1.48}$$

Instead of the absorption cross section, it is more practical to use the decadic molar extinction coefficient (Eq. (1.11)) so that

$$B_{l0\to u} = \frac{2303}{6.022\times 10^{23}}\frac{c}{hn}\int\frac{\varepsilon(\nu)}{\nu}\mathrm{d}\nu \tag{1.49a}$$

$$B_{l0\to u} = 3.82\times 10^{-21}\frac{c}{hn}\int\frac{\varepsilon(\nu)}{\nu}\mathrm{d}\nu \tag{1.49b}$$

Equation (1.49) relates the Einstein B coefficient for absorption to a quantity that can be measured experimentally in a simple way. The absorption occurs from the 0th vibrational level of the lower state to all vibrational levels of the upper state.

For compounds that show a clear mirror relationship between absorption and emission, one can assume that $B_{l0\to un} = B_{u0\to ln'}$, and one can then obtain the Einstein A coefficient for spontaneous emission by the Einstein relation, Eq. (1.43), as

$$A_{u0\to lm} = 8\pi\left(\frac{h\nu n}{c}\right)^3 B_{l0\to un} \tag{1.50}$$

Strickler and Berg have further shown that the intrinsic radiative decay rate, τ_0, can be related to the Einstein coefficients in the following way. Since $A_{un\to lm}$ is the probability coefficient for spontaneous emission, which occurs from the 0th vibrational level of the upper state to all vibrational levels of the lower state, it follows that A relates to τ_0 as

$$\tau_0^{-1} = A_{u0\to l} = \sum_a A_{u0\to la} \tag{1.51}$$

Their calculations show that

$$\frac{1}{\tau_0} = A_{u0\to l} = \frac{8\cdot 2303\pi n^2}{c^2\times 6.022\times 10^{23}}\frac{1}{\langle\nu^{-3}\rangle}\int\frac{\varepsilon(\nu)}{\nu}\mathrm{d}\nu = \frac{8\pi hn^3}{c^3}\frac{1}{\langle\nu^{-3}\rangle}B_{l0\to u} \tag{1.52}$$

where $1/\langle\nu^{-3}\rangle = \int I(\nu)\mathrm{d}\nu/\int\nu^{-3}I(\nu)\mathrm{d}\nu$. $I(\nu)$ is the fluorescence intensity measured in number of photons per frequency interval. Instead of using the frequency $\nu = c/\lambda$ in units s^{-1}, one may prefer to use wavenumbers $\tilde{\nu} = 1/\lambda$ in units cm^{-1}. c and λ are the velocity and wavelength of light, respectively. Equation (1.52) then reads

$$A_{u0\to l} = \frac{1}{\tau_0} = 2.880\times 10^{-9}\frac{n^2}{\langle\tilde{\nu}^{-3}\rangle}\int\frac{\varepsilon(\tilde{\nu})}{\tilde{\nu}}\mathrm{d}\tilde{\nu} \tag{1.53}$$

This is the familiar form of the *Strickler–Berg equation* that relates radiative lifetime to the absorption spectrum. If the band is sharp and the absorption and fluorescence occur at the same wavelength, $\tilde{\nu}$ can be considered a constant and can be removed from under the integral. This is the case for most atomic transitions, where Eq. (1.53) reduces to

$$\frac{1}{\tau_0} = 2.880\times 10^{-9}n^2\tilde{\nu}^2\int\varepsilon(\tilde{\nu})\mathrm{d}\tilde{\nu} \tag{1.54}$$

This equation is also useful for order-of-magnitude calculations on molecules.

So far, we have seen how the Einstein coefficients relate to the absorption spectrum and to the radiative lifetime, both being experimentally accessible quantities. It is also possible to relate the Einstein coefficients to the quantum mechanical matrix element for a dipole transition. Let us use the abbreviation $|\boldsymbol{\mu}_{\mathrm{if}}|^2 = |\langle\Psi_{\mathrm{el,i}}|e\hat{\boldsymbol{r}}|\Psi_{\mathrm{el,f}}\rangle|^2$ for the electronic factor in the Fermi Golden rule expression for a radiative transition. One can show that

$$B_{l0\to u} = \frac{8\pi^3}{3h^2}|\boldsymbol{\mu}_{\mathrm{if}}|^2 \tag{1.55}$$

where $|\boldsymbol{\mu}_{\mathrm{if}}|^2$ is in electrostatic units (e.s.u.). A derivation of this expression can be found in Appendix 13 and 17 of [64]. Equating (1.55) with (1.49b) yields

$$|\boldsymbol{\mu}_{\mathrm{if}}|^2 = \frac{2303}{6.022\times 10^{23}}\frac{3ch}{8\pi^3 n}\int\frac{\varepsilon(\nu)}{\nu}\mathrm{d}\nu \tag{1.56}$$

thus directly linking the experimental with the quantum mechanical quantity.

In practice, it has been found convenient to define a measure for the strength of an optical transition. The *oscillator strength* f has been defined as

$$f = \frac{mc}{\pi e^2 n}\int\sigma'(\nu)\mathrm{d}\nu \tag{1.57}$$

which can be expressed in terms of the extinction coefficient and wavenumbers using Eq. (1.11)

$$f = \frac{2303}{6.022\times 10^{23}}\frac{mc^2}{\pi en}\int\varepsilon(\tilde{\nu})\mathrm{d}\tilde{\nu} \tag{1.58a}$$

$$f = \frac{4.39\times 10^{-9}}{n}\int\varepsilon(\tilde{\nu})\mathrm{d}\tilde{\nu} \tag{1.58b}$$

The oscillator strength can also be related to the Einstein coefficients. Equation (1.48) can be approximated by using an average frequency $\langle\nu\rangle$ to

$$B_{l0\to u} = \frac{c}{hn}\int\frac{\sigma'(\nu)}{\nu}\mathrm{d}\nu \approx \frac{c}{hn}\frac{1}{\nu}\int\sigma'(\nu)\mathrm{d}\nu \tag{1.59}$$

Inserting this into Eq. (1.57) yields

$$f = \frac{mh\langle\nu\rangle}{\pi e^2}B_{l0\to u} \tag{1.60}$$

Combining this with Eq. (1.55) and using $\langle\nu\rangle = c\langle\tilde{\nu}\rangle$ readily gives

$$f = \frac{8m\pi^2 c\tilde{\nu}}{3he^2}|\boldsymbol{\mu}_{\mathrm{if}}|^2 \tag{1.61a}$$

$$f = 4.70\cdot 10^{29}\langle\tilde{\nu}\rangle|\boldsymbol{\mu}_{\mathrm{if}}|^2 \tag{1.61b}$$

with $\tilde{\nu}$ in cm^{-1} and $\boldsymbol{\mu}_{\mathrm{if}}$ in electrostatic units. If SI units are used for $\tilde{\nu}$ and $\boldsymbol{\mu}_{\mathrm{if}}$, this translates into

$$f = 5.23\times 10^{6}\langle\tilde{\nu}\rangle|\boldsymbol{\mu}_{\mathrm{if}}|^2 \tag{1.61c}$$

The oscillator strength was initially introduced in the context of the Lorentz oscillator model. For a classical, single, three-dimensional oscillator it has its maximum value of 1. Equation (1.58b) can be used to estimate the maximum possible value for the decadic extinction coefficient. The integral can be approximated to

$$\int\varepsilon(\tilde{\nu})\mathrm{d}\tilde{\nu} \approx \varepsilon_{\max}\Delta\tilde{\nu} \tag{1.62}$$

where $\varepsilon_{\max}$ is the value of the extinction coefficient at the maximum of absorption and $\Delta\tilde{\nu}$ is the full width at half the maximum height of the absorption band $\varepsilon_{\max}$. Taking the refractive index to be one and a minimum value for $\Delta\tilde{\nu}$ to be $2000\,\mathrm{cm}^{-1}$, Eq. (1.58b) gives $1 = 4.39\cdot 10^{-9}\cdot\varepsilon_{\max}\cdot 2000\,\mathrm{cm}^{-1}$ which implies

$$\varepsilon_{\max} \approx 10^{5}\,\mathrm{cm}^{-1} \tag{1.63}$$

In a similar way, the maximum radiative decay rate can be estimated from the oscillator strength. Approximating the radiative lifetime by employing Eq. (1.54), and combining it with Eq. (1.58b) yields

$$\frac{1}{\tau_0} \approx n^3\tilde{\nu}^2 f \tag{1.64}$$

Using a refractive index of 1, a transition wavelength of 400 nm, that is, $25\,000\,\mathrm{cm}^{-1}$, Eq. (1.64) gives an upper limit for the radiative decay rate $k_{\mathrm{r}} = \tau_0^{-1} \approx 1\cdot(2.5\cdot 10^4)^2\cdot 1 = 6.25\cdot 10^8$, that is, the maximum possible radiative decay rate is on the order of

$$k_{\mathrm{r,max}} = 10^{9}\,\mathrm{s}^{-1} \tag{1.65}$$

We shall add two final remarks. First, we note that in this derivation involving the Einstein coefficients, we have considered the lower and upper states to have the same degeneracy, that is, both being singlets or both being triplet states. For transitions between singlets and triplets, a degeneracy factor of 3 needs to be taken into account appropriately [83].

Second, the definition of the oscillator strength in Eq. (1.57) may seem somewhat arbitrary. It is equivalent to the expression $f = \sigma_{\mathrm{classical}}/\sigma_{\mathrm{QM}}$, that is, a definition as the ratio between the absorption cross section $\sigma_{\mathrm{classical}}$ of a classical, three-dimensional single-electron oscillator in the Lorentz oscillator model and the absorption cross section σ_{QM} calculated from the Einstein B coefficient. When the correct units are used, this leads to the expression given in Eq. (1.57). As the Einstein B

coefficient also relates to the quantum mechanical transition dipole operator (Eq. (1.55)), the oscillator strength is a measure for how much a calculated transition rate differs from the maximum possible one that is realized in the model of the three-dimensional single-electron oscillator. A full derivation can be found in [101–103] (the latter is a revised version of the earlier manuscript).

1.4.4 Non-Radiative Transitions: Internal Conversion and Intersystem Crossing

A non-radiative transition is an *isoenergetic* transition that occurs from the zeroth vibrational level of the initial state to a *k*th vibrational level of the final state. It is usually followed by the fast and irreversible dissipation of vibrational energy to the surrounding (thermal relaxation). The isoenergetic non-radiative transition between two different electronic states is not to be confused with the subsequent vertical thermal relaxation within one electronic state. While the radiative transitions treated in the previous chapter can be indicated in a configuration coordinate diagram by a single vertical arrow, the non-radiative transition is represented by a horizontal arrow (Figure 1.26). The thermal relaxation that follows the non-radiative transition may be indicated by a sequence of vertical arrows.

Non-radiative transitions are referred to as *internal conversion*, with a rate k_{IC}, when they take place between states of the same spin manifold (e.g., $S_2 \rightarrow S_1$, $T_2 \rightarrow T_1$) and as *intersystem crossing,* with a rate k_{ISC}, when a change of spin is involved (e.g., $S_1 \rightarrow T_1$, $T_1 \rightarrow S_0$). Intersystem crossing from S_1 can occur either from the zero-point vibrational level of S_1 or from thermally populated vibrational levels of S_1. It may take place either into an excited vibrational level of T_1 or into a higher excited triplet state T_2 (or T_3, T_4, etc.) that is closer in energy to S_1. Intersystem crossing can also occur in the reverse direction, that is, from T_1 to S_1. When the energy difference between the two states is small, thermal activation of T_1 to a vibrational level that is isoenergetic with S_1 allows for the $T_1 \rightarrow S_1$ intersystem crossing. The luminescence that then results from S_1 is referred to as *thermally activated delayed fluorescence* .

The theory of radiationless transitions has been developed in the early 1960s by Siebrand, Robinson, Frosch, Jortner, Englmann, and coworkers [85, 104–110], and was found in good agreement with the experimental facts. Experimentally, the radiationless transition that has been investigated most extensively is the $T_1 \rightarrow S_0$ transition in aromatic hydrocarbons, notably polyacenes [111–119]. At later times, scientific attention also included the radiationless deactivation of this transition in organometallic complexes [120, 121]. Despite their relevance to the quantum yields of luminescence

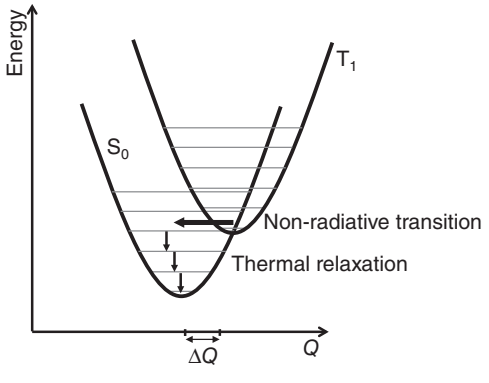

Figure 1.26 Potential energy diagram illustrating a nonradiative transition from T_1 to S_0, followed by thermal relaxation.

and photocurrent, non-radiative transitions are hardly covered in common textbooks, with the exception of the book by Birks [87], which is out of print. We shall therefore give a more extensive treatment.

The rate for a non-radiative transition can be written as

$$k_{if} = \frac{2\pi}{\hbar}\left|\left\langle \Psi_{el,i}\Psi_{vib,i}\Psi_{spin,i}\left|\hat{H}'\right|\Psi_{el,f}\Psi_{vib,f}\Psi_{spin,f}\right\rangle\right|^2\rho \tag{1.66}$$

where the perturbing Hamiltonian $\hat{H}'$ that induces the radiationless transition is the nuclear kinetic energy operator $\partial/\partial Q$. Q is a normal mode displacement. When treating nonradiative transitions, one has to go beyond the Born–Oppenheimer approximation. Siebrand [85, 122] does this by first integrating over the electronic coordinates, thus writing Eq. (1.66) as

$$k_{if} = \frac{2\pi}{\hbar}|\langle\Psi_{vib,i}|\mathcal{J}|\Psi_{vib,f}\rangle|^2\rho \;\text{ with }\; \mathcal{J} = \langle\Psi_{el,i}\Psi_{spin,i}|\hat{H}'|\Psi_{el,f}\Psi_{spin,f}\rangle \tag{1.67}$$

and then inserting molecular wavefunctions and operators. In this way, he was able to separate Eq. (1.66) into the different components [85]. He arrives at the expression

$$k_{if} = \frac{2\pi}{\hbar}\rho J^2 F \tag{1.68}$$

where J contains the electronic coupling between the two states, while the overlap of the vibrational wavefunctions of initial and final state is contained in the Franck–Condon factor F. Formally, the rate equations for the radiative and nonradiative transitions, Eqs. (1.4) and (1.68), are thus similar. We shall now discuss the factors F and J.

1.4.4.1 The Franck–Condon Factor *F* and the Energy Gap Law

The Franck–Condon factor F is given by the overlap of the overall vibrational wavefunction $|\langle\Psi_{vib,i}|\Psi_{vib,f}\rangle|^2$, where the initial state vibrational wavefunction has vibrational energy of 0, $\Psi_{vib,i} = \Psi_{vib,i}(0)$, and the final state vibrational wavefunction has a vibrational energy E, $\Psi_{vib,f} = \Psi_{vib,f}(E)$. $\Delta E = (E - 0)$ is the energy gap between the 0-0 energies of the initial and final state. Siebrand, Robinson and Frosch calculated how the Franck–Condon Factor changes with increasing energy difference ΔE [85, 104].

To describe the experimental results, it is sufficient to consider only one vibrational mode of the final state, that is the one with the highest frequency ω_M. Its vibrational quantum number υ_M is given by $\upsilon_M = \Delta E/\hbar\omega_M$. The Franck–Condon Factors for the limiting cases of a displaced oscillators and a distorted oscillator are given in Box 1.11. For the general case of a displaced and distorted oscillator, evaluation of the Franck-Condon Factor results in an exponential dependence on $\Delta E/\hbar\omega$. As J is constant with energy, this leads to an exponential dependence of the nonradiative transition rate on the energy difference between the initial and the final states. This is well known as the *energy gap law* and is expressed as

$$k_{if} \propto \exp\left(-\gamma\frac{\Delta E}{\hbar\omega_M}\right) \tag{1.69}$$

with $\hbar\omega_M$ being the vibrational quanta of the highest frequency mode, and γ is a term that can be expressed through molecular parameters [85, 104, 105, 110]. The mode involved in the Franck–Condon overlap is called an *accepting mode*. When several high-frequency modes are to be considered (Box 1.12), a correspondingly weighted term can be used though the limitation to the highest frequency mode is usually sufficient. Experimentally, the energy gap law has been well confirmed, both for organic aromatic hydrocarbons as well as for organometallic complexes and polymers (Figure 1.27).

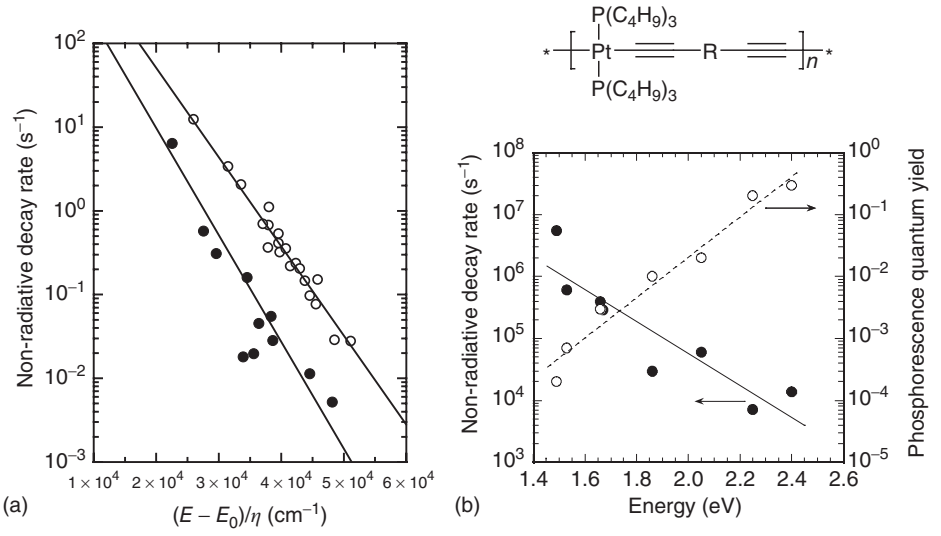

Figure 1.27 The energy gap law. (a) Example for aromatic hydrocarbons: Dependence of the non-radiative decay rate k_{nr} for a number of normal (open symbols) and deuterated (filled symbols) aromatic hydrocarbons on the normalized triplet energy $(E_T - E_0)/\eta$. η is the relative fraction of hydrogen or deuterium atoms in the molecule. E_0 is a minor correction factor related to the Franck–Condon factor crossing for displaced and distorted oscillators, and it is $E_0 = 4000\,\text{cm}^{-1}$ (0.5 eV) for protonated compounds and $E_0 = 5500\,\text{cm}^{-1}$ (0.68) for deuterated compounds. Totally deuterated molecules included are (in order of decreasing τ) benzene, triphenylene, acenaphthene, naphthalene, phenanthrene, chrysene, biphenyl, *p*-terphenyl, pyrene, 1,2-benzanthracene, anthracene. (After Siebrand and Williams [123].) (b) Example for organometallic polymers: k_{nr} and phosphorescence quantum yield as a function of the triplet state energy for a series of Pt-polymers with R = phenylene, alkoxy-substituted phenylene, thiophene, quinoline, bithiophene, quinoxaline, terthiophene, benzothiadiazole (in order of decreasing T_1 energy). The lines indicate exponential fits. (Data from Wilson *et al*. [124].)

Box 1.12 Franck–Condon Factors Involving Several Modes

A real molecule has not just one but several normal mode vibrations. This renders the expressions for the Franck–Condon factors a little more complicated [85]. When several normal modes n with frequency ω_n, vibrational quantum number m_n, and vibrational wavefunctions χ_n are involved, the overall vibrational wavefunction needs to be written as a product, $\Psi_{\text{vib,f}}(E) = \prod_n \chi_n(m_n)$. Further, the transition may take place into any state $\Psi_{\text{el,f}}\Psi_{\text{vib,f}}\Psi_{\text{spin,f}}$ with suitable total energy, implying that the general Franck–Condon factor in Eq. (1.26) becomes a sum $F = \sum_P P\left[\prod_{\substack{n=1\\ n\neq p}}^{N} |\langle\chi_{n,i}(0)|\chi_{n,f}(m_n)\rangle|\right]^2$. The operator $\sum_P P$ permutates the vibrational quanta m_n among the N normal modes. This permutation is subject to the energy conservation condition $\sum m_n \hbar\omega_n = E$. In the end, the energy gap law is recovered. Owing to the exponential dependence on the vibrational frequency, however, the use of a single highest-energy frequency is fully sufficient for most cases.

1.4.4.2 The Electronic Coupling J

J contains the coupling between the initial and final electronic state. J can be evaluated by first expanding the operator $\mathcal{J}$ in terms of normal mode displacements around the equilibrium position Q_0,

$\mathcal{J} = \sum_{n=1}^{N} \partial\mathcal{J}/\partial Q_n (Q_n - Q_0)$. This is inserted into Eq. (1.67) and evaluated to yield Eq. (1.68). In this process, Siebrand [85, 122] assumes that a single oscillator p accounts for most of the induced transition probability, and that this oscillator is only slightly perturbed by the transition. With this, he arrives at

$$J = \frac{\partial \mathcal{J}}{\partial Q_\mathrm{p}} \frac{\hbar\omega_\mathrm{p}}{2k_\mathrm{p}} \langle \chi_{\mathrm{p,i}}(0) | \chi_{\mathrm{p,f}}(0) \rangle \tag{1.70}$$

$\hbar\omega_\mathrm{p}$ is the vibrational quantum of the mode that induces the transition, k_p is the force constant of that oscillation. The mode associated with J is called a *promoting mode* for the transition.

The electronic coupling contains the electronic and spin wavefunctions (see Eq. (1.67)), implying that for spin, symmetry, and parity considerations the same selection rules apply as for the corresponding radiative transitions. Internal conversion between states of the same parity may occur nevertheless, since the radiationless transition occurs into a higher vibronic level of the final state that may differ in symmetry and parity from the zero-point level of the final state [87].

Regarding the spin, Eq. (1.67) implies that spin–orbit coupling is required for intersystem crossing to occur. A large spin–orbit-coupling thus allows for a large intersystem crossing rate. This agrees with experimental observations on the intersystem crossing rate. For example, the $S_1 \rightarrow T_1$ transition rate can be measured directly when an S_1 state is created by an excitation pulse, and then the time is measured for a $T_n \leftarrow T_1$ absorption signal to appear. Such measurements are referred to as pump–probe experiment, transient absorption measurement, or flash photolysis spectroscopy. Typical intersystem crossing rates for $S_1 \rightarrow T_1$ are $k_\mathrm{ISC} \approx 10^{12}\,\mathrm{s}^{-1}$ for organometallic complexes and $k_\mathrm{ISC} \approx 10^6 - 10^9\ \mathrm{s}^{-1}$ for organic oligomers (see also Table 1.4 further below) [96]. Intersystem crossing rates into higher triplet states are often faster due to the smaller energy gap. For example, for terthiophene, the dominant intersystem crossing channels from S_1 are the exothermic $S_1 \rightarrow T_3$ pathway and the endothermic $T_4 \leftarrow S_1$ pathway, while the $S_1 \rightarrow T_1$ route is negligible [96]. Intersystem crossing rates for the $T_1 \rightarrow S_0$ transition depend exponentially on the T_1 energy and are in the range of $0.1 - 10\,\mathrm{s}^{-1}$ for aromatic hydrocarbons [87, 93] and $10^3 - 10^6\,\mathrm{s}^{-1}$ for organometallic compounds (see Figure 1.27) [124]. This compares against corresponding radiative rates of 0.1 and $10^3\,\mathrm{s}^{-1}$, respectively.

1.4.4.3 Accepting Modes, Promoting Modes, and the Isotope Rule

From Eq. (1.68) it is evident that both, accepting and promoting modes play a role in the non-radiative transition. While the significance of the accepting modes was evident early on, the contribution of the promoting mode has only become apparent in the course of time, in particular through work on organometallic complexes and rare earth complexes [120, 121].

It may be helpful to associate some intuitive picture with these modes. To illustrate this, consider the $T_1 \rightarrow S_0$ transition in the molecule shown in Figure 1.28. Normal modes of high frequency in this molecule include the stretching vibration of the C–H bond on the benzene ring, the stretching vibration of the C–C triple bond and a breathing mode of the benzene ring. As detailed in Box 1.9, the associated vibrational quanta for these modes are $3000\,\mathrm{cm}^{-1}$ (378 meV), $2100\,\mathrm{cm}^{-1}$ (260 meV), and $1600\,\mathrm{cm}^{-1}$ (198 meV), respectively. Next consider the equilibrium geometries in the T_1 state and in the S_0 state. The calculated changes in bond lengths between S_0 and T_1 are indicated in Figure 1.28 for the model trimer phenylene ethynylene. Evidently, changing the electronic state from T_1 to S_0 is associated with changes in the carbon–carbon bond lengths in the benzene ring and along the molecular axis in the range of 2–3 pm. In contrast, the carbon–hydrogen bond length changes by 3 fm, that is, it remains largely unaffected by the electronic transition. Therefore, the electronic transition can couple to the C–C triple bond stretching vibration and to the benzene ring breathing mode, as is evident in the vibrational structure of the phosphorescence spectra. The converse also applies – these vibrations can act as promoting modes to the isoenergetic non-radiative transition from T_1 into S_0. The electronic energy associated with T_1 now needs to be accepted by an overtone of a vibration in S_0, the accepting mode, which will then dissipate it to the environment. For this transfer of energy

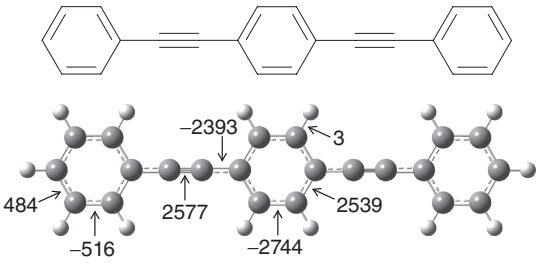

Figure 1.28 The geometry of a phenylene–ethynylene model trimer. The changes in bond length from the geometry of the ground state S_0 to excited state T_1 are indicated for selected bonds in 10^{-15} m.

to be efficient, the Franck–Condon Factor should be large, implying that the accepting mode should have a high frequency (cf. Eq. (1.69)). In the case of the phenylene ethynylene model molecule shown in Figure 1.28 as well as for the Pt-polymer show in Figure 1.27 with R = phenylene [81], the highest energy mode is the C–H stretching mode. However, the C–H mode does not couple to the electronic $T_1 \rightarrow S_0$ transition, as evidenced by its negligible displacement. This is understandable since it oscillates nearly orthogonal to the direction of both, the changes in the nuclei positions and the changes of the electron density, that accompany the electronic $T_1 \rightarrow S_0$ transition. So, despite its high frequency, the C–H mode does not act as an accepting mode. The C–C triple bond stretch, in contrast, couples well and has a high vibrational frequency that makes it suitable as an accepting mode. In this example, the C–C triple bond stretching vibration acts as both, a promoting mode and as an accepting mode. In the general case, they can differ.

The well-established way to investigate whether a mode controls the non-radiative decay as an accepting mode is to replace an atom involved by an isotope of different mass. The vibrational frequency of a mode depends on the effective mass μ of the atoms involved and the force constant k by $\omega = \sqrt{k/\mu}$. For the simple case of a stretching vibration between two atoms with mass m_1 and m_2, $\mu = m_1 m_2/(m_1 + m_2)$. Replacing one of them with a heavier atom increases the effective mass and reduces the vibrational frequency. This, in turn, decreases the nonradiative transition rate according to Eq. (1.69). A classic example for this is the replacement of hydrogen by deuterium in aromatic hydrocarbons such as polyacenes. This reduces the frequency of the C–H streching vibration from about 3000 cm^{-1} to about 2200 cm^{-1} and leads to a concomitant observed reduction in the non-radiative decay rate (Figure 1.27).

1.4.4.4 Implications of the Energy Gap Law

The energy gap law (Eq. (1.69)) has a number of consequences. One of it is that internal conversion from $S_2 \rightarrow S_1$ or from $T_2 \rightarrow T_1$ is usually fast ($\sim 10^{12}$ s^{-1}) compared to the radiative decay rate of $S_2 \rightarrow S_0$ ($\sim 10^9$ s^{-1}) or $T_2 \rightarrow S_0$, as the $S_2 - S_1$ and $T_2 - T_1$ energy gaps are small. As a result, emission always occurs from the lowest excited state of a spin manifold. This is empirically known as *Kasha's rule*. This no longer applies when the $S_2 - S_1$ energy difference becomes large, such as in excess of 1 eV, and emission from S_2 can be observed. As this was first observed for Azulene and later also for its derivatives, this phenomenon is referred to as *Azulene anomaly* [87, 125–128].

Another implication of the energy gap law is that an endothermic transition to an energetically close state may provide a faster non-radiative decay channel than an exothermic transition to a state that is at much lower energy. The temperature-dependence of the non-radiative transition rate is empirically frequently found to take a form of

$$k_{nr}(T) = k_{nr}^0 + k'_{nr} \exp\left(-\frac{E_a}{kT}\right) \tag{1.71}$$

with k_{nr}^0, k'_{nr} being independent of temperature and E_a being an activation energy.

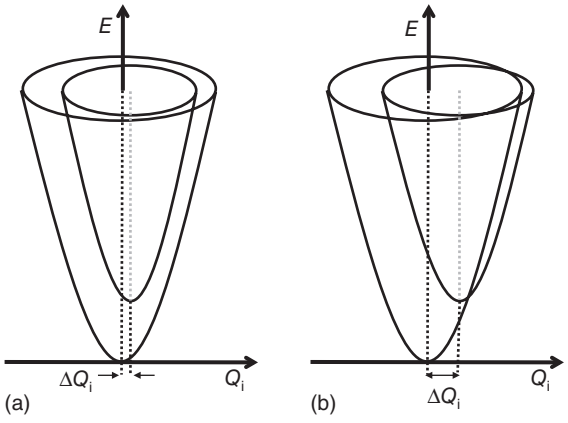

Figure 1.29 The potential energy curves (a) for the case of weak coupling and (b) for the case of strong coupling between the two states. (After Englman and Jortner [110].)

Finally, the energy gap law is also the reason why non-radiative decay rate seriously competes with the radiative rate for the $T_1 \rightarrow S_0$ transition – note that intersystem crossing is required in both cases – while for the $S_1 \rightarrow S_0$ transition, internal conversion to the ground state is negligible compared to the radiative decay. Common T_1 energies are in the range of 1–2 eV, while S_1 energies often range from 2 to 3 eV.

1.4.4.5 The Strong Coupling Limit

In general, the theory distinguishes between the two limiting cases of weak coupling and strong coupling illustrated in Figure 1.29. The above considerations and equations of sections (i)–(iv) apply to the weak coupling limit. This is the case when the potential energy surfaces of initial and final state are only weakly displaced so that the surfaces only intersect far away from the minimum of the upper state surface. For aromatic hydrocarbons, this is considered to be fulfilled [110].

Strong coupling applies when the minima of the potential energy curves of initial and final state are strongly displaced so that the potential curves intersect near to the potential minimum of the higher energy state. This case has been considered for some metal complexes, where the metal-ligand bond length can change significantly for a transition between two states [121]. The geometric reorganization energy $E_{\mathrm{rel}} = \sum_j S_j \hbar\omega_j$ is taken as a quantitative criterion to distinguish the two limits. If it is smaller than the mean vibrational energy $\hbar\langle\omega\rangle = \sum_j \hbar\omega_j/N$ of the molecule, the weak coupling limit is fulfilled. Mathematically, $E_{\mathrm{rel}} \lesssim \hbar\langle\omega\rangle$ implies the weak coupling limit and $E_{\mathrm{rel}} \gg \hbar\langle\omega\rangle \tanh(\hbar\langle\omega\rangle/2kT)$ identifies the strong coupling limit [110]. A more practical, equivalent condition is $\sum_j S_j \lesssim 1$ for the weak coupling limit and $\sum_j S_j \gg 2$ for the strong coupling limit.

In the strong coupling limit, the nonradiative transition rate becomes

$$k_{\mathrm{nr}} \propto \frac{1}{\sqrt{E_{\mathrm{rel}}}} \exp\left(-\frac{2E_{\mathrm{A}}}{\hbar\omega}\right), \quad E_{\mathrm{A}} = \frac{(\Delta E - E_{\mathrm{rel}})^2}{4E_{\mathrm{rel}}} \tag{1.72}$$

where ΔE is the energy gap between the two states. Equation (1.72) applies at "low" temperature, that is, $\hbar\omega \gg kT$, which is usually fulfilled. Compared to the weak coupling case, there are two major differences. First, the dependence on the energy gap is not exponential but Gaussian. Second, the rate is not controlled by the highest energy vibrational mode but by an effective mode of mean energy. Essentially, all vibrations can act equally as accepting modes. As a result, replacing an atom by an isotope has little effect on the transition rate. In the unlikely situation of the molecule being immersed

in a heat bath such that $\hbar\omega \ll kT$, the functionality obtained is

$$k_{\mathrm{nr}} \propto \frac{1}{\sqrt{E_{\mathrm{rel}}}} \exp\left(-\frac{E_{\mathrm{A}}}{kT}\right) \tag{1.73}$$

One may notice the formal similarity to the Marcus equation of charge transfer [129]. When Englman comes to this equation after an about 10-page-long derivation in his original paper, he succinctly comments "This equation has a general appearance of a conventional rate equation, where the energy E_{A} plays the role of the activation energy as might have been guessed by the intelligent chemist on intuitive grounds" [110].

The questions on which coupling limit applies, and on the role of accepting modes and promoting modes in the weak coupling limit have been addressed in particular for metal, organometallic, and rare earth complexes [121]. In these materials, the nonradiative decay can be very competitive to the radiative decay channel. The non-radiative decay can be reduced by replacing the atom involved in the vibrations with heavier ones, for example, replacing C–H by C–D. This method is applicable only if the nonradiative decay is controlled by a high-frequency accepting mode in the weak-coupling regime. In the strong coupling limit, this does not work.

1.4.5
Basic Photophysical Parameters: Lifetimes and Quantum Yields

Those interested in organic semiconductor devices may ask, quite justifiably, why they should care about the origins of a radiative or nonradiative transition rates. The answer is that the radiative and nonradiative decay rates control the lifetime τ of an excited state, the quantum yield of emission from an excited state, and the quantum yield of transitions between states. In this way, k_{r} and k_{nr} determine whether an organic semiconductor material is suitable for application in a LED or solar cell. This is illustrated in Figure 1.30. By definition, the radiative decay rate k_{r} gives the number of radiative decays per second, and a non-radiative decay rate k_{nr} corresponds to the number of non-radiative decays per second. Since their sum is the total number of decays per second, the inverse of it defines the lifetime of an excited state, also called the *natural lifetime*.

$$\tau = \frac{1}{k_{\mathrm{r}} + k_{\mathrm{nr}}} \tag{1.74}$$

This is the experimentally measured lifetime that appears as the decay constant in the mono-exponential intensity decay of the luminescence intensity of a state, $I(t) = I_0 \mathrm{e}^{-t/\tau}$. This is consequence of the fact that the luminescence intensity is equal to the concentration of excitations that decay per second, $I(t) = k_{\mathrm{r}} n(t)$, with $n(t) = n_0 \mathrm{e}^{-t/\tau}$ denoting the time-dependent concentration of excitations. One may also define a *radiative lifetime* $\tau_0 = 1/k_{\mathrm{r}}$ that gives the theoretical maximum lifetime the excited state may have assuming no nonradiative decay channels present.

There is usually only one significant radiative pathway that contributes to k_{r}. For a S_1 state, that is the $S_1 \rightarrow S_0$ transition. In contrast, several processes with individual rates k_{nr_i} add to the overall nonradiative decay rate $k_{\mathrm{nr}} = \sum_i k_{\mathrm{nr}_i}$. When considering an individual molecule, the nonradiative processes that can occur are the fundamental ones discussed in Section 1.4.3, that is, internal conversion with a rate k_{IC} and intersystem crossing with k_{ISC}. In a condensed phase such as a solution or a film, an excited state may further dissociate into free carriers with a rate k_{diss} or transfer its energy to another state with k_{ET}. The mechanisms for dissociation and energy transfer are discussed in Chapter 3. A general expression for the lifetime of an excited state of a molecule in the gas phase is thus

$$\tau = \frac{1}{k_{\mathrm{r}} + \sum_i k_{\mathrm{nr}_i}} \tag{1.75}$$

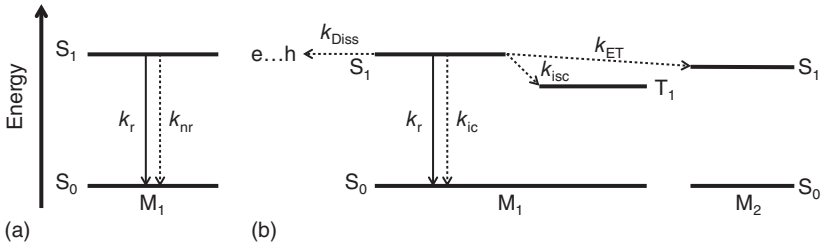

Figure 1.30 State diagram (a) indicating the radiative and nonradiative decay from S_1 to S_0 with rates k_r and k_{nr} in a general fashion. In (b) several nonradiative decay routes with their respective rates are indicated, such as internal conversion (k_{ic}), intersystem crossing (k_{isc}), energy transfer (k_{ET}) from molecule M_1 to molecule M_2, and exciton dissociation (k_{diss}).

which may include contributions such as

$$\tau = \frac{1}{k_r + k_{IC} + k_{ISC} + k_{diss} + k_{ET}} \tag{1.76}$$

as exemplified in Figure 1.30. Evidently, rates that are more than two orders of magnitude lower than others do not need to be considered in practice. For example, for the singlet excited state of an individual molecule, the internal conversion rate is insignificant, thus $\tau_{S1} = (k_{Fl} + k_{ISC})^{-1}$, while $\tau_{T1} = (k_{Ph} + k_{IC,T1})^{-1}$ for the triplet state of the same molecule. k_{Fl} and k_{Ph} denote the rate of fluorescence and of phosphorescence, respectively.

The ratio of the radiative decay rate to the total decay rate of an excited state defines its photoluminescence efficiency. Since it measures the fraction of photon quanta that decay radiatively per unit time, it is also referred to as *photoluminescence quantum yield* Φ_{PL}. The PL quantum yield thus becomes

$$\Phi_{PL} = \frac{k_r}{k_r + \sum_i k_{nr_i}} = \tau k_r = \frac{\tau}{\tau_0} \tag{1.77}$$

Accordingly, the quantum yield for fluorescence of a molecule in the gas phase is given by $\Phi_{Fl} = k_{Fl}/(k_{Fl} + k_{ISC}) = k_{Fl}\tau_{S1}$ (assuming that internal conversion is insignificant). For the phosphorescence yield, the generation efficiency of the triplet excited state needs to be taken into account. The T_1 state is formed by intersystem crossing with a quantum yield

$$\Phi_{ISC} = \frac{k_{ISC}}{k_{ISC} + k_{Fl} + k_{nr,S1}} \tag{1.78}$$

The ratio between the photon quanta emitted from the triplet state to the absorbed photon quanta is therefore

$$\Phi_{Ph} = \Phi_{ISC} \cdot \frac{k_{Ph}}{k_{Ph} + \sum_i k_{nr_i}} = \Phi_{ISC} \cdot \frac{k_{Ph}}{k_{Ph} + k_{IC,T1}} = \Phi_{ISC} k_{Ph} \tau_{T1} \tag{1.79}$$

It is useful to have some idea about the magnitudes of different photophysical parameters. Tables 1.1–1.4 provide compilation of a few selected data for a basic orientation. More extensive

Table 1.1 Experimentally measured fluorescence lifetimes.

Position	Compound	τ_{S1} (ns)	References
1	MeLPPP	0.30	[130]
2	MEH–PPV in toluene solution at 295 K	0.45	[31]
	MEH–PPV in $CHCl_3$ solution at 295 K	0.35	[131]
3	PFO	0.43	[32]
4	OPV3, OPV4, OPV5, OPV6, OPV7 in $CHCl_3$ solution at 295 K	1.70, 1.32, 0.73, 0.52, 0.45	[132]
5	PF-trimer, -pentamer, -heptamer in thin film at 295 K	0.67, 0.58, 0.52	[79]
6	Biphenyl, *p*-terphenyl, *p*-quaterpheny in cyclohexane at 295 K	16, 1.0, 0.8	[87]
7	Fluorene in cyclohexane at 295 K	10	[87]
8	Benzene naphthalene, anthracene, tetracene in cyclohexane at 295 K	30, 100, 5, 6	[87]
9	Pyrene in cyclohexane at 295 K	450	[87]
10	Perylene in cyclohexane at 295 K	6	[87]

information can be found in the books by Birks, Pope & Swenberg, and Turro for the class of organic molecules, in the book by Yersin & Finkenzeller for organometallic complexes and, for the polymers and oligomers, in the original papers quoted in Tables 1.1 to 1.4 [11, 72, 86, 87].

From the tables it is evident that the fluorescence lifetime of polymers tends to be below 1 ns. As the radiative rate for a fully allowed transition is at most 10^9 s^{-1}, the short lifetime in polymers reflects a comparable nonradiative decay rate. The reduction in lifetime with oligomer length observed for the oligomers can be attributed to both, an increase in the oscillator strength of the transition, evident from the increase in extinction coefficient, and an increase in non-radiative decay [132]. The low oscillator strength for the $S_1 \leftarrow S_0$ transitions for benzene, naphthalene, and pyrene is due to the fact that this transition is partially forbidden by symmetry selection rules. The "obvious" transition seen in the absorption spectra is therefore the allowed $S_2 \leftarrow S_0$ transition. For longer polyacenes, the energy of the allowed transition decreases below that of the symmetry-forbidden transition, thus resulting in an intense $S_1 \leftarrow S_0$ signal. Fluorescence quantum yields for polymers vary and depend on sample morphology and also purity. In contrast, quantum yields for molecules or oligomers are more uniform. Phosphorescence lifetimes for organic compounds are in the range of milliseconds to seconds, unless the T_1 state is very low as for MEH–PPV. The phosphorescence lifetime in organometallic compounds are in the microsecond regime and depend on the triplet state energy, according to the energy gap law.

1.5 Spectroscopic Methods

Photophysical parameters such as the fluorescence and phosphorescence lifetimes and quantum yields, as well as their spectra are usually measured in a film or in solution. The solution may be liquid (at room temperature), frozen (for temperatures below room temperature) , or solid (i.e., frozen at room temperature) . Typical organic solvents employed for a *liquid solution* include toluene, xylene,

Table 1.2 Fluorescence quantum yields and extinction (Eq. (1.10)) or absorption (Eq. (1.8)) coefficients. Extinction coefficients are given at the peak of the $S_1 \leftarrow S_0$ transition unless stated otherwise.

Positon	Compound	Φ_{Fl}	ϵ ($mol^{-1}\,cm^{-1}$)	References
1	PFO as (glassy phase) thin film, nematic glass, or crystal, all at 20 K	0.8 – 0.9	—	[32]
	PFO in the β-phase at 20 K	0.42		[32]
	PFO as amorphous thin film or β-phase at 295 K	0.53, 0.55		[32]
	PFO as crystal or nematic glass at 295 K	0.65, 0.80		[32]
	PF0 as glassy phase thin film		Here, α is given instead: $\alpha = 250\,000\,cm^{-1}$	[84]
2	PPV as thin film at 10 K, at 295 K	0.40, 0.08	—	[133]
	MEH – PPV in $CHCl_3$ solution at 295 K	0.35	—	[131]
3	OPV3 in $CHCl_3$ solution at 295 K	0.62	44 000	[132]
	OPV4 in $CHCl_3$ solution at 295 K	0.76	68 000	—
	OPV5 in $CHCl_3$ solution at 295 K	0.49	88 000	—
	OPV6 in $CHCl_3$ solution at 295 K	0.41	107 000	—
	OPV7 in $CHCl_3$ solution at 295 K	0.25	142 000	—
4	PF-trimer	0.41	85 100	[79]
	PF-pentamer	0.42	135 900	—
	PF-heptamer	0.44 All in thin film at 295 K	196 800 All in chlorobenzene solution at 295 K	—
5	Biphenyl	0.15	17 000 for S_2 at 5.0 eV (S_1 not observed), in light petroleum	[87]
	p-Terphenyl	0.77	33 100 for S_1 at 4.46 eV in heptane	—
	p-Quaterphenyl	0.74 All in cyclohexane at 295	36 300 for S_1 at 4.28 eV in heptane	—
6	Fluorene	0.66 In cyclohexane at 295 K	10 000 for S_1 in heptane	[87]
7	Benzene	0.06	250 for S_1 at 4.87 eV 8 800 for S_2 at 6.08 eV	[87]
	Naphthalene	0.19	270 for S_1 at 4.12 eV, 5 600 for S_2 at 4.51	—
	Anthracene	0.30	8 500 for S_1 at 3.31 eV	—
	Tetracene All absorptions in heptane All emissions in cyclohexane at 295 K	0.17	14 000 at 2.63 eV	—
8	Pyrene	0.65 in cyclohexane at 295 K	510 for S_1 at 3.53 eV 55 000 for S_2 at 3.70 eV, in light petroleum	[87]
9	Perylene in cyclohexane at 295 K	0.89	39 500 for S_1 at 2.85 eV	[87]

Table 1.3 Experimentally measured phosphorescence lifetimes.

Position	Compound	τ_{T1}	References
1	MeLPPP in mixed toluene:MTHF solution at 77 K	1.0 s	[134]
	MeLPPP in film at 10 and at 295 K	0.5 and 10^{-4} s	[135]
2	PhPPV in film at 295 K	20 µs	[136]
	OPV2, OPV3, OPV4, OPV5, OPV6, OPV7 in MTHF at 80 K	7.9, 3.6, 3.4, 3.7, 2.9 ms	[132]
3	FIrpic in CDBP matrix at 295 K	1.4 µs	[137]
4	$Ir(ppy)_3$ in solution at 295 and at 2 K	2.6, 140 µs	[72]
5	Pt-polymers in thin films at 20 K with T_1 from 2.5 to 1.5 eV	100 to 0.1 µs	[124]

Table 1.4 Illustration of the heavy atom effect on naphthalene [87].

Compound	Φ_{Fl}	k_{Fl} (s^{-1})	k_{ISC} (s^{-1})
Naphthalene	~0.2	$\sim 10^6$	5×10^6
1-Chloronaphthalene	~0.05	$\sim 10^6$	5×10^8
1-Bromonaphthalene	~0.002	$\sim 10^6$	$\sim 10^9$
1-Iodonaphthalene	~0.000	$\sim 10^6$	$\sim 10^{10}$

tetrahydrofuran (THF), chloroform ($CHCl_3$), dichloromethane (CH_2Cl_2), and many others. Good solubility of a material is obtained when the Hildebrandt solubility parameter of the solvent and the material to be dissolved, the solute, are similar (see Box 1.13). While chlorinated solvents such as chloroform and dichloromethane are popular since they dissolve many semiconducting polymers particularly well, one should keep in mind that they are more harmful than most nonchlorinated solvents and the solutions are chemically less stable.

Box 1.13 Solvents and the Hildebrand Solubility Parameter

The character of a solvent can be parameterized in terms of the Hildebrand solubility parameter δ [138]. It gives a measure for the attractive strength between molecules of a material and corresponds to the square root of the cohesive energy density. The enthalpy of mixing, ΔH, between the polymer and the solvent depends on the difference in the solubility parameters of polymer and solvent according to

$$\frac{\Delta H}{V} = (\delta_{\text{polymer}} - \delta_{\text{solvent}})^2 \Phi_{\text{polymer}} \Phi_{\text{solvent}} \qquad \text{(B1.13.1)}$$

where V is the volume of the mixture and Φ is the volume fraction. Consequently, good mixing is observed when polymer and solvent have the same δ. A few illustrative values are listed below for selected solvents and polymers. For many compounds, values of δ are quoted in common handbooks or in the technical report by the International Union of Pure and Applied Chemistry (IUPAC) [139], which also contains the refractive indices and dielectric constants of many solvents. Be aware that δ may be given either in the popular units of $\sqrt{\text{cal cm}^{-3}}$ or in SI units $\text{MPa}^{1/2}$, with

2.046 δ ($MPa^{1/2}$) = 1 δ ($cal^{1/2}\,cm^{-3/2}$). There are also other solubility parameters available that use different definitions such as the Hansen solubility parameter (Table B1.13.1).

Table B1.13.1 List of Hildebrand solubility parameters.

Compound	$cal^{1/2}\,cm^{-3/2}$	$MPa^{1/2}$
n-Hexane [139]	7.3	14.9
m-Xylene, *p*-xylene [139]	8.8	18.0
Toluene [139]	8.9	18.2
o-Xylene [139]	9.0	18.4
Ethyl acetate [139]	9.0	18.4
Chloroform [139]	9.2	18.9
Tetrahydrofuran [139]	9.3	19.0
Acetone [139]	9.6	19.7
Dichloromethane [139]	9.9	20.3
Cyclopentanone [139]	10.4	21.3
Acetonitrile [139]	11.8	24.2
Polystyrene [140]	9.1	18.7
Poly(methyl methacrylate), PMMA [140]	9.3	19.0
PFO [141]	9.1–9.3	—
MEH–PPV [142, 143]	8.9–9.4	—
P3HT [138]	9.3	—

A *frozen solution* may become crystalline or form a glass, depending on the solvent. The term *solid solution* refers to the situation where a small amount of the molecule of interest, such as a chromophore or polymer, is dissolved in an electronically inert material, the matrix. Typical matrix materials are polystyrene (PS) and polymethyl methacrylate (PMMA), also known as *plexiglass*. Both are transparent in the visible spectral range and electrically insulating. Thin films of a solid solution can be prepared by spin-coating. This is done by mixing the two materials, adding an organic solvent, putting a droplet of the liquid onto a rotating substrate and waiting for the organic solvent to evaporate.

For spectroscopic investigations, thin films of neat material, of blends or of solid solutions may be prepared on transparent substrates by a variety of techniques such as spin-coating, dip-coating, or blade-coating. Dip-coating consists essentially in dipping the substrate into the solution of material and retracting it, while blade-coating implies distributing the solvent over the substrate with a horizontal, steadily moved blade. The preferred substrate is the quartz-glass Spectrosil B, which is transparent far into the UV. Be aware that even apparently transparent substrates may have a weak absorption or emission feature that is worth checking for when observing a weak unexpected feature in a spectrum.

1.5.1
Photoluminescence Spectra, Lifetimes, and Quantum Yields

Any luminescence measurement consists of the same generic setup shown in Figure 1.31. Light from an excitation source is directed onto the sample using suitable optics. The light emitted from the sample is collected, again by suitable optics, and recorded by a detector. If one is interested in the spectrum, the emitted light needs to be dispersed in some way, for example, by placing a monochromator

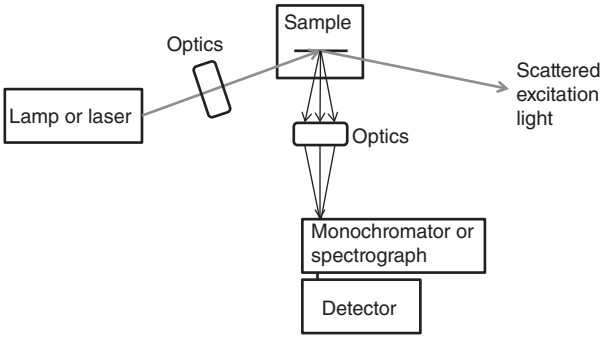

Figure 1.31 Generic setup for measuring photoluminescence. The excitation source may be a tungsten or xenon lamp, or a pulsed or continuous laser. The sample is typically either a thin film in a vacuum chamber (as shown here) or a solution in a cuvette. Optical components such as lens systems or glass fiber bundles direct the excitation and emission light. The emitted light is detected after dispersion.

or spectrograph in front of the detector. The signal recorded by the detector needs to be corrected for the spectral response of the measurement unit, that is, the spectral response of the excitation source, the optical pathway of the light, and the spectral response of the detector. This is usually done by taking a reference measurement with illumination yet without sample and dividing by it. Frequently, this step is already included in the software of the detection unit (provided it was calibrated after incorporation into the experimental setup).

If one is interested in the lifetime of the emitting state, a light pulse is used to excite the sample and the emitted light intensity is recorded as a function of time. Correction for the temporal response of the detection unit is only required when the decay time of the signal comes close to the temporal response of the detection unit.

The various measurement techniques differ only by the choice of excitation source and detection unit. These choices are dictated by the excitation mode needed (continuous or pulsed) and the time scale desired for the detection. Concerning the optics, a combination of lenses may be used or, alternatively, a glass fiber bundle. While combining lenses requires a little knowledge about the laws of optics, glass fiber bundles are very easy to use.

1.5.1.1 Steady State Spectra and Quantum Yields

A simple way to measure the time-integrated luminescence spectrum is to place the sample in a fluorescence spectrometer and to press the "run" button. In these machines, light from a xenon lamp or a deuterium lamp is directed onto the sample, which may be a film on a substrate or a solution in a cuvette. The light emitted from the sample is then dispersed by a monochromator and detected using a photomultiplier tube or a photodiode. Such fluorescence spectrometers provide a convenient means to measure a large number of samples in a short space of time. When using them for thin film measurements, care should be taken that the sample space containing the film is well purged with nitrogen to avoid accidental photooxidation of the sample. Solutions should be well dilute, preferably at concentrations below 10^{-6} mol of chromophore per liter of solvent, to avoid self-absorption (Figure 1.32). Self-absorption happens if light emitted from a higher-energy chromophore is reabsorbed by a lower-energy chromophore. (Keep in mind that the energy of chromophores varies slightly due to interactions with the solvent as detailed in Chapter 2, so that there is always a distribution of chromophores at different energies present in a sample.) In a spectrum, self-absorption can be identified if the energetic spacing between the 0-0 and 0-1 peaks reduce with increasing concentration, while the spacing from the 0-1 to 0-2 peaks remains constant.

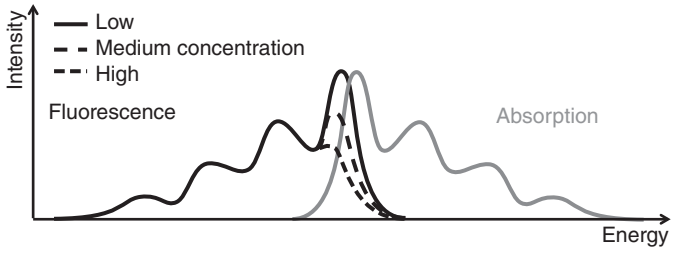

Figure 1.32 Schematic illustration of the spectral changes associated with self-absorption. The increased re-absorption of emitted light when the sample is more concentrated reduces the intensity of the 0-0 vibrational peak and leads to an apparent shift of the peak position to lower energies.

The advantages of a home-made set-up are a larger flexibility in the choice of excitation and detection components and a precise control over the measurement geometry. Instead of a monochromated xenon or deuterium lamp, one may use continuous wave (cw) lasers (argon-ion lasers, helium-cadmium lasers, or solid state lasers) which deliver high excitation intensities albeit at discrete wavelengths. For temperature control, the sample may be placed in a nitrogen or helium cryostat, preferably in vacuum or alternatively in an inert gas to prevent photooxidation. The traditional time-consuming method of detecting the emitted light with a photomultiplier behind a monochromator and then scanning the monochromator through a wavelength range is largely replaced by the use of a spectrograph in front of a CCD-camera (charge-coupled-device-camera). A monochromator and a spectrograph both consist of a box with grating in it that disperses the incoming light. The only difference is that a monochromator has a small exit slit so that the exiting light has a narrow wavelength range of 1 nm or less, while a spectrograph has a wide exit hole that yields a dispersed band of light that may be as wide as 400 nm. A CCD camera has a detector array. When the dispersed light band falls onto the detector array, each pixel records the light intensity of a particular wavelength interval. For example, if 400 nm are mapped onto 1240 pixels, each pixel records roughly the intensity from a 0.3 nm interval. The intensities obtained by the different pixels can be read out electronically, yielding the spectrum immediately.

When time-integrated spectra are recorded, one measures the emission from the state with the highest quantum yield. For organic compounds, this is the fluorescence from the S_1 state. In organometallic complexes, this is mostly the phosphorescence from T_1. When the spectral shape changes as a function of temperature, for example, when heating from 10 K to room temperature, then this reflects a temperature activation of a transition rate between two states. This can be a temperature-dependent change between emission from two different conformations of a molecule, or between emission from a monomeric state and an excimer state, or between fluorescence and phosphorescence, or between a donor and an acceptor molecule, provided the energy transfer requires thermal activation.

To measure the photoluminescence quantum yield (PL QY) of a thin film, one needs to know the number of absorbed photons and the number of photons that are emitted from the film in any direction. This is best obtained by placing the film in the middle of a nitrogen-purged sphere that is coated with a diffuse, uniformly reflective paint. Such a sphere is called *Ulbricht-sphere* or *integrating sphere*. Emitted light hitting the surface of the sphere is reflected multiple times. This creates a uniform photon flux in the sphere that is independent of the initial direction in which the light was emitted. A first-order estimate of the quantum yield can be obtained from a sequence of two measurements. First, a small laser beam is let into the empty sphere through a small hole. Through another small hole, the spectrum in the sphere due to the scattered laser light is collected using a glass fiber coupled to a spectrograph and a CCD camera. It shows an intense peak at the laser wavelength. Next, the sample is placed in the middle of the sphere, and the laser is directed to hit the sample. Again, the spectrum of the scattered light is collected. It shows the light emitted by the sample as well as the scattered laser light. The intensity of the peak by the laser is now reduced since some of the laser light had been

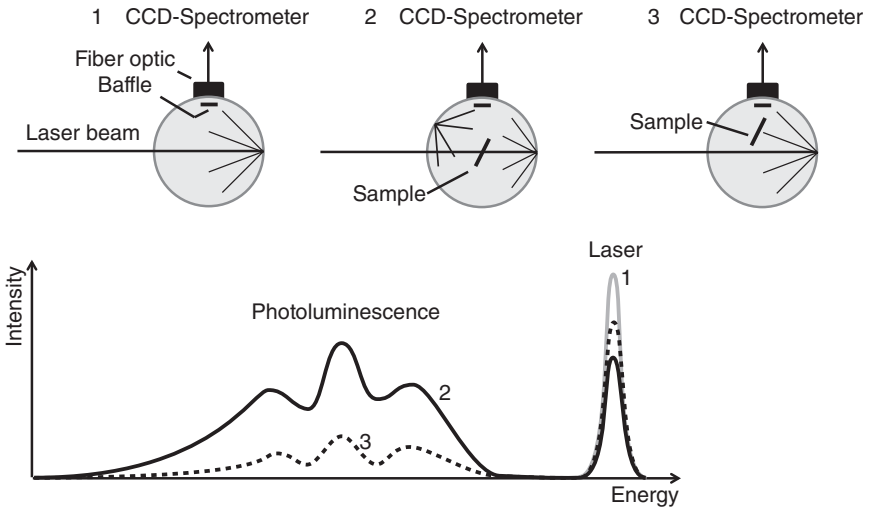

Figure 1.33 Illustration of the measurements conducted to measure PL QY showing the configuration of the sphere (top) and the spectrum obtained (bottom). First, the laser is directed into the empty sphere (1), giving the photon flux at the laser wavelength (gray line). Next, the sample is placed in the sphere and excited (2), giving the photon flux of fluorescence and the flux of the incident laser photons reduced by the absorbed laser photons (black line). Finally, a measurement with the sample in the sphere and the laser missing it is made (3) to correct for absorption of scattered laser light (dotted line). (After deMello *et al*. [144].)

absorbed by the sample. The difference in the area under the laser peak measured with and without the sample in the integrating sphere corresponds to the number of absorbed photons. The area under the spectrum in the wavelength region where the sample emits gives the number of emitting photons. The ratio of the emitted photons to the absorbed photons is the quantum yield. The principle of this measurement is easy. For an accurate measurement on thin films, however, one needs to correct for the fact that some of the laser light is initially reflected from the sample, then reflected from the surface of the sphere, and then absorbed by the sample. This is done by a third measurement with the sample inside the sphere, and the laser hitting the surface of the sphere (not the sample). For the detailed mathematical treatment, we refer to Ref. [144] (Figure 1.33).

While the principle of this quantum yield measurement is simple, a few things need to be attended to. First, to determine the quantum yield with good accuracy, the third measurement that corrects for absorption of the scattered laser light is essential. There are meanwhile fluorescence spectrometers available that offer integrating sphere measurements. Some of them do not correct for reabsorption. Second, the sphere needs to be well-purged with nitrogen to avoid photooxidation in the case of fluorescence measurement and to avoid triplet state quenching for phosphorescence measurements (Box 1.14). Third, it is recommendable to take the measurement at a range of excitation intensities, starting from very low ones. The results are trustworthy as long as the numbers obtained for different excitation intensities match. When the quantum yield starts reducing with increasing excitation power, unwanted bimolecular process take place and the quantum yield is no longer reliable, even though the signal-to-noise ratio may be better. Finally, this experiment relies on dividing two quantities, that is, the number of emitted photons by the number of absorbed photons. When the exciting laser is very blue, such as at 405 nm or even shorter wavelength, the detecting unit (CCD camera or photodiode) may operate at the border of its measurement range. The number of absorbed photons is then determined with significant error, and the resulting quantum yield needs to be viewed with caution. This can, of course, be avoided by appropriate detector choice.

Box 1.14 Quenching by Molecular Oxygen

Molecular oxygen, O_2, is a very efficient quencher for phosphorescence. The HOMOs of the oxygen molecule are two antibonding degenerate π-orbitals, so that the electronic ground state formed is a triplet state T_0 (Figure B1.14.1). The next higher excited states are two singlet states, S_1 and S_2, with energies of 0.98 and a 1.63 eV above the ground state. In the gas phase at low pressure, the associated excited state lifetimes are 2700 and 7 s. In solutions, these lifetimes reduce significantly, e.g. to values ranging from about 10 – 500 microseconds for S_1, depending on the solvent used. The first optically allowed transition is to a triplet state at 6.2 eV [86]. The T_0, S_1, and S_2 states are frequently denoted by the spectroscopic symbols for diatomic molecules, in this case $^3\Sigma_g$, $^1\Delta_g$, and $^1\Sigma_g$, respectively. The index 3 and 1 denote the triplet or singlet state, g indicates a *gerade* parity and the Greek letter Σ or Δ indicates the angular momentum of the molecular state along the O–O axis, analogous to the terms s and d for the angular momentum of atomic states.

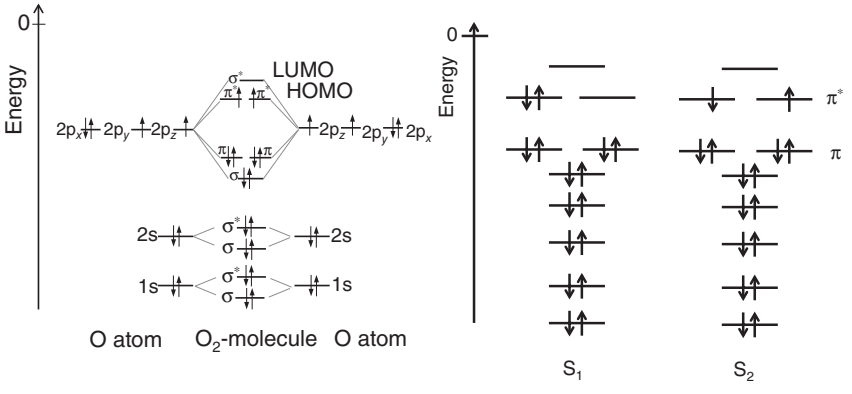

Figure B1.14.1 (a) Simple molecular orbital (MO) diagram showing how interaction of two oxygen atoms results in the triplet ground state of O_2. Note that the two degenerate HOMOs are anti-bonding π-orbitals. (b) Simple MO diagram of the first and second singlet excited state of O_2.

When a chromophore molecule in an excited triplet state, $^3M^*$, is adjacent to an oxygen molecule in the triplet ground state, $^3O_2$, energy transfer can take place. This results in an oxygen molecule in an excited singlet state ("singlet oxygen"), $^1O_2{}^*$, and a chromophore molecule in the ground state, ^1M, so that phosphorescence is no longer possible. This process may be written as

$$^3M^* + {}^3O_2 \rightarrow {}^1M + {}^1O_2{}^*$$

Since the energy level of singlet oxygen is only at 0.98 eV, this mechanism can quench most of the triplet states encountered in organic semiconductors. Singlet oxygen is chemically very reactive during its lifetime and may attack the π-bonds in organic semiconductors. This reduces the luminescence efficiency of a material and the lifetime of an OLED made with it. A common reaction, for example for polyacenes, is a peroxidation reaction of the type $^1M + {}^1O_2{}^* \rightarrow MO_2$. In the case of anthracene peroxide, the oxygen molecule bridges the (9,10-)positions of the anthracene molecule. Other well-known defects due to the reaction of (singlet or triplet) oxygen with organic semiconductors include the formation of keto-defects (C=O), for example, when breaking the vinyl bond in PPV, or when transforming a fluorene unit with incomplete sidechains into a fluorenone. Figure B1.14.2 Polyfluorenes containing such a fluorenone defect show a broad emission at 2.3 eV (540 nm), in addition to the usual, structured emission at 2.9 eV (420 nm).

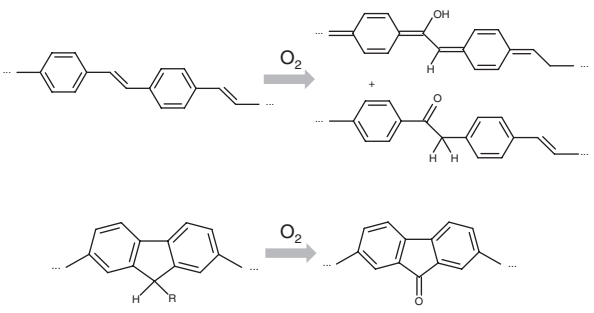

Figure B1.14.2 Defects introduced by molecular oxygen (a) at poly(*para*-phenylene vinylene) (PPV), after [145] (b) at a fluorene unit in a poly(fluorene). R may be any alkyl group, for example, C_8H_{17}. (After List *et al*. [146].)

In passing we note that ground state triplet oxygen may quench not only phosphorescence, but also fluorescence. Furthermore, it is well established that chemical defects in π-conjugated compounds occur in particular when the sample is exposed to oxygen and UV light simultaneously. A photoexcited molecule is more reactive than a molecule in the ground state and may react with the electronegative oxygen comparatively easily. This is in particular true for photoexcited π-systems, where electrons are only weakly bound. A good practice is therefore to store samples in a dark, oxygen free atmosphere, for example, in nitrogen, and to remove any residual oxygen prior to any optical measurement.

Techniques to remove oxygen from a sample involve keeping the sample under vacuum for an extended period in case of a film. For a solution, oxygen can be removed effectively by freezing the solution in a closed cuvette and then pumping off the oxygen that has been released as a gas into the space above the frozen solution. Then close the valve to the pump, bring the solution to room temperature and repeat the procedure several times. The alternative method of bubbling an inert gas such as nitrogen through the solution from a needle connected to a nitrogen line for a certain time is not as efficient.

More information on the photophysics and photochemistry of molecular oxygen may be found in [86, 87].

1.5.1.2 **Spectra and Lifetimes in the Nanosecond to Second Range**

In organic compounds, phosphorescence cannot be measured by a steady state measurement due to the low phosphorescence rate compared to the much higher fluorescence rate. It implies that the phosphorescence signal cannot be discerned from the tail of the much more intense fluorescence signal. Therefore, the excitation source needs to be a pulsed laser such as an Nd:YAG laser with ns pulses or a pulsed Xenon lamp, both operated at 10 Hz or lower frequency (to avoid re-excitation before the triplet has entirely decayed). The detection unit consists of a spectrograph coupled to a gated intensified charge-coupled-device-camera (iCCD). After the excitation pulse, one waits until all of the fluorescence has decayed, typically a few nanoseconds. Then the detector gate is opened and left open for a sufficiently long time to collect any of the few photons possibly emitted from the triplet state. This may take between a microsecond and a few seconds, depending on the phosphorescence rate. The read-out of the detector array then yields the phosphorescence spectrum. Sometimes, one observes an additional signal that is identical to the steady state fluorescence in spectral shape and wavelength range, even though the delay time between laser pulse and detection far exceeds the fluorescence lifetime, and this additional signal may have a long lifetime such as a few microseconds. In this case, the S_1 state has been repopulated from a long-lived state such as the T_1 state or a CT state, and the emission is referred to as *delayed fluorescence*. In the recent literature, obtaining delayed

fluorescence from T_1 has also been described as *non-resonant triplet up-conversion* [147–149]. Different mechanisms that cause delayed fluorescence are discussed in Chapter 3.

The lifetime of the phosphorescence (or any other type of luminescence) can be determined by measuring the decay of the luminescence intensity as a function of time and fitting this to an exponential decay function

$$I(t) = I_0 e^{-\frac{t}{\tau}} + c \tag{1.80}$$

where c is the baseline given by the detector noise level. To this end, one excites the sample with a nanosecond pulse. The emitted light is dispersed through a monochromator and detected by a photomultiplier connected to an oscilloscope, which records the decay curve. Alternatively, the emitted light is recorded as a spectrum, by using a spectrograph coupled to iCCD, and the delay time between pulse and detection window is shifted stepwise (with a step width exceeding the gate width to avoid overlap). The intensity at a particular wavelength is then read off the spectrum for different delay times, and by this the decay curve is constructed. Sometimes, there are two distinct decay channels by which an excited state can decay. In this case, the use of a biexponential decay curve

$$I(t) = I_1 \exp\left(-\frac{t}{\tau_1}\right) + I_2 \exp\left(-\frac{t}{\tau_2}\right) + c \tag{1.81}$$

can be appropriate. The two lifetimes τ_1 and τ_2 should then always be quoted in combination with the two amplitudes I_1 and I_2, as the four quantities are not independent of each other. Fitting more than two exponentials to a non-mono-exponential decay curve rarely has any physical meaning. In disordered organic semiconductors, there frequently is a statistical distribution of radiative or non-radiative transition rates, and subsequently of lifetimes. This is the case, for example, when there is energy transfer to an acceptor or quencher that is randomly distributed in the sample. When a Gaussian distribution function is convoluted with an exponential decay function, this leads to a functional dependence known as *stretched exponential*,

$$I(t) = I_0 \exp\left(-\left[\frac{t}{\tau_1}\right]^{\alpha}\right) + c \tag{1.82}$$

as illustrated in (Figure 1.34) [150–152]. It is convenient to display Eq. (1.82) on a double logarithmic plot as $\ln(\ln(I(t)/I_0))$ against $\ln(t/\tau_1)$, which gives a straight line with slope α. This form is also known as *Kohlrausch–Williams–Watt plot*. For $\alpha = 1$, a mono-exponential decay is recovered, while $\alpha = 1/2$, 1/3, and 1/6 can indicate a 3D, 2D, and 1D energy transfer process, respectively, to a random distribution of acceptors (see also Förster transfer, Chapter 2).

1.5.1.3 Spectra and Lifetimes in the Picosecond to Nanosecond Range

To measure the time evolution of fluorescence spectra, one excites using a fast pulse such as a 100 fs pulse from a Ti:Sapphire laser. The emission can be detected using a spectrograph with a *streak camera* attached. Similar to the case of a CCD camera, a wide band of emitted light falls onto the camera thus providing the spectral dispersion required. The light falls onto a photocathode where it hits out electrons. Under the influence of a (horizontal) electric field, the electrons move to a counter electrode that is covered with a phosphor, just as in a cathode ray tube. To obtain the temporal dispersion needed, one applies a vertical electrical field that increases with time (the "streak"), as in an oscilloscope. The first photons to arrive at the camera will experience only a small vertical electric field and will be deflected little, while the photons arriving later will be subjected to a larger vertical field resulting in a larger deflection. In this way, a two-dimensional picture is created on the phosphor, with the horizontal axis corresponding to the wavelength dispersion and the vertical axis mapping the temporal dispersion. Behind the phosphor, there is a two-dimensional CCD array to read out the signal intensity at each point. The resulting data is three dimensional and is usually displayed as a color-coded, two-dimensional picture. The abscissa displays the wavelength range, the ordinate gives the time range, and the color or grayscale encodes the intensity (Figure 1.35). From this, the spectrum at a specific time and the decay curve at a specific wavelength can be readily extracted.

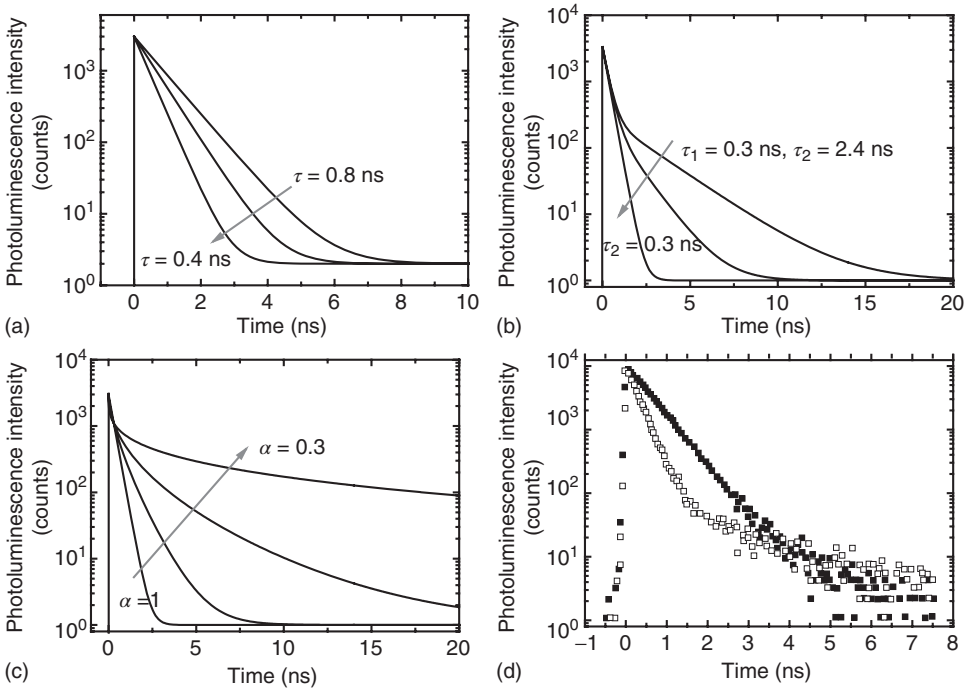

Figure 1.34 Luminescence decays. (a) Schematic of a monoexponential decay $I(t) = I_0 e^{-t/\tau} + c$ with lifetimes of $\tau = 0.8$, 0.6, and 0.4 ns. (b) Schematic of a monoexponential decay with $\tau_1 = 0.3$ ns and two bi-exponential decays according to $I(t) = I_0 \exp(-t/\tau_1) + I_0 \exp(-t/\tau_2) + c$ with τ_1 kept at 0.3 ns and $\tau_2 = 1.2$ and 2.4 ns, respectively, shown on a semilogarithmic scale. (c) Schematic of a stretched exponential decay $I(t) = I_0 \exp(-[t/\tau_1]^{\alpha}) + c$ with $\tau = 0.3$ ns on a semi-logarithmic scale for different values of α. (d) Experimental example for a monoexponential with $\tau_1 = 0.8$ ns (full symbols) and an bi-exponential luminescence decay signal with $I(t) = 10^4 \exp(-t/0.8\,\text{ns}) + 10^2 \exp(-t/1.7\,\text{ns}) + 1$. The data is taken from a thin film at room temperature containing a fluorene-trimer (full symbols) and a fluorene-trimer doped with 2 mol% of an anthracene derivative (open symbols). (Data from Albuquerque *et al.* [79].) For an experimental example of a stretched-exponential decay, see Figure 50 in Chapter 3.

A different technique to record the decay curve is *Time-Correlated Single-Photon Counting (TCSPC)*. Here, the sample is excited with a pulsed diode laser at low intensity. After the excitation pulse, a timer counts the time until the detector (a photomultiplier tube after a monochromator) records the arrival of a single photon. This procedure is repeated many times. Displaying the number of photon counts against time then yields the decay curve. When this is done for multiple wavelengths, a spectrum can be constructed.

1.5.1.4 Spectra and Time Scales below the Picosecond Range

A technique to measure emission with spectral resolution below the picosecond time regime is *two-photon upconversion*. This experiment requires some knowledge and skill in non-linear optics. A laser pulse, for example, the 120 fs pulse from a Ti:Sapphire laser, is divided into two beams using a beam-splitter. One beam (1) is used to excite the sample, and the emitted fluorescence is directed into a non-linear optical crystal. The other beam (2) is directed over a longer light path to create a well-controlled time delay Δt between beam 1 and beam 2 and then also enters the non-linear crystal. Non-linear crystals have the property that if a light with frequency ω_1 and light with frequency ω_2 meet at the same time (and under the right angle), some light with the sum frequency

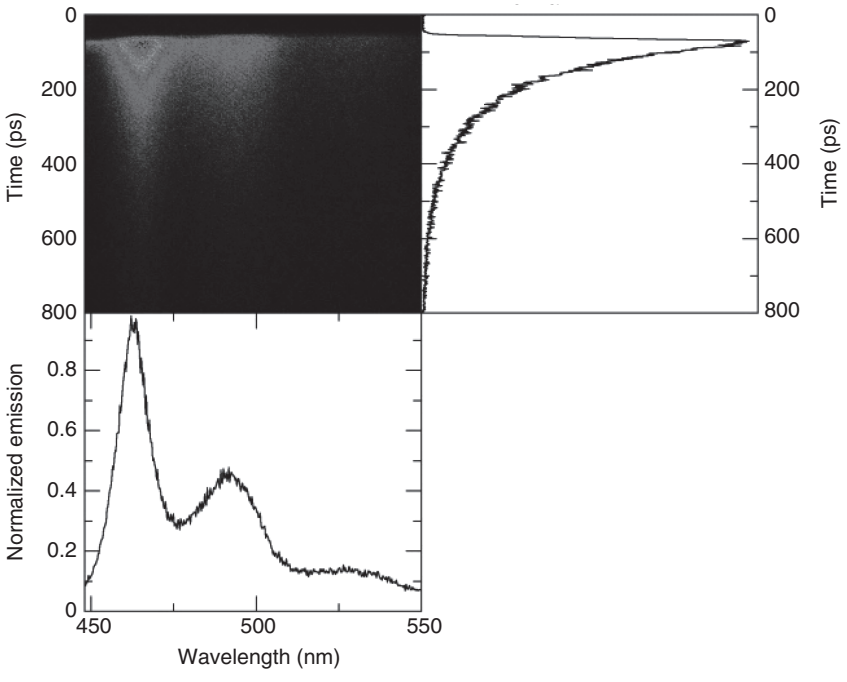

Figure 1.35 Two-dimensional plot of a lifetime measurement for MeLPPP. The abscissa indicates the wavelength, the ordinate indicates the time, the color or gray scale indicates the intensity. A cut at a fixed lifetime yields a spectrum, shown on bottom. A cut at a fixed wavelengths results in a decay curve, plotted on the right. (Data from R. Hildner, Bayreuth.)

$\omega_3 = \omega_1 + \omega_2$ is emitted. Thus, if beam 2 and the beam of the sample fluorescence meet at Δt in the non-linear crystal, light at a shifted frequency is emitted. This light can be dispersed by a spectrograph and recorded using a CCD camera to yield a spectrum. A high time resolution can be obtained by adjusting the time delay of beam 2 with respect to excitation beam 1. In a refined version of this experiment, no separate nonlinear crystal is employed. Rather, the organic semiconductor sample also acts as nonlinear material.

1.5.2 Excited State Absorption Spectra

The approach taken to measure the absorption from a molecule in the ground state has already been introduced in Section 1.4.2. Absorption can also occur from an excited state during the lifetime of that state. The only requirement is that the excited state absorption (ESA) rate is higher than the excited state decay rate. This experiment requires two excitation sources. One source is used to illuminate the sample such as to create an excited state. For obvious reasons, this light beam is called the *pump beam*. The other source is employed to measure the absorption of the excited sample. This is the probe beam. Its attenuation by the sample is measured with a detector unit (Figure 1.36). Analogous to the photoluminescence measurements, different time regimes for this experiment require different excitation and detection equipment.

1.5.2.1 Steady State Spectra (Photoinduced Absorption)

When the probe beam is continuous, this technique is also called *photoinduced absorption* measurement and abbreviated with PiA or PA. The pump beam is typically an intense beam of about

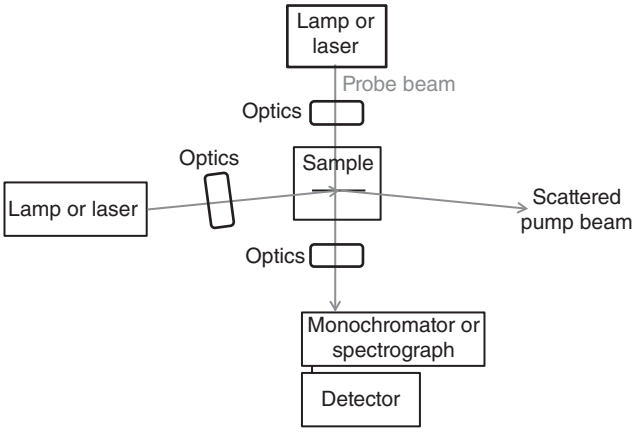

Figure 1.36 Generic setup to measure photoinduced absorption. The sample (film or solution) may be excited ("pumped") using a continuous or pulsed laser. The absorption of the excited sample is recorded using a "probe" beam from a continuous tungsten lamp, a pulsed xenon lamp, or a pulsed white-light continuum from a laser and non-linear crystal. The detector may be a CCD camera coupled to a spectrograph or, less frequently, a photodiode behind a monochromator. Time-resolution can be obtained by using pulsed light sources and delaying the probe beam with respect to the pump beam.

100 mW cm^{-2} from a laser such as an argon-ion laser. The sample is placed in vacuum to avoid photooxidation, or an oxygen-free solution is used (Box 1.14). The probe beam comes usually from a tungsten lamp. Tungsten lamps can run very stably and are particularly intense in the visible and near infrared spectral range. This is just the range where the absorption features from excited states tend to appear. The probe beam hits the sample normally to its surface and is transmitted. The transmitted light is directed into a monochromator, and the dispersed light is collected at the monochromator exit by a silicon photodiode or a similar detector. The quantity detected is the relative transmission with and without the pump beam, $\Delta T/T$, which is typically in the range of $\Delta T/T = 10^{-4}$. In order to measure the transmission with and without pump beam, ΔT, a mechanical chopper is placed in the path of the pump beam, and the signal detected by the photodiode is recorded with a lock-in amplifier. To get a spectrum, the monochromator needs to be stepped through the desired wavelength range, and the PiA signal is recorded at each point. To normalize, a transmission spectrum without laser excitation, T, is also taken with the sample in the setup. No correction is required to account for the spectral response of the experimental setup as this is implicitly included when forming $\Delta T/T$.

With such a cw probe beam, the absorption features one measures are the ones from long-lived excited states such as triplet states, CT states or from charges that have been created after dissociation of an excited state. The $T_1 \rightarrow T_n$ transition is typically found around 1.5 ± 0.2 eV (830 ± 100 nm) for semiconducting polymers and at higher energy for oligomers [132, 153] (Figure 1.37).

It is possible to measure the lifetime of these states by changing the frequency of the mechanical chopper and recording the change in signal intensity. When the period with ("on") and without ("off") pump beam becomes shorter than the decay time of the excited state, an excited state population is still present in the "off" period. Consequently, the difference in transmission between the "on" and the "off" period reduces, and the lock-in detector records a drop in intensity. Dellepiane and coworkers used the rate equations for the photogenerated species to show that the intensity relates to the chopper frequency ω and excited state lifetime τ as

$$I(\omega, \tau) = A \frac{\tau}{\sqrt{1 + (\omega\tau)^2}} \tag{1.83}$$

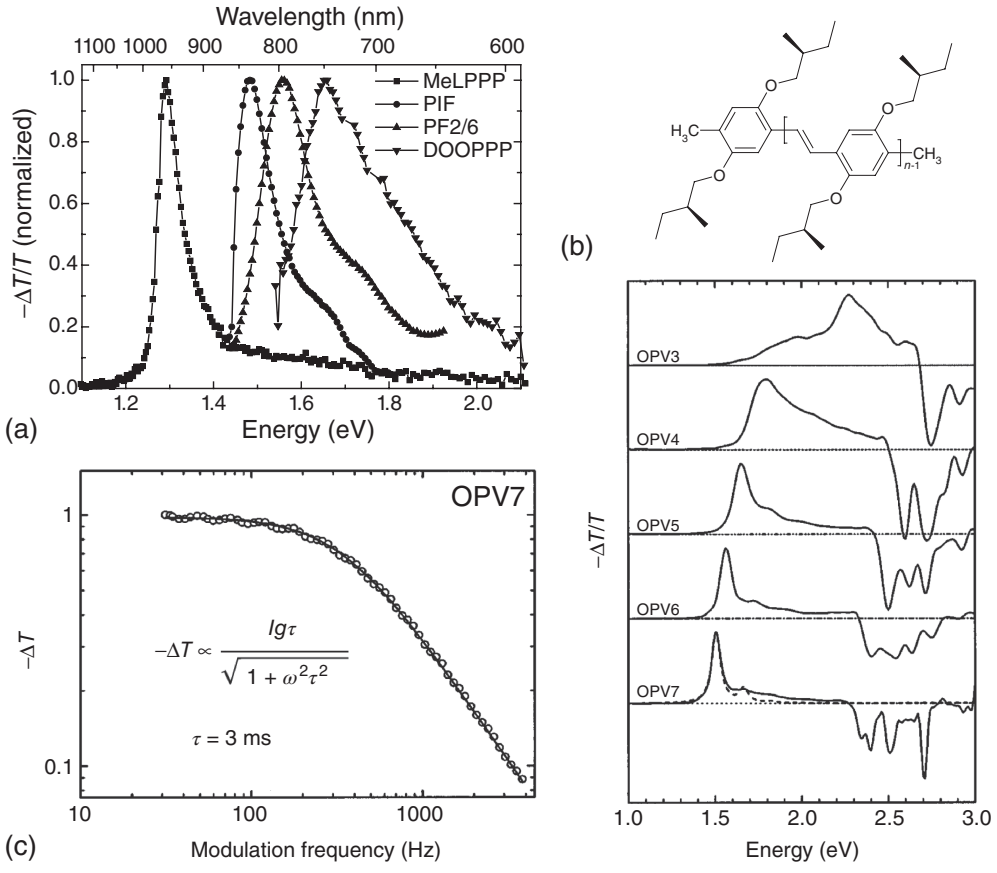

Figure 1.37 Steady-state photoinduced absorption (a) of the $T_n \leftarrow T_1$ absorption in thin films of the polymers MeLPPP, PIF (poly(indenofluorene)), PF and DOOPPP, taken at 5 K, from K. Huber, Bayreuth, and (b) of the $T_n \leftarrow T_1$ absorption at 1.5–2.3 eV of the OPVs (oligo-phenylene vinylenes) shown above in MTH solutions at 100 K. The signals with inverse sign above 2.3 eV are due to the ground state bleach (see below) (Data from [132].) (c) Intensity dependence of the PIA (photoinduced absorption) band at 1.50 eV of OPV7 in 2MeTHF at 100 K as a function of the modulation frequency of the excitation beam, as well as a fit to the equation shown. (Data from Peeters *et al*. [132].)

with A being a fitting constant [154]. This equation holds for a monomolecular decay. Their paper also treats the bimolecular case. This method is limited to excited state lifetimes of milliseconds and longer by the fact that mechanical choppers do not rotate stably beyond 4000 Hz.

1.5.2.2 Spectra in the Nanosecond Range (Flash Photolysis)

The same measurement at higher time resolution is known as a *transient absorption measurement* or *flash photolysis*. It is a well-established technique that has been widely employed to record the transient absorption from triplet excited states or charged states in organic molecules, as its time resolution matches the lifetime of triplet and charged states. In this experiment, one uses a pulsed excitation source, for example, an Nd:YAG laser with 7 ns pulses at 10 Hz. The probe beam is typically a pulsed xenon lamp (a "flash lamp"). Operating the lamp in pulsed mode allows for high light intensities. The difference in transition from the Xenon lamp with and without the laser pulse, normalized to the total transition, $\Delta T/T$, can now be obtained for different delay times between the pump beam

and the probe beam, and this is what yields the time resolution of the measurement. Analogous to the case of emission measurements, two detection modes are possible. One may either record how the intensity of $\Delta T/T$ changes with time at a fixed wavelength by placing for example, a Si-diode behind a monochromator, or one may take the spectrum of $\Delta T/T$ at a certain time after excitation by using a spectrograph coupled to an iCCD camera.

1.5.2.3 Spectra in the Femtosecond Range (fs Pump–Probe Measurements)

A correspondingly higher time resolution is required for excited states with a shorter lifetime. As already mentioned, the time dependence in the measurement results from the time-delay between the excitation (pump) pulse and the probe pulse. Of course, there is no point in having, say, a 300 fs delay between pump and probe pulse if the pump pulse itself has a width of 7 ns. For a high time resolution one therefore requires short pump pulses, such as pulses of about 100 fs duration supplied from a Ti:Sapphire laser. This laser emits around 800 nm, while most molecules require excitation in the blue spectral range. This can be arranged by sending a laser pulse with suitable polarization and incident angle through a nonlinear crystal (e.g., β-barium borate (BBO)). In the crystal, a nonlinear optical process converts incoming high-intensity light of one wavelength such as 800 nm into lower intensity light with half the wavelength, that is, 400 nm (*frequency-doubling*). Next, one needs a probe beam with a well-defined delay with respect to the pump beam. This can be obtained by splitting the pump with a semitransparent mirror into two parts. Part one is still used as pump beam and is directed onto the sample. Part two is employed as probe beam. The time delay with respect to the pump is obtained by directing the probe beam over a longer optical path distance using mirrors. When the mirrors are set on translation stages (delay stage), control over the pump–probe time delay is easily reached by modifying the path length. For example, a total path difference of 150 µm between pump and probe translates into a time delay of 500 fs, according to $\Delta x = c\Delta t$ with c being the speed of light, $c = 3 \cdot 10^8\,\mathrm{m\,s^{-1}}$. With this, the setup consists of a short pump pulse and an equally short probe pulse with a well-defined delay time between them, but, unfortunately, also with the same wavelength. For a useful experiment, the probe beam needs to be at a different wavelength, preferably even dispersed to cover at a range of wavelengths. This can be obtained by directing the probe beam (at suitable polarization and incident angle) through a sapphire plate that, by a nonlinear optical process, disperses it into a beam with wavelengths covering the visible spectral range (*white light*). The UV pump beam now excites the sample, and at a fixed delay, the white-light probe beam is transmitted through it. The spectrum of the probe beam, with and without pump, is recorded by a CCD camera for different pump–probe delays. The time evolution of the signal at a particular wavelength is constructed by reading the intensity in the spectra taken at different times.

A typical example for a femtosecond pump–probe signal is shown in Figure 1.38 for a range of polymers. Changes in the absorption signal that occur upon pumping are illustrated in Figure 1.39 and include [155]

- a reduced absorption (*ground state bleach*) (GSB) since some of the chromophores are still in an excited state, so they cannot absorb incident light,
- an additional absorption from the chromophore in the S_1 singlet excited state to a higher lying singlet excited state ESA or $PA_{S\text{-}EXC}$. At longer delay times, an additional absorption may also occur from the T_1 triplet excited state to a higher lying triplet state (ESA or $PA_{T\text{-}EXC}$),
- an additional absorption from a charged chromophore (*polaron absorption*) (PA_{CS}) that is formed when the S_1 state created by the pump pulse dissociates into a positive and negative charge (see Chapter 2),
- an additional photoluminescence (*SE*) that occurs because photons from the probe beam stimulate emission from the S_1 state generated by the pump beam.

PA signals show up in the spectra as a reduction in the transmission (i.e., negative sign of $\Delta T/T$), SE and GSB signals give an increased transmission. The GSB is easily identified as it occurs at the wavelength of the usual absorption signal. Similarly, the SE coincides with the fluorescence spectrum.

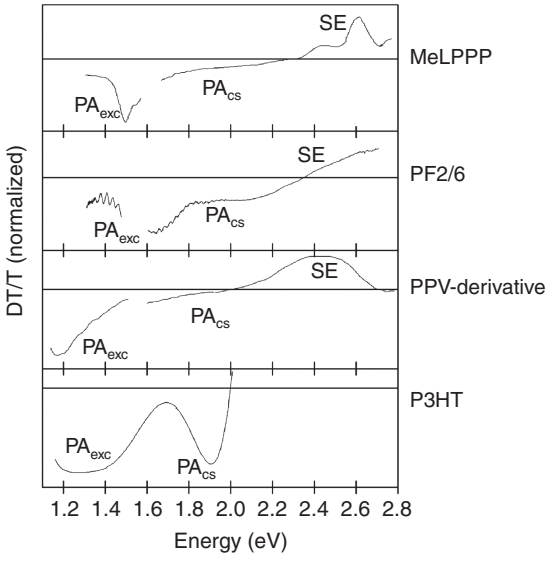

Figure 1.38 The photoinduced absorption spectra of the polymers indicated taken with a pump-probe delay in the range of 100 fs to 10 ps. (Figure adapted from Cabanillas-Gonzalez [155] with data from Cerullo *et al*., Cabanilla-Gonzalez *et al*., and Kraabel *et al*. [156–159].) SE, PA_{cs}, PAexc denote the processes of stimulated emission, photoinduced absorption from a charged state, and photoinduced absorption from a (singlet or triplet) exciton, respectively.

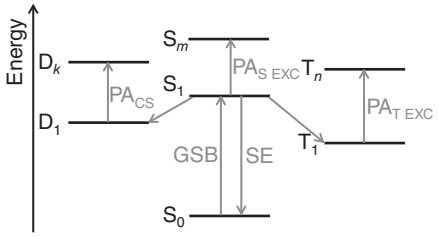

Figure 1.39 Schematic of the different transitions that may be observed in photoinduced absorption spectra (gray thick arrows). S, T, and D denote a singlet exciton, triplet exciton and a charged state, respectively. PA, SE, and GSB stand for photoinduced absorption, stimulated emission, and ground state bleach. Dotted lines indicated nonradiative transitions after excitation.

In polymers, PA signals from $T_n \leftarrow T_1$ transitions are frequently observed around 1.5 ± 0.2 eV, while PA signals from charges are common somewhere broadly around 2 eV and around 0.5 eV (see also Chapter 2). A simple way to confirm the PA signal of a charged molecule is to dope the molecule extrinsically and to measure the normal, linear absorption spectrum for comparison (see Chapter 2). PA signals from triplet and singlet state absorption can be differentiated by their lifetime, with the triplet needing more time to form and more time to decay.

1.5.3
Fluorescence Excitation Spectroscopy

In a conventional absorption experiment, one measures the difference in the transmission of the light beam with and without the absorber in the path of the light. For weak absorbers, this can become

difficult. In that case, *fluorescence excitation spectroscopy* (FLE) is a helpful technique, provided that the sample is fluorescent. One detects the fluorescence of the sample as a function of the excitation energy. If the non-radiative decay from the sample is independent of excitation energy, then the emission intensity will be proportional to the absorption of the sample, and one obtains a direct portrait of the absorption spectrum. For some samples, a different non-radiative decay path may become accessible upon increasing the excitation energy. In that case, the FLE spectrum differs from the absorption spectrum, and concomitantly, this difference can be employed to identify such processes, which may include energy transfer processes or photodissociation.

When conducting the experiment, the measurement geometry needs to be selected with care to avoid artifacts from self-absorption. A geometry where the exciting laser beam hits the sample surface (film or cuvette) under a flat angle of incidence while the emitted luminescence is detected normally tends to work well (as illustrated in Figure 1.31). The standard geometry in commercial luminescence spectrometers, where a 1 cm cuvette of solution is excited and the luminescence is detected at 90° angle only works for very dilute solutions and is particularly prone to self-absorption effects.

1.6 Further Reading

The electronic properties of organic semiconductors require knowledge from a wide range of fields. The topics covered in this first chapter draw from the areas of synthetic chemistry, polymer science, crystallography, quantum mechanics, photophysics, and spectroscopy. Later chapters will further include issues from semiconductor physics, device physics, engineering, and material science. This book can merely give an introduction to the electronic properties of organic semiconductors. It aims to provide an initial orientation that allows the reader to follow up different threads in more depth. We list here some literature that may be useful to this purpose. By nature of being a selection, it is not comprehensive and it reflects our own preferences. The literature is listed in the context of the section that it substantiates further.

Section 1.2 on Different Organic Semiconductor Materials: More information about the structure of crystalline organic semiconductors can be found in the book by Schwoerer and Wolf, *Organic Molecular Solids* [12]. For a brief introduction into polymer physics, we recommend Chapter 2 in the book *Introduction to Soft Matter* by Hamley [56] and Chapter 5 in the book *Soft Condensed Matter* by Jones [160], while more extensive treatment is given in the book *The Physics of Polymers* by Strobl [161]. Issues pertaining to the synthesis of semiconducting polymers are discussed in a number of edited books, for example, Chapters 1 and 2 in the book *Semiconducting Polymers*, edited by Hadziioannou and Malliaras [62, 63].

Section 1.3 on Electronic States of a Molecule: The concepts of bonding, molecular orbitals, and states are very well explained in the books *Molecular Physics* by Demtröder and *Molecular Quantum Mechanics* by Atkins and Friedman [64, 65].

Section 1.4 on Transitions between Molecular States: There are a number of books that introduce these topics. Pope and Swenberg, as well as Birks, have written the corresponding chapters of their books with a particular view to organic semiconductors, and both books may be considered classic for those working in the field. The book by Birks, *Photophysics of Aromatic Molecules*, is highly recommendable [87]. Its only disadvantage is that it is out of print, though available in many scientific libraries. Pope and Swenberg's book *Electronic Processes in Organic Crystals and Polymer*s is available as a second edition [11]. Another good introduction to transitions between molecular states can be found in *Modern Molecular Photochemistry* by Turro and the expanded version *Modern Molecular Photochemistry of Organic Molecules* by Turro, Ramamurthy, and Scaiano [86]. It has a strong emphasis on visualizing the photophysical and photochemical processes. A classical approach is given in *Excited states and Photochemistry of Organic Molecules* by Klessinger and Michl [162]. A clear and concise introduction can also be found in *Modern Spectroscopy* by Hollas [163].

Section 1.5 on Spectroscopic Methods: A detailed and practical introduction into the techniques of absorption and luminescence spectroscopy can be found in *Principles of Fluorescence Spectroscopy* by Lakowicz. The examples mostly use biologically relevant molecules [164]. A stronger focus on organic molecules and electronic transitions is given by Valeur in *Molecular Fluorescence* [165].

References

1. Pochettino, A. (1906) Sul comportamento fotoelettrico dell' antracene. *Rendiconti*, **15**, 355.
2. Königsberger, J. and Schilling, K. (1910) Über Elektrizitätsleitung in festen Elementen und Verbindungen. *Ann. Phys.*, **32**, 179.
3. Stark, J. and Steubing, W. (1908) Fluorescence and light electrical sensitivity of organic substances. *Phys. Z.*, **9**, 481.
4. Pauli, W.E. (1913) Lichtelektrische Untersuchungen an fluoreszierenden Substanzen. *Ann. Phys.*, **345** (4), 677.
5. Bernanose, A., Comte, M., and Vouaux, P. (1953) A new method of emission of light by certain organic compounds. *J. Chim. Phys.*, **50**, 64.
6. Pope, M., Magnante, P., and Kallmann, H.P. (1963) Electroluminescence in organic crystals. *J. Chem. Phys.*, **38** (8), 2042.
7. Helfrich, W. and Schneider, W.G. (1965) Recombination radiation in anthracene crystals. *Phys. Rev. Lett.*, **14** (7), 229.
8. Helfrich, W. and Schneider, W.G. (1966) Transients of volume-controlled current and of recombination radiation in anthracene. *J. Chem. Phys.*, **44** (8), 2902.
9. Tang, C.W. and VanSlyke, S.A. (1987) Organic electroluminescent diodes. *Appl. Phys. Lett.*, **51** (12), 913.
10. Burroughes, J.H. *et al.* (1990) Light-emitting diodes based on conjugated polymers. *Nature*, **347**, 539.
11. Pope, M. and Swenberg, C.E. (1999) *Electronic Processes in Organic Crystals and Polymers*, Clarendon Press, Oxford, ISBN: 978-0195129632
12. Schwoerer, M. and Wolf, H.C. (2007) *Organic Molecular Solids*, Wiley-VCH Verlag GmbH, Weinheim, ISBN: 978-3-527-40540-4, 3527405402.
13. Scher, H. and Montroll, E.W. (1975) Anomalous transit-time dispersion in amorphous solids. *Phys. Rev. B*, **12**, 2455.
14. Borsenberger, P.M. and Weiss, D.S. (1998) *Organic Photoreceptors for Xerography*, Marcel Dekker, Inc., New York.
15. Heeger, A.J. (2001) Semiconducting and metallic polymers: the fourth generation of polymeric materials (Nobel lecture). *Angew. Chem. Int. Ed.*, **40** (14), 2591.
16. Chiang, C.K. *et al.* (1977) Electrical-conductivity in doped polyacetylene. *Phys. Rev. Lett.*, **39** (17), 1098.
17. Su, W.P., Schrieffer, J.R., and Heeger, A.J. (1979) Solitons in polyacetylene. *Phys. Rev. Lett.*, **42** (25), 1698.
18. Su, W.P., Schrieffer, J.R., and Heeger, A.J. (1980) Soliton excitations in polyacetylene. *Phys. Rev. B*, **22** (4), 2099.
19. Sariciftci, E.N.S. (1997) *Primary Photoexcitations in Conjugated Polymers: Molecular Exciton Versus Semiconductor Band Model*, World Scientific, Singapore, ISBN: 978-9810228804.
20. Scholes, G.D. and Rumbles, G. (2006) Excitons in nanoscale systems. *Nat. Mater.*, **5**, 683.
21. Silinsh, E.A. and Capek, V. (1994) *Organic Molecular Crystals*, AIP Press, New York, ISBN: 978-1563960697.
22. Wright, J.D. (ed.) (1994) *Molecular Crystals*, Cambridge University Press, ISBN: 978-0521465106
23. Kitaigorodskii, A.I. (1973) *Molecular Crystals and Molecules*, Academic Press, New York, ISBN: 978-0124105508.
24. Hasegawa, T. and Takeya, J. (2009) Organic field-effect transistors using single crystals. *Sci. Technol. Adv. Mater.*, **10** (2), 024314.
25. Podzorov, V. *et al.* (2004) Intrinsic charge transport on the surface of organic semiconductors. *Phys. Rev. Lett.*, **93**, 086602.
26. Zeis, R. *et al.* (2006) Field effect studies on rubrene and impurities of rubrene. *Chem. Mater.*, **18** (2), 244.
27. Wang, L. *et al.* (2007) Electric-field-dependent charge transport in organic thin-film transistors. *J. Appl. Phys.*, **101**, 054515.
28. Minari, T., Nemoto, T., and Isoda, S. (2006) Temperature and electric-field dependence of the mobility of a single-grain pentacene field-effect transistor. *J. Appl. Phys.*, **99**, 034506.
29. Bässler, H. and Köhler, A. (2012) Charge Transport in Organic Semiconductors. *Top. Curr. Chem.*, **312**, 1.

30. Sirringhaus, H. *et al.* (1999) Two-dimensional charge transport in self-organized, high-mobility conjugated polymers. *Nature*, **401** (6754), 685.
31. Rothberg, L. (2006) Photophysics of conjugated polymers, in *Semiconducting Polymers* (eds G. Hadziioannou and G.G. Malliaras), Wiley-VCH Verlag GmbH, Weinheim, ISBN: 978-3-527-31271-9.
32. Ariu, M. *et al.* (2002) The effect of morphology on the temperature-dependent photoluminescence quantum efficiency of the conjugated polymer poly(9, 9-dioctylfluorene). *J. Phys. Condens. Matter*, **14** (42), 9975.
33. Silva, C. *et al.* (2002) Exciton and polaron dynamics in a step-ladder polymeric semiconductor: the influence of interchain order. *J. Phys. Condens. Matter*, **14** (42), 9803.
34. Hayer, A. *et al.* (2005) Morphology dependence of the triplet excited state formation and absorption in polyfluorene. *Phys. Rev. B*, **71** (24), 241302.
35. Mauer, R., Kastler, M., and Laquai, F. (2010) The impact of polymer regioregularity on charge transport and efficiency of P3HT:PCBM photovoltaic devices. *Adv. Funct. Mater.*, **20** (13), 2085.
36. Scherf, U. and List, E.J.W. (2002) Semiconducting polyfluorenes -towards reliable structure-property relationships. *Adv. Mater.*, **14** (7), 477.
37. Burn, P.L. *et al.* (1992) Precursor route chemistry and electronic-properties of poly(p-phenylene-vinylene), poly[(2,5-dimethyl-p-phenylene)vinylene] and poly[(2,5-dimethoxy-p-phenylene)vinylene]. *J. Chem. Soc., Perkin Trans.*, **1** (23), 3225.
38. Png, R.Q. *et al.* (2010) High-performance polymer semiconducting heterostructure devices by nitrene-mediated photocrosslinking of alkyl side chains. *Nat. Mater.*, **9** (2), 152.
39. Müller, C.D. *et al.* (2003) Multi-colour organic light-emitting displays by solution processing. *Nature*, **421** (6925), 829.
40. Jandke, M. *et al.* (2001) Polarized electroluminescence from photocrosslinkable nematic fluorene bisacrylates. *Proc. SPIE*, 4105.
41. Scheler, E. and Strohriegl, P. (2010) Three color random fluorene-based oligomers for fast micrometer-scale photopatterning. *Chem. Mater.*, **22** (4), 1410.
42. Prigodin, V.N. *et al.* (2008) Electron-ion interaction in doped conducting polymers. *Phys. Rev. B*, **78** (3), 035203.
43. Lee, H.J., Lee, J., and Park, S.M. (2010) Electrochemistry of conductive polymers. 45. nanoscale conductivity of PEDOT and PEDOT:PSS composite films studied by current-sensing AFM. *J. Phys. Chem. B*, **114** (8), 2660.
44. Jung, J.W., Lee, J.U., and Jo, W.H. (2010) High-efficiency polymer solar cells with water-soluble and self-doped conducting polyaniline graft copolymer as hole transport layer. *J. Phys. Chem. C*, **114** (1), 633.
45. Li, D., Huang, J.X., and Kaner, R.B. (2009) Polyaniline nanofibers: a unique polymer nanostructure for versatile applications. *Acc. Chem. Res.*, **42** (1), 135.
46. Lee, K.H. *et al.* (1998) Nature of the metallic state in conducting polypyrrole. *Adv. Mater.*, **10** (6), 456.
47. Hulea, I.N. *et al.* (2005) Doping, density of states, and conductivity in polypyrrole and poly(p-phenylene vinylene). *Phys. Rev. B*, **72** (5), 054208.
48. Banerjee, S. and Kumar, A. (2010) Dielectric behavior and charge transport in polyaniline nanofiber reinforced PMMA composites. *J. Phys. Chem. Solid*, **71** (3), 381.
49. Kirchmeyer, S. and Reuter, K. (2005) Scientific importance, properties and growing applications of poly(3,4-ethylenedioxythiophene). *J. Mater. Chem.*, **15** (21), 2077.
50. MacDiarmid, A.G. (2001) "Synthetic metals": a novel role for organic polymers (Nobel lecture). *Angew. Chem. Int. Ed.*, **40** (14), 2581.
51. Smela, E., Lu, W., and Mattes, B.R. (2005) Polyaniline actuators – Part 1. PANI(AMPS) in HCl. *Synth. Met.*, **151** (1), 25.
52. Kroto, H.W. *et al.* (1985) C-60 – Buckminsterfullerene. *Nature*, **318** (6042), 162.
53. Dresselhaus, M.S., Dresselhaus, G., and Eklund, P.C. (1993) Fullerenes. *J. Mater. Res.*, **8** (8), 2054.
54. Dresselhaus, M.S., Dresselhaus, G., and Saito, R. (1995) Physics of carbon nanotubes. *Carbon*, **33** (7), 883.
55. Dresselhaus, M.S., Dresselhaus, G., and Jorio, A. (2004) Unusual properties and structure of carbon nanotubes. *Annu. Rev. Mater. Res.*, **34**, 247.
56. Hamley, I. (2007) *Introduction to Soft Matter*, Wiley-VCH Verlag GmbH, ISBN: 9780470516102.
57. Chandrasekha, S. (1994) *Liquid Crystals*, Cambridge University Press, ISBN: 978-0521417471.
58. Mccullough, R.D. and Lowe, R.D. (1992) Enhanced electrical-conductivity in regioselectively synthesized poly(3-alkylthiophenes). *J. Chem. Soc., Chem. Commun.*, (1), 70.
59. Stein, P.C. *et al.* (1991) NMR-studies of poly(3-alkylthiophenes). *Synth. Met.*, **41** (1-2), 559.

60. Yamamoto, T. *et al.* (1992) Preparation of pi-conjugated poly(thiophene-2,5-diyl), poly(para-phenylene), and related polymers using zero valent nickel-complexes – Linear structure and properties of the pi-conjugated polymers. *Macromolecules*, **25** (4), 1214.
61. Miyaura, N. and Suzuki, A. (1995) Palladium-catalyzed cross-coupling reactions of organoboron compounds. *Chem. Rev.*, **95** (7), 2457.
62. Bolognesi, A. and Pasini, M.C. (2007) Synthetic methods for semiconducting polymers, in *Semiconducting Polymers* (eds G. Hadziioannou and G.G. Malliaras), Wiley-VCH Verlag GmbH, Weinheim, ISBN: 978-3-527-31271-9.
63. Kallitsis, J.K., Tsolakis, M.C., and Andreopoulou, A.K. (2007) Processable semiconducting polymers containing oligo-conjugated blocks, in *Semiconducting Polymers* (eds G. Hadziioannou and G.G. Malliaras), Wiley-VCH Verlag GmbH, Weinheim, ISBN: 978-3-527-31271-9.
64. Atkins, P.W. (1983) *Molecular Quantum Mechanics*, 2nd edn, Oxford University Press, ISBN: 0-19-855170-3.
65. Demtröder, W. (2005) *Molecular Physics*, Wiley-VCH Verlag GmbH, ISBN: 978-3527405664.
66. Atkins, P.W. and Friedman, R.S. (1996) *Molecular Quantum Mechanics*, 3rd edn, Oxford University Press, Oxford.
67. Demtröder, W. (2003) *Molekülphysik*, Oldenbourg Wissenschaftsverlag GmbH, München.
68. Miller, R.D. (1989) Polysilanes – A new look at some old materials. *Angew. Chem., Int. Ed. Engl.*, **28** (12), 1733.
69. Stolka, M. *et al.* (1990) Manifestation of glass-transition in electronic charge transport in Si and Ge backbone polymers. *Synth. Met.*, **37** (1-3), 295.
70. Bredas, J.L. (2014) Mind the gap! *Mater. Horiz.*, **1**, 17.
71. Haken, H. and Wolf, H.C. (2006) *Molekülphysik und Quantenchemie*, Springer, ISBN: 978-3540435518
72. Yersin, H. and Finkenzeller, W.J. (2007) Triplet emitters for organic Light-emitting diodes: basic properties, in *Highly Efficient OLEDs with Phosphorescent Materials* (ed. H. Yersin), Wiley-VCH Verlag GmbH, ISBN: 978-3-527-62131-6
73. Köhler, A. and Bässler, H. (2009) Triplet states in organic semiconductors. *Mater. Sci. Eng., R*, **66**, 71.
74. Johnston, M.B. *et al.* (2003) Low-energy vibrational modes in phenylene oligomers studied by THz time-domain spectroscopy. *Chem. Phys. Lett.*, **377** (1-2), 256.
75. Karabunarliev, S. *et al.* (2000) Rigorous Franck-Condon absorption and emission spectra of conjugated oligomers from quantum chemistry. *J. Chem. Phys.*, **113** (24), 11372.
76. Mariani, M.M. and Deckert, V. (2012) Raman spectroscopy: principles, benefits and applications. *Bunsen-Magazin*, **4**, 136.
77. Hollas, J.M. (1992) *Modern Spectroscopy*, 2nd edn, John Wiley & Sons, Ltd, Chichester.
78. Liu, Y. *et al.* (2002) Photophysics of monodisperse platinum-acetylide oligomers: delocalization in the singlet and triplet excited states. *J. Am. Chem. Soc.*, **124** (42), 12412.
79. Albuquerque, R.Q. *et al.* (2011) Diffusion-limited energy transfer in blends of oligofluorenes with an anthracene derivative. *J. Phys. Chem. B*, **115** (25), 8063.
80. Khan, A.L.T. (2005) Analysis of electron-phonon coupling from the luminescence of conjugated polymers, in PhD thesis, *Cavendish Laboratory*, University of Cambridge, Cambridge.
81. Köhler, A. *et al.* (2012) The role of C-H and C-C stretching modes in the intrinsic non-radiative decay of triplet states in a Pt-containing conjugated phenylene ethynylene. *J. Chem. Phys.*, **136**, 094905.
82. Kearwell, A. and Wilkinson, F. (1969) in *Transfer and Storage of Energy by Molecule* (eds Q.M. Burnett and A.M. North), John Wiley & Sons, Inc., New York.
83. Strickler, S.J. and Berg, R.A. (1962) Relationship between absorption intensity and fluorescence lifetime of molecules. *J. Chem. Phys.*, **37** (4), 814.
84. Sandee, A.J. *et al.* (2004) Solution-processible conjugated electrophosphorescent polymers. *J. Am. Chem. Soc.*, **126** (22), 7041.
85. Siebrand, W. (1967) Radiationless transitions in polyatomic molecules. I. Calculation of Franck-Condon factors. *J. Chem. Phys.*, **46** (2), 440–447.
86. Turro, N.J. (1991) *Modern Molecular Photochemistry*, 2nd edn, University Science Books, Sausalito, CA, ISBN-13: 978-0935702712 and Turro, N.J., Ramamurthy V., and Scaiano, J. (2010) Modern Molecular Photochemistry of Organic Molecules, Palgrave Macmillan, ISBN: 978-189138925.
87. Birks, J.B. (1970) *Photophysics of Aromatic Molecules*, Wiley-Interscience, London, ISBN: 978-0471074205

88. Wilson, J.S. *et al.* (2003) Polarization of singlet and triplet excited states in a platinum-containing conjugated polymer. *Phys. Rev. B*, **67** (12), 125206.
89. King, S.M., Vaughan, H.L., and Monkman, A.P. (2007) Orientation of triplet and singlet transition dipole moments in polyfluorene, studied by polarised spectroscopies. *Chem. Phys. Lett.*, **440** (4-6), 268.
90. Mcglynn, S.P. *et al.* (1962) External heavy-atom spin-orbital coupling effect. 3. Phosphorescence spectra and lifetimes of externally perturbed naphthalenes. *J. Phys. Chem.*, **66** (12), 2499.
91. Mcglynn, S.P., Kasha, M., and Azumi, T. (1964) External heavy-atom spin-orbital coupling effect. V. absorption studies of triplet states. *J. Chem. Phys.*, **40** (2), 507.
92. Lupton, J.M. *et al.* (2002) Intrinsic room-temperature electrophosphorescence from a pi-conjugated polymer. *Phys. Rev. Lett.*, **89** (16), 167401.
93. Turro, N.J. (1965) *Molecular Photochemistry (Frontiers in Chemistry)*, W.A. Benjamin, New York.
94. Forrest, S.R., Bradley, D.D.C., and Thompson, M.E. (2003) Measuring the efficiency of organic light-emitting devices. *Adv. Mater.*, **15** (13), 1043.
95. McGlynn, S.P., Azumi, T., and Kinoshita, M. (1969) *Molecular Spectroscopy of The Triplet State*, Prentice-Hall, Englewood Cliffs, NJ, ISBN: 978-0135996621
96. Beljonne, D. *et al.* (2001) Spin-orbit coupling and intersystem crossing in conjugated polymers: a configuration interaction description. *J. Phys. Chem. A*, **105** (15), 3899.
97. Klingshirn, C.F. (1997) *Semiconductor Optics*, Springer-Verlag, Berlin, ISBN: 978-3540583127.
98. Paus, H.J. (2007) *Physik in Experimenten und Beispielen*, 3rd edn, Hanser-Verlag, München, ISBN: 978-3-446-41142-5.
99. Demtröder, W. (2010) *Atome, Moleküle und Festkörper. Experimentalphysik*, Vol. 3, Springer, Berlin, ISBN: 978-3540214731
100. Einstein, A. (1917) Zur Quantentheorie der Strahlung. *Phys. Z.*, **18**, 121.
101. Hilborn, R.C. (1982) Einstein coefficients, cross-sections, f values, dipole-moments, and all that. *Am. J. Phys.*, **50** (11), 982.
102. Hilborn, R.C. (1983) Correction. *Am. J. Phys.*, **51** (5), 471.
103. Hilborn, R.C. (2002) Einstein coefficients, cross sections, *f* values, dipole moments, and all that, *http://arxiv.org/abs/physics/0202029* (accessed 6 September 2014).
104. Robinson, G.W. and Frosch, R.P. (1962) Theory of electronic energy relaxation in solid phase. *J. Chem. Phys.*, **37** (9), 1962.
105. Robinson, G.W. and Frosch, R.P. (1963) Electronic excitation transfer and relaxation. *J. Chem. Phys.*, **38** (5), 1187.
106. Siebrand, W. (1966) Mechanism of radiationless triplet decay in aromatic hydrocarbons and magnitude of Franck-Condon factors. *J. Chem. Phys.*, **44** (10), 4055.
107. Gelbart, W.M., Freed, K.F., and Rice, S.A. (1970) Internal rotation and breakdown of adiabatic approximation – Many-phonon radiationless transitions. *J. Chem. Phys.*, **52** (5), 2460.
108. Jortner, J., Rice, S.A., and Hochstrasser, R.M. (1969) Radiationless transitions in photochemistry. *Adv. Photochem.*, **7**, 149.
109. Freed, K.F. and Jortner, J. (1970) Multiphonon processes in nonradiative decay of large molecules. *J. Chem. Phys.*, **52** (12), 6272.
110. Englman, R. and Jortner, J. (1970) Energy gap law for radiationless transitions in large molecules. *Mol. Phys.*, **18** (2), 145.
111. Craig, D.P. and Ross, I.G. (1954) The triplet-triplet absorption spectra of some aromatic hydrocarbons and related substances. *J. Chem. Soc.*, 1589, DOI: 10.1039/JR9540001589
112. Kellogg, R.E. and Schwenker, R.P. (1964) Temperature effect on triplet state lifetimes in solid solutions. *J. Chem. Phys.*, **41** (9), 2860.
113. Kellogg, R.E. and Bennett, R.G. (1964) Radiationless intermolecular energy transfer. 3. Determination of phosphorescence efficiencies. *J. Chem. Phys.*, **41** (10), 3042.
114. Lim, E.C. and Laposa, J.D. (1964) Radiationless transitions + deuterium effect on luminescence of some aromatics. *J. Chem. Phys.*, **41** (10), 3257.
115. Azumi, T. and Mcglynn, S.P. (1963) Delayed fluorescence of solid solutions of polyacenes. 2. Kinetic considerations. *J. Chem. Phys.*, **39** (5), 1186.
116. Kellogg, R.E. (1966) Second triplet state of anthracene. *J. Chem. Phys.*, **44** (1), 411.
117. Hilpern, J.W., Stief, L.J., and Porter, G. (1964) Decay of triplet state. I. First-order processes in solution. *Proc. R. Soc. London, Ser. A: Math. Phys. Sci.*, **277** (1370), 437.
118. Ermolaev, V.L. (1963) Perenos Energii V Organicheskikh Sistemakh S Uchastiem Tripletnogo Sostoyaniya. 3. Tverdye Rastvory I Kristally. *Usp. Fiz. Nauk*, **80** (1), 3.
119. Ermolaev, V.L. (1963) English translation. *Sov. Phys.-Usp.*, **6**, 333.
120. Kober, E.M. *et al.* (1986) Application of the energy-gap law to excited-state

decay of osmium(Ii) polypyridine complexes – Calculation of relative nonradiative decay-rates from emission spectral profiles. *J. Phys. Chem.*, **90** (16), 3722.

121. Browne, W.R. and Vos, J.G. (2001) The effect of deuteration on the emission lifetime of inorganic compounds. *Coord. Chem. Rev.*, **219**, 761.

122. Siebrand, W. (1967) Radiationless transitions in polyatomic molecules. 2. Triplet-ground-state transitions in aromatic hydrocarbons. *J. Chem. Phys.*, **47** (7), 2411.

123. Siebrand, W. and Williams, D.F. (1967) Isotope rule for radiationless transitions with an application to triplet decay in aromatic hydrocarbons. *J. Chem. Phys.*, **46** (1), 403.

124. Wilson, J.S. *et al.* (2001) The energy gap law for triplet states in Pt-containing conjugated polymers and monomers. *J. Am. Chem. Soc.*, **123** (38), 9412.

125. Beer, M. and Longuethiggins, H.C. (1955) Anomalous light emission of azulene. *J. Chem. Phys.*, **23** (8), 1390.

126. Viswanath, G. and Kasha, M. (1956) Confirmation of the anomalous fluorescence of azulene. *J. Chem. Phys.*, **24** (3), 574.

127. Sidman, J.W. and Mcclure, D.S. (1956) Electronic and vibrational states of azulene. *J. Chem. Phys.*, **24** (4), 757.

128. Ruzevich, Z.S. (1963) Fluorescence and absorption spectra of azulene in frozen crystalline solutions. *Opt. Spektrosk.*, **15** (3), 357.

129. Marcus, R.A. (1956) On the theory of oxidation-reduction reactions involving electron transfer. 1. *J. Chem. Phys.*, **24** (5), 966.

130. Rissler, J. *et al.* (2001) Excited states of ladder-type poly-p-phenylene oligomers. *Phys. Rev. B*, **64** (4), 045122.

131. Samuel, I.D.W. *et al.* (1993) The efficiency and time-dependence of luminescence from poly(p-phenylene vinylene) and derivatives. *Chem. Phys. Lett.*, **213** (5-6), 472.

132. Peeters, E. *et al.* (2000) Singlet and triplet excitations of chiral dialkoxy-p-phenylene vinylene oligomers. *J. Chem. Phys.*, **112** (21), 9445.

133. Ho, P.K.H. *et al.* (2001) Photoluminescence of poly(p-phenylenevinylene)–silica nanocomposites: evidence for dual emission by Franck–Condon analysis. *J. Chem. Phys.*, **115**, 2709.

134. Romanovskii, Y.V. and Bässler, H. (2000) Phosphorescence from a ladder-type conjugated polymer in solid solutions at low temperature. *Chem. Phys. Lett.*, **326** (1-2), 51.

135. Hoffmann, S.T. *et al.* (2010) Triplet energy transfer in conjugated polymers. III. An experimental assessment regarding the influence of disorder on polaronic transport. *Phys. Rev. B*, **81** (16), 165208.

136. Laquai, F. *et al.* (2003) Sensitized intrinsic phosphorescence from a poly(phenylenevinylene) derivative. *Chem. Phys. Lett.*, **375** (3-4), 286.

137. Tanaka, I. and Tokito, S. (2007) Energy-transfer processes between phosphorescent guest and fluorescent host molecules in phosphorescent OLEDs, in *Highly Efficient OLEDs with Phosphorescent Materials* (ed. H. Yersin), Wiley-VCH Verlag GmbH, ISBN: 978-3527405947.

138. Brandrup, J., Immergut, E.H., and Grulke, E.A. (1999) *Polymer Handbook*, 4th edn, John Wiley & Sons, Inc., New York, ISBN: 978-0471166283.

139. Abboud, J.L.M. and Notario, R. (1999) Critical compilation of scales of solvent parameters. Part I. Pure, non-hydrogen bond donor solvents – Technical report. *Pure Appl. Chem.*, **71** (4), 645.

140. Vandenburg, H.J. *et al.* (1999) A simple solvent selection method for accelerated solvent extraction of additives from polymers. *Analyst*, **124** (11), 1707.

141. Grell, M. *et al.* (1998) Chain geometry, solution aggregation and enhanced dichroism in the liquid-crystalline conjugated polymer poly(9,9-dioctylfluorene). *Acta Polym.*, **49** (8), 439.

142. Cossiello, R.F., Akcelrud, L., and Atvars, D.Z. (2005) Solvent and molecular weight effects on fluorescence emission of MEH-PPV. *J. Braz. Chem. Soc.*, **16** (1), 74.

143. Chen, H.C. *et al.* (2009) Full color light-emitting electrospun nanofibers prepared from PFO/MEH-PPV/PMMA ternary blends. *J. Polym. Sci., Part B: Polym. Phys.*, **47** (5), 463.

144. deMello, J.C., Wittmann, H.F., and Friend, R.H. (1997) An improved experimental determination of external photoluminescence quantum efficiency. *Adv. Mater.*, **9** (3), 230.

145. Zoppi, L. *et al.* (2008) Defect-induced effects on carrier migration through one-dimensional poly(para-phenylenevinylene) chains. *Phys. Rev. B*, **78**, 165204.

146. List, E.J.W. *et al.* (2002) The effect of keto defect sites on the emission properties of polyfluorene-type materials. *Adv. Mater.*, **14** (5), 374.

147. Endo, A. *et al.* (2011) Efficient up-conversion of triplet excitons into a singlet state and its application for organic light emitting diodes. *Appl. Phys. Lett.*, **98** (8), 083302.

148. Baluschev, S. *et al.* (2006) Up-conversion fluorescence: noncoherent excitation by sunlight. *Phys. Rev. Lett.*, **97** (14), 143903.
149. Keivanidis, P.E. *et al.* (2011) Electron-exchange-assisted photon energy up-conversion in thin films of pi-conjugated polymeric composites. *J. Phys. Chem. Lett.*, **2** (15), 1893.
150. Mollay, B. *et al.* (1994) Dynamics of singlet excitations in conjugated polymers – Poly(phenylenevinylene) and poly(phenylphenylenevinylene). *Phys. Rev. B*, **50** (15), 10769.
151. Brunner, K. *et al.* (2000) Site torsional motion and dispersive excitation hopping transfer in pi-conjugated polymers. *J. Phys. Chem. B*, **104** (16), 3781.
152. Herz, L.M. *et al.* (2004) Time-dependent energy transfer rates in a conjugated polymer guest-host system. *Phys. Rev. B*, **70** (16), 165207.
153. Wasserberg, D. *et al.* (2005) Comparison of the chain length dependence of the singlet- and triplet-excited states of oligofluorenes. *Chem. Phys. Lett.*, **411** (1-3), 273.
154. Dellepiane, G. *et al.* (1993) Long-lived photoexcited states in symmetrical polydicarbazolyldiacetylene. *Phys. Rev. B*, **48** (11), 7850.
155. Cabanillas-Gonzalez, J., Grancini, G., and Lanzani, G. (2011) Pump-probe spectroscopy in organic semiconductors: monitoring fundamental processes of relevance in optoelectronics. *Adv. Mater.*, **23** (46), 5468.
156. Cerullo, G. *et al.* (1998) Excited-state dynamics of poly(para-phenylene)-type ladder polymers at high photoexcitation density. *Phys. Rev. B*, **57** (20), 12806.
157. Cabanillas-Gonzalez, J. *et al.* (2005) Photophysics of charge transfer in a polyfluorene/violanthrone blend. *Phys. Rev. B*, **71** (1), 014211.
158. Kraabel, B. *et al.* (2000) Unified picture of the photoexcitations in phenylene-based conjugated polymers: universal spectral and dynamical features in subpicosecond transient absorption. *Phys. Rev. B*, **61** (12), 8501.
159. Korovyanko, O.J. *et al.* (2001) Photoexcitation dynamics in regioregular and regiorandom polythiophene films. *Phys. Rev. B*, **64** (23), 235122.
160. Jones, R.A.L. (2002) *Soft Condensed Matter*, Oxford University Press, ISBN: 978-0198505891.
161. Strobl, G.R. (2007) *The Physics of Polymers*, 3rd edn, Springer, ISBN: 978-3-540-25278-8.
162. Klessinger, M. and Michl, J. (1995) *Excited States and Photochemistry of Organic Molecules*, VCH Publishers, New York, ISBN: 978-0471185765.
163. Hollas, J.M. (2008) *Modern Spectroscopy*, 4th edn, John Wiley & Sons, Ltd, Chichester, ISBN: 978-0-470-84416-8.
164. Lakowicz, J.R. (2006) *Principles of Fluorescence Spectroscopy*, 3st edn, Springer, ISBN 978-0-387-31278-1
165. Valeur, B. (2002) *Molecular Fluorescence*, Wiley-VCH Verlag GmbH, Weinheim, ISBN: 978-3-527-29929-5.